

# **Characterization of 3C-Silicon Carbide for Advance Applications**

A thesis submitted in fulfillment of the requirements for the degree of Doctor of Philosophy

Nashrul Fazli Mohd Nasir

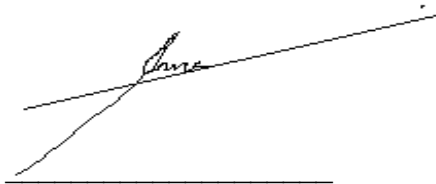
B. Biomed (Eng.), M.Sc. (Biomedical Engineering)

School of Electrical and Computer Engineering  
College of Science, Engineering, and Technology  
RMIT University

August 2012

# Declaration

I certify that except where due acknowledgement has been made, the work is that of the author alone; the work has not been submitted previously, in whole or in part, to qualify for any other academic award; the content of the thesis is the result of work which has been carried out since the official commencement date of the approved research program; and, any editorial work, paid or unpaid, carried out by a third party is acknowledged.

A handwritten signature in black ink, appearing to read 'Nashrul', is written over a horizontal line. The signature is slanted upwards from left to right.

Nashrul Fazli Mohd Nasir

August 2012

# Acknowledgements

*“Alhamdulillah Rabbil Alamin.”*

I would firstly express my special gratitude to Assoc. Prof. Dr. Anthony S. Holland for his guidance, encouragement and tremendous support throughout my PhD. program. Special thanks to Dr. Elena Pirogova who was in the first place to receive me with open hands at the RMIT University. And not to forget, the mentoring I received from Dr. Patrick W. Leech who is a very selfless person and the man of example in science. Here, I would like to thank Assoc. Prof. Dr. Geoffrey K. Reeves where his discoveries in the ohmic contact Transmission Line Model (TLM) test structure parameters laid the foundation of my work. Special thanks to Mr. Mark Aaron Collins for developing the Matlab software to calculate the ohmic contact TLM test structure parameters.

I would like to thank my parents, Haji Mohd Nasir Abdullah and Hajjah Norfishah Zainul Abidin for their continuous prayers and support whilst completing my studies. And to mention the sacrifices of my wife, Rozita Bibi Ismail and three sons, Irham Danish Zayani, Irfan Amsyar Harraz and Izzul Wazif Akram (expected to be born in the end of this September, 2012) whose passions and support throughout this period allowed me to keep on the track and finish this work on time.

This doctoral program cannot be completed without the support from Dr. Taghrid Istivan who supported me during the critical time at Bundoora and also Dr. Emily Gan and Dr. Ravi Shukla

who taught me the techniques and tips for the biocompatibility and hemocompatibility studies which are very valuable for my future career in Biomedical Engineering.

Here, I would like to thank Mr. Paul Jones, Mr. Yunxun Cao and Mrs. Chi-Ping Wu for the valued support they gave me at the Microelectronics and Materials Technology Centre. I also acknowledged the guidance I received from Mr. Eltaher Elshagmani and Mrs. Layla Mehdi Alhasan during my time in Bundoora Campus. The assistance from Mr. Phil Francis, Mr Peter Rummel, Ms Arwen Pagon and A/Prof. Johan du Plessis of the School of Applied Science (Physics), the RMIT University and Dr Brett Johnson of the School of Physics, the University of Melbourne for the material characterization of 3C-SiC is much appreciated and acknowledged. Thank you also to Miss Karen Hewitt and Mrs. Laurie Clinton for their wonderful assistance throughout my PhD studies.

I would like to thank those who are supporting me persistently from my home University, Universiti Malaysia Perlis (UniMAP), Pn. Sharifah Husna Syed Idrus, Prof. Dr. Sazali Yaacob, Prof. Dr. Abdul Hamid Adom, Prof. Dr. Zul Azhar Zahid Jamal and Brig. Jen. Dato' Prof. Dr. Kamarudin Hussin. And lastly, my sponsor, Ministry of Higher Education, (MOHE) and the government of Malaysia, who provided funds for my PhD studies and my stipend at the RMIT University, Melbourne.

# CONTENTS

<b>DECLARATION</b>	<b>ii</b>
<b>ACKNOWLEDGEMENTS</b>	<b>iii</b>
<b>CONTENTS</b>	<b>v</b>
<b>LIST OF FIGURES</b>	<b>x</b>
<b>LIST OF TABLES</b>	<b>xviii</b>
<b>ABSTRACT</b>	<b>xix</b>
<b>1 INTRODUCTION</b>	<b>1</b>
1.1 Motivation	1
1.2 Major Works Included in This Research	5
1.3 Author's Achievements	8
1.3.1 Awards	8
1.3.2 Peer Reviewed Conference Proceedings Publications	9
1.3.3 Journal Papers	9
1.4 Thesis Outline	10
1.5 References	11
<b>2 FABRICATION OF 3C-SILICON CARBIDE MEMBRANES</b>	<b>18</b>
2.1 Experimental	19
2.1.1 Photolithography	19
2.1.2 Reactive Ion Etching	21
2.1.3 Wet Etching of Si in KOH	22

2.2 Results and Discussions	26
2.2.1 Reactive Ion Etching	26
2.2.2 Wet Etching of Si in KOH	27
2.3 Conclusion	30
2.4 References	31
<b>3 MATERIAL CHARACTERIZATION OF 3C-SILICON CARBIDE MEMBRANES</b>	<b>34</b>
3.1 Experimental	35
3.1.1 Scanning Electron Microscopy (SEM)	35
3.1.2 Raman Spectroscopy	35
3.1.3 Visible Transmission Spectra	35
3.1.4 X-Ray Photoelectron Spectroscopy (XPS)	36
3.1.5 Thin Film Adhesion Test	36
3.2 Scanning Electron Microscopy	37
3.3 Raman Spectroscopy	38
3.4 Visible Transmission Spectra	45
3.5 X-Ray Photoelectron Spectroscopy	47
3.6 Thin Film Adhesion Test	49
3.7 Conclusion	51
3.8 References	53

<b>4 ELECTRICAL CHARACTERIZATION OF 3C-SILICON CARBIDE MEMBRANES</b>	<b>58</b>
4.1 Influence of Fluorinated Plasma on Metal Contacts/3C-SiC Electrical Behavior	59
4.1.1 Experimental Methods	59
4.1.2 Results and Analysis of the Symmetrical (Dot to Dot) Contacts	60
4.1.3 Results and Analysis of the Asymmetrical (Dot to Ring) Contacts	62
4.2 Characterization of Ohmic Contact Transmission Line Model Test Structure Parameters	64
4.2.1 Introduction	64
4.2.2 Measurements of $\rho_c$ for metal contacts/3C-SiC membranes	67
4.2.2.1 <i>Experimental Methods</i>	67
4.2.2.2 <i>Results and Analysis of I-V Characteristics of Al, Pd and Ni/Ti/Au on 3C-SiC membranes</i>	70
4.2.2.3 <i>Results and Analysis of <math>\rho_c</math> for Al, Pd and Ni/Ti/Au on 3C-SiC membranes</i>	72
4.3 Analysis of the Substrate Influence on the Current Paths at the 3C-SiC/Si Interface	77
4.3.1 Measurements of Two Symmetrical Contacts on Etched and Unetched Substrate	77
4.3.1.1 <i>Fabrication of Symmetrical Al Contact Patterns</i>	77
4.3.1.2 <i>Results and Analysis of the Measurements of Two Symmetrical Al Contacts on Etched and Unetched Substrates</i>	78
4.3.2 Measurements of $R_{sh}$ with Linear TLM	79
4.3.2.1 <i>Fabrication of Linear TLM</i>	79
4.3.2.2 <i>Results and Analysis of the <math>R_{sh}</math> Measurements</i>	81
4.4 Conclusion	84
4.5 References	86

<b>5 BIOCOMPATIBILITY AND HEMOCOMPATIBILITY ASSESSMENT OF 3C-SILICON CARBIDE THIN FILMS</b>	<b>91</b>
5.1 Introduction	92
5.2 Experimental	93
5.2.1 Basic Cell Culture Technique	93
5.2.2 Cell Counting	94
5.2.3 Cell Viability Studies	96
5.2.3.1 <i>MTT Assay</i>	96
5.2.3.2 <i>PrestoBlue™ Reagent</i>	97
5.2.4 Hemolysis Assay	97
5.2.5 Environmental Scanning Electron Microscopy (ESEM)	98
5.3 Results and Discussions	100
5.3.1 Basic Cell Culture Technique	100
5.3.2 Optical Microscopy	101
5.3.2.1 <i>Cell Lines Cultured on Materials</i>	101
5.3.2.2 <i>Cell Lines Cultured on Plate Well Surface</i>	104
5.3.3 Environmental Scanning Electron Microscopy (ESEM)	109
5.3.4 Cell Counting	111
5.3.4.1 <i>Total Cells Counting</i>	111
5.3.4.2 <i>Living Cells Counting</i>	112
5.3.4.3 <i>Cell Viability Percentage</i>	113
5.3.5 Cell Viability Tests	115
5.3.5.1 <i>MTT Assay</i>	115
5.3.5.2 <i>PrestoBlue™ Reagent</i>	117
5.3.6 Hemolysis Assay	118
5.4 Conclusion	119
5.5 References	122



<b>6 CONCLUSION AND FUTURE WORK</b>	<b>127</b>
6.1 Conclusion	127
6.1.1 Fabrication of 3C-Silicon Carbide Membranes	128
6.1.2 Material Characterization of 3C-Silicon Carbide Membranes	129
6.1.3 Electrical Characterization of 3C-Silicon Carbide Membranes	130
6.1.4 Biocompatibility and Hemocompatibility Assessment of 3C-Silicon Carbide Thin Films	131
6.1.5 Author’s Conclusion Statement	132
6.2 Future Work	133
6.2.1 Fabrication and Finite Element Modeling of MEMS Structures Based on 3C-SiC Membranes	133
6.2.2 Mechanical Characterization of 3C-SiC Membranes	133
6.2.3 Investigation of Schottky Behavior and Other Electrical Properties of Metal/3C-SiC Contacts	134
6.2.4 Fabrication of Potential Microdevices Based on 3C-SiC Membranes and Its Biocompatibility Study	134
<b>A Appendix A</b>	<b>135</b>
A.1 Etching Simulation	135
A.2 Simulation Results	137
A.3 References	139
<b>B Appendix B</b>	<b>140</b>
B.1 Micromilling	140
B.2 References	142
<b>C Appendix C</b>	<b>143</b>
C.1 PrestoBlue™ Reagent Calculation	143
C.2 References	145

# LIST OF FIGURES

2.1	A profilometry showing a step height measured from differences of the surface of 3C-SiC and the photoresist. The thickness of the photoresist was about 7.8 $\mu\text{m}$ .	21
2.2	a) KOH Etching of a Si substrate coated with SiC. The RIE etched window pattern in the SiC film on the backside of the Si substrate allows etching of the Si in the KOH solution. (SiC is highly resistive to KOH etching and therefore is an excellent etch mask material for silicon etching) b) In this early version of experimental set up, a 3C-SiC etched with RIE was suspended with a plastic holder in the KOH solution for wet etching.	23
2.3	3C-SiC samples were taped at the bottom of the beaker or holder to ensure KOH can react with SiC throughout the etching period.	24
2.4	3C-SiC samples were put in a plastic holder and covered by another plastic holder to ensure KOH can react with SiC throughout the etching period	25
2.5	Schematic illustration of 3C-SiC membrane fabrication process	25
2.6	The etch rate of 3C-silicon carbide using Reactive Ion Etching ( $\text{CF}_4$ , 22 sccm, 80 mTorr and 100W)	27
2.7	The final produce of the wet etching using different masks a) double circular mask b) square mask and c) rectangular	27
2.8	(a) $0.5 \times 0.5 \text{cm}^2$ 3C-SiC membrane (0.95 $\mu\text{m}$ thick) structure produced after 63 hours of KOH etching of Si (650 $\mu\text{m}$ thick substrate). (b) $1.5 \times 1.0 \text{cm}^2$ 3C-SiC membrane (0.95 $\mu\text{m}$ thick) structure produced after 63 hours of KOH etching of Si (650 $\mu\text{m}$ thick substrate). (c) Probing of two aluminum contacts on the intact membrane (arbitrary metal tracks can be seen below the SiC membrane). (d) Schematic diagram of SiC membrane structure.	28

	(e) Cross section schematic showing the etched Si layer and the SiC membrane window.	
2.9	A membrane structure in 0.285 $\mu\text{m}$ 3C-SiC produced over an area of 0.5 $\times$ 0.5 $\text{cm}^2$ by 28 hours of KOH etching at 80 $^\circ\text{C}$ .	29
3.1	Scanning electron micrographs showing the backside of a membrane at a magnification of a) 200 $\times$ b) 1000 $\times$ and c) 4000 $\times$ .	37
3.2	a) Positions of measurement taken on the 3C-SiC/Si sample: Position “1”: Underneath the 3C-SiC membrane, Position “2”: Underneath 3C-SiC/Si, Position “3”: On top of the 3C-SiC membrane and Position “4”: On top of 3C-SiC/Si. b) Raman spectra taken from the positions mapped as in a) where the 3C-SiC transverse optic (TO) peaks is approximately 795 $\text{cm}^{-1}$ and the 3C-SiC longitudinal optic (LO) peak is approximately 970 $\text{cm}^{-1}$ . Silicon spectra is included for reference.	39
3.3	PL spectrum of the 3C-SiC free standing membrane and 3C-SiC/Si at room temperature corresponding to positions as mapped in Figure 3.3 (a).	40
3.4	The transverse optic (TO) and longitudinal optic (LO) Raman peaks of 3 different sizes of 3C-SiC free standing films.	42
3.5	PL spectra of 3 different sizes of 3C-SiC free standing films at room temperature.	43
3.6	a) Optical micrograph showing features on a free standing 3C-SiC membrane at 40 $\times$ magnifications. Two sizes of visual microstructures defects were apparent on the film. b) The formation of microstructure defects due to the KOH etching of Si substrate leaving Si <111> as the visual microstructure defects.	44
3.7	Raman spectrum taken from region of the microstructure defects on the free standing films (NOTE: surrounding SiC influences the spectra as the sample region is larger than the defect). Raman Spectra of the microstructures defects in comparison to the spectra at Position “1” (same side of SiC film but away from any defect) which represents 3C-SiC membrane interfacing Si substrate.	44

3.8	Visible transmission spectra of 0.285 $\mu\text{m}$ 3C-SiC membrane.	45
3.9	Visible transmission spectra of 0.95 $\mu\text{m}$ 3C-SiC membrane.	45
3.10	Visible transmission spectra of 1.18 $\mu\text{m}$ 3C-SiC membrane.	46
3.11	Comparison of XPS spectra of 0.285 $\mu\text{m}$ thick 3C-SiC thin film samples which had (i) no surface treatment, (ii) wet etching in KOH and (iii) reactive ion etching with tetrafluoromethane ( $\text{CF}_4$ ).	47
3.12	Comparison of XPS spectra of 0.95 $\mu\text{m}$ thick 3C-SiC thin film samples which had (i) no surface treatment, (ii) wet etching in KOH and (iii) reactive ion etching with tetrafluoromethane ( $\text{CF}_4$ ).	48
4.1	Schematic illustration showing the probing of aluminum contact patterns on large area 3C-SiC; a) Current-voltage measurement from dot to dot contacts. b) Current-voltage measurement from dot to ring contacts. c) Schematic illustration, geometry and dimensions of the contact electrodes for the electrical measurements.	60
4.2	(a) Current-voltage plots from dot to dot metal contacts for (i) the samples that had not been treated, (ii) the samples which were only treated by the KOH and (iii) the samples which were KOH treated and RIE treated. (b) Inset figure shows the comparison between the I-V curves of the untreated samples and the samples influenced by RIE.	61
4.3	a) Current-voltage plots from dot to ring metal contacts for (i) the samples that has not been treated, (ii) the samples which was only treated by the KOH and (iii) the samples which were KOH treated and RIE treated. b) Comparison is made between the I-V curves of the untreated samples and the samples influenced by RIE as shown in the inset figure.	63
4.4	Schematic illustrations showing the CTLM contact geometry. a) $R_1$ is the resistance measured between the central dot and the inner ring. $R_2$ is the resistance measured between the inner ring and the outer metal surrounding. b) A schematic diagram	65

which shows  $R_c$  measurement. Voltage is measured by probing the centre pad to the second ring. Current is supplied to the second ring and the surrounding metal portion. c)  $r_0$  represents the radius of the central dot,  $r_1$  represents the inner radius of the first ring contact,  $r_1$  represents the outer radius of the first ring contact and  $r_2$  represents the inner radius of the second ring contact. The grey area representing the metal and the white representing the substrate/material.

- 4.5 a) Geometry and dimensions of electrodes in the Circular TLM pattern used in the measurement of specific contact resistance. b) Optical micrographs of CTLM. 68
- 4.6: a) CTLM patterns fabricated in Ni/Ti/Au metallization on the upper surface of a membrane. b) The underside of a membrane with the etched recess coated with a resin layer. c) Clear resin fills the backside allowing the front surface (Al metallization) to be probed without breaking the membrane. d) The backside of the 3C-SiC thin film in which a thin layer of Si substrate was left unetched to mechanically reinforce the fragile membrane. 69
- 4.7 Current-voltage plots for a) Al (300 nm) as-deposited on membrane b) Pd (300 nm) annealed at 600 °C, 5 mins on a membrane and substrate and c) Ni (50 nm)/Ti (50 nm)/Au annealed at 950 °C, 5 mins on membrane and on substrate. 70
- 4.8 Schematic illustration of the membrane showing the alternate current paths for contacts located on the membrane and on the 3C-SiC/Si substrate. 71
- 4.9 Measurements of  $\rho_c$  for a) Al/SiC and b) Pd/3C-SiC contacts located both on and off the membranes, with pre-treatment by RIE or KOH solutions and after annealing. 73
- 4.10 Formation of blisters after annealing Al at 600°C. 75
- 4.11 Measurements of  $\rho_c$  for as –deposited Al/3C-SiC contacts on wafers 1-3 with a partial etch through the Si substrate. 76

4.12	Schematic illustration showing the probing of aluminum circular patterns on the etched and unetched Si substrate to determine current leakage.	78
4.13	3C-SiC chip with different gaps length of Al pads for measuring the sheet resistance.	80
4.14	Schematic diagram describing the fabrication process of obtaining samples to measure sheet resistance by shallow isolation of the 3C-SiC thin film from the substrate and complete dicing of the samples.	81
4.15	A linear graph representing a plot of total resistance, $R_T$ , against pad spacing. The value of $2R_C$ is obtained from the intercept of the plotting at Y axis.	82
4.16	Schematic illustration of the membrane showing the current paths for contacts located on the etched and unetched Si substrate. The current shows preference to flow in the epitaxial layer of 3C-SiC rather than leaking into the substrate.	83
5.1	Optical micrograph of CHO cells grown for 24 hours and reached 90% confluent at 4× magnifications. The cells were ready to be used for cell counting and cell viability tests.	100
5.2	Optical micrograph of CHO cells cultured overnight on Thermanox™ Coverslip (positive control) at 4 × magnifications.	101
5.3	Optical micrograph of CHO cells cultured overnight on Thermanox™ Coverslip treated with Bovine Serum Albumin (BSA) (negative control) at 4× magnifications.	101
5.4	Optical micrograph of CHO cells cultured overnight on Si at 20× magnifications.	102
5.5	Optical micrograph of CHO cells cultured overnight on 3C-SiC/Si untreated at 20× magnifications.	102
5.6	Optical micrograph of CHO cells cultured overnight on 3C-SiC/Si treated with KOH solution at 20× magnifications.	103

5.7	Optical micrograph of CHO cells cultured overnight on 3C-SiC/Si treated with KOH solution and reactive ion etching at 20× magnifications.	103
5.8	Optical micrograph of CHO cells cultured overnight on the 6 well plate surface previously subcultured on Thermanox™ Coverslip (positive control) at 4× magnifications.	104
5.9	Optical micrograph of CHO cells cultured overnight on the 6 well plate's surface previously subcultured on Thermanox™ Coverslip treated with BSA (negative control) at 4× magnifications.	104
5.10	Optical micrograph of CHO cells cultured overnight on the 6 well plate's surface previously subcultured on Si at 4× magnifications.	105
5.11	Optical micrograph of CHO cells cultured overnight on the 6 well plate's surface previously subcultured on 3C-SiC/Si untreated at 4× magnifications.	106
5.12	Optical micrograph of CHO cells cultured overnight on the 6 well plate's surface previously subcultured on 3C-SiC treated with KOH solution at 4× magnifications.	106
5.13	Optical micrograph of CHO cells cultured overnight on the 6 well plate's surface previously subcultured on 3C-SiC treated with KOH solution and reactive ion etching at 4× magnifications.	107
5.14	ESEM micrographs showing CHO cells cultured on Si a) 400× and b) 1200×.	109
5.15	ESEM micrographs showing CHO cells cultured on untreated 3C-SiC a) 400× and b) 1200×.	109
5.16	ESEM micrographs showing CHO cells cultured on 3C-SiC treated with KOH solution a) 400× and b) 1200×.	110
5.17	ESEM micrographs showing CHO cells cultured on 3C-SiC treated with	110

KOH solution and reactive ion etching a) 400× and b) 1200×.

- 5.18 The number of total cells cultured on the materials after incubated overnight, stained by Trypan blue dye and counted using Countess® Automated Cell Counter (Invitrogen). The cells cultured on Thermanox™ coverslip were used as positive control and the cells cultured on Thermanox™ coverslip treated with Bovine Serum Albumin (BSA) were used as negative control. The total cells counted include living cells and dead cells. 111
- 5.19 The amount of living cells cultured on the materials after incubated overnight, stained by Trypan blue dye and and counted using Countess® Automated Cell Counter (Invitrogen). The cells cultured on Thermanox™ coverslip were used as positive control and the cells cultured on Thermanox™ coverslip treated with Bovine Serum Albumin (BSA) were used as negative control. 112
- 5.20 The viability percentage of the cells after had been cultured on the materials, incubated overnight and stained by Trypan blue dye and. The cell viability percentage was obtained using Countess® Automated Cell Counter (Invitrogen). The cells cultured on Thermanox™ coverslip were used as positive control and the cells cultured on Thermanox™ coverslip treated with Bovine Serum Albumin (BSA) were used as negative control. 114
- 5.21 CHO cells viability percentage on the materials against control using MTT assay (Invitrogen, USA) assay. The tests were performed in triplicates and the reported values are expressed as  $\bar{x} \pm \sigma_m$ . The cells cultured on Thermanox™ coverslip were used as positive control and the cells cultured on Thermanox™ coverslip treated with Bovine Serum Albumin (BSA) were used as negative control. 115
- 5.22 CHO cells viability percentage on the materials against control using Prestoblue™ Cell Viability reagent (Invitrogen, USA) assay. The tests were performed in triplicates and the result is expressed as  $\bar{x} \pm \sigma_m$ . The cells cultured on Thermanox™ coverslip were used as positive control and the cells cultured 117



on Thermanox™ coverslip treated with Bovine Serum Albumin (BSA) were used as negative control.

5.23	Hemolytic activity of hRBC with the materials. The tests were performed in triplicates and the reported values are expressed as $\bar{x} \pm \sigma_m$ . Results from PBS (where no hemolysis should occur) is set to zero and compared to the hemolysis results from other materials interacting with hRBC.	118
A.1	The parameters set for the simulations of KOH etching of Si and the shape of masks used in the fabrication of 3C-SiC membranes, a) round mask and b) square mask c) rectangular mask	136
A.2	The final outcome of the simulated etching of Si using circular mask.	137
A.3	The final outcome of the simulated etching of Si using square mask.	138
A.4	The final outcome of the simulated etching of Si using rectangular mask.	138
B.1	isel CPM 3020 which was used to remove the 3C-SiC layer exposing the substrate for KOH wet etching of Si.	141

# LIST OF TABLES

3.1	Transverse optic (TO) and Longitudinal optic (LO) of Raman peaks according to 3C-SiC free standing films sizes.	41
3.2	3C-SiC membranes thicknesses and their corresponding transmission percentage.	46
3.3	The list of the metals deposited on the 3C-SiC thin films and the quality of the adhesion. *Nickel adhered better if the 3C-SiC/Si samples were plasma etched for surface cleaning (Condition: CF <sub>4</sub> /O <sub>2</sub> , 14/5 sccm, 70mTorr, 100W). Other metals showed the same adhesion quality with or without plasma treatment.	50
4.1	Resistivity values measured compared to the resistivity values in literatures	85
C.1	The values for OD <sub>595</sub> , OD <sub>630</sub> and the OD <sub>595</sub> -OD <sub>630</sub>	144
C.2	The background corrected values	144

# Abstract

3C-Silicon Carbide (SiC) is currently under intense study as a potential material for biomedical microdevices due to its excellent electrical, material and biocompatibility properties. In this work, the fabrication processes for n-type 3C-SiC membranes using epitaxial 3C-SiC layers grown on Silicon (Si) substrate is presented and discussed in detail. Membranes of n-type 3C-SiC were successfully fabricated using standard photolithography, reactive ion etching (RIE) and wet etching of Si substrates and could withstand small forces applied. Subsequently, the membranes were able to be patterned with patterns such as Circular Transmission Line Models (CTLM) patterns.

Scanning electron microscope (SEM) micrographs were used to observe the structure of the membrane and the wall formed by the Si wet etching. The quality of the 3C-SiC membranes were observed using Raman Spectroscopy and Visible Transmission Spectra. The remains of  $\langle 111 \rangle$  Si substrate which was unetched during the Si wet etching were represented with the formation of microstructure defects which showed distinct peaks in comparison to the high quality 3C-SiC membranes at different position. X-Ray Photoelectron Spectroscopy (XPS) revealed the effect of RIE where fluorinated plasma had introduced fluorine elements into the membranes' surface.

Surface modification due to reactive ion etching (RIE) process had significant impact on the electrical properties of the sample. The non linearity of current-voltage (I-V) characteristics for the samples treated with fluorinated plasma was observed which were absent for the control 3C-

SiC samples. Measurements of specific contact resistance,  $\rho_c$  for Al/3C-SiC and Pd/3C-SiC contacts with pre-treatment by reactive ion etching in  $CF_4$  plasma were 3 orders of magnitude higher ( $\rho_c = 2 \times 10^{-1} \Omega\text{cm}^2$ ) than for as-grown SiC or KOH treated surfaces ( $\rho_c = 4 \times 10^{-5} - 8.9 \times 10^{-4} \Omega\text{cm}^2$ ). Annealing of Al/3C-SiC contacts resulted in a progressive increase in  $\rho_c$  with increase in temperature to 600 °C. In this program, it is found that the substrate effect on the electrical characteristic properties of 3C-SiC/Si can be neglected at room temperature. However, the application of 3C-SiC membrane to determine the electrical characteristics is the best way to eliminate any possibility of current leakage into the substrate for this type of system.

Cells grown on 3C-SiC were stellular and flattened showing good adhesion to the material as compared to cells on Si. The number of the cells grown on the 3C-SiC samples showed superior figure in comparison to Si which indicates higher biocompatibility. However, the number of cells was found to be less for the plasma treated samples, even compared with Si. This result was annulled after a series of experiments using typical assay used for cell viability detection such as MTT assay and PrestoBlue™ reagent where the plasma treated samples had the best cell viability percentage of all. By using hemolytic activity assessment, the plasma treated 3C-SiC was found to be decisively hemocompatible.

As a conclusion, fabrication processes of 3C-SiC membrane had altered the properties of 3C-SiC. Thus, the utilization of RIE should compromise the effect outlined by the author in order to achieve best performance for the biomedical microdevices.

# Chapter 1

## Introduction

### 1.1 Motivation

Microelectromechanical (MEMS) devices with high biocompatibility can be used for new and effective medical devices in human disease prevention and detection systems. The best condition for human physiological measurements is to avoid disruption of a patient's normal activity and this can be achieved by implantable biomedical microdevices [1]. BioMEMS technology offers

prospective devices which have low power consumption and production cost together with the miniaturization of size and weight for implants and allows continuous patient monitoring [2]. However, apart from the electronic design and fabrication issues, the material that should be chosen for these types of applications should firstly be shown to be biocompatible and ideally be suitable for use in conventional Silicon (Si) microfabrication technology [3, 4]. Park et al. [5] defines biocompatibility as “the acceptance of the artificial implant by the surrounding tissue and by the body as a whole”. Apart from using SiC as a bulk material, 3C-SiC can be epitaxially grown on Si substrates which can lead to reduced costs allows structures to be made to a significant extent using Si micromachining processes.

In regard to its use for BioMEMS devices, Silicon carbide has the properties and characteristics that could meet the requirements mentioned in the previous paragraph together with excellent electrical, mechanical and chemical properties [3, 4]. 3C-SiC can tolerate 20% lattice mismatch and 8% thermal mismatch which allows low cost and large area growth of SiC on <100> Si substrates [6]. SiC devices have included automotive pressure and acceleration sensors used in harsh environments, motors with resistance to high temperature, electronics for high radiation applications and microswitches with improved power capability [7]. Thus, most of the reports and reviews on application of silicon carbide are mostly in regard to its use in MEMS devices, particularly in high temperature applications [7-19].

Before SiC can be successfully used as a MEMS device, it has to be characterized in order to understand its electrical properties. The major problem which hinders appropriate electrical characterization of 3C-SiC/Si is related to heterojunction leakage current where the current is susceptible to flow especially at temperature higher than 150°C into the Si substrate [8]. It is also reported that this phenomenon can occur at room temperature [20, 21]. Thus, to enable 3C-SiC to

be used in high temperature applications, electrical insulation of the SiC layer from the Si substrate was performed either using Silicon on Insulator (SOI) system or by the introduction of a SiO<sub>2</sub> layer [10, 22-24]. Although there is a high chance of substrate effect phenomenon, attempts were made to electrically characterize the ohmic contact Transmission Line Model (TLM) test structure parameters (contact resistance, contact end resistance, sheet resistance and specific contact resistance) of metal contacts deposited straight onto the 3C-SiC layer at room temperature [14, 25] and even at elevated temperatures [26-28]. In this thesis, the possibility of substrate effects can be ruled out through a series of appropriately designed experiments. The electrical characterization of the transmission line model test structure parameters for the 3C-SiC/Si system at room temperature is presented and shown in detail. However, the electrical characterization of 3C-SiC via application of membrane is the best method to eliminate substrate effects on the measurements since the current definitely has to flow only through one path which is via the membrane.

SiC is also currently getting significant attention as a biomedical material of interest. Vigorous biocompatibility studies were performed on the devices fabricated from hexagonal crystal variants of SiC, either 6H-SiC or 4H-SiC [29-32]. For example, the application of amorphous SiC (a-SiC) as a coronary stent coating shows contrary findings [33-35]. a-SiC was found to reduce coronary events in patients, but, in another study, restenosis was shown in both patients implanted with bare stents and SiC coated stents after 6 months of surgery [34, 35]. This proposes a further investigation on the biocompatibility and suitability of SiC as a material for implants.

Despite these advances for amorphous silicon carbide, the application of 3C-SiC as a biomaterial is an area ripe for development. However, only few biocompatibility studies have

been taken place on 3C-SiC using testing procedures in accordance to ISO 10993 which serves as a guideline to evaluate the biological and immunotoxic responses and risks of medical devices prior to clinical study [3, 36]. Kotzar et al. was the first to intensively evaluate the cytocompatibility of 3C-SiC. Currently, further investigation on the biocompatibility of 3C-SiC as a biomaterial of interest is performed by a group led by Stephen E. Saddow from the University of South Florida [37-41]. Subsequently, a successful brain-machine interface device has been constructed by the group [39]. Apart from these studies, 3C-SiC has been proposed as a basic material for superlenses used in near-field scanning optical microscopy (NSOM) [42] and as a capacitive sensor used for invasive blood pressure monitoring [43]. But no further testing was conducted to prove the biocompatibility or hemocompatibility (this term refers to the appropriateness of the material or the device to be used in blood contacting applications [44]) of these devices. In this thesis, further studies on the biocompatibility and hemocompatibility of 3C-SiC is performed and presented. Related studies on the effect of the fabrication process in semiconductor such as potassium hydroxide (KOH) etching of silicon substrate and reactive ion etching (RIE) on the biocompatibility of AlGaIn/GaN [45] and polyimide [46] have been reported. The authors of these studies concluded that these processes posed little effect on the materials biocompatibility and cytotoxicity. Thus, the effect of typical fabrication steps used in semiconductor devices production on cell viability and hemolytic nature of 3C-SiC is established and included in this thesis.



## 1.2 Major Works Included in This Research

In this PhD thesis, the author demonstrates the processes for fabricating 3C-SiC membranes using standard micromachining procedures which involves standard photolithography, reactive ion etching (RIE), micromilling and potassium hydroxide (KOH) etching. One of the objectives of membrane fabrication in this PhD program is to eliminate the possibility of leakage current at the 3C-SiC/Si heterojunction which subsequently enable electrical characterization of 3C-SiC without the substrate effect.

The 3C-SiC thin films with thickness of 0.285, 0.950 or 1.18  $\mu\text{m}$  were grown using low pressure chemical vapour deposition (LPCVD) at the Queensland Microtechnology Facility, Griffith University [47, 48]. Consequently, RIE was used to remove a portion of 3C-SiC which revealed Si substrate. The Si was further etched by KOH etching and the 3C-SiC thin films eventually formed into membranes: 5 mm  $\times$  5 mm membranes and 10 mm  $\times$  15 mm membranes. Before using standard photolithography to produce test structures, metal masks (etched patterned brass shims) were used to create circular dots on the membrane which proved the ability of the membrane to be patterned. Subsequently, dot and ring patterns and Circular Transmission Line Models (CTLM) patterns were made on the membranes using standard photolithographically. These processes demonstrated that 3C-SiC membranes were able to be produced using standard micromachining steps and test structures were patterned without difficulties which enabled electrical, material and biological characterization to be made.

Characterization of 3C-SiC thin films and membranes in this program involved the application of Scanning Electron Microscopy (SEM), Raman Spectroscopy, Ultra Violet Visible Infra Red Spectroscopy (UV-VIS) and X-Ray Photoelectron Spectroscopy (XPS) and Thin Film

Adhesion Test. The morphology of the membrane was observed by the author using an SEM. The SEM micrographs show the etched cavity of the <100> Si substrate and the formation of membrane structures with.

Micro-Raman measurements using Raman spectroscopy showed the differences of Raman peaks (transverse optic and longitudinal optic peaks) and photoluminescence (PL) peaks of 3C-SiC membranes and the 3C-SiC/Si. The influence of Si to the membrane was apparent to the backside of the membrane which previously interfaced the Si substrate. The front side of the 3C-SiC membrane was smooth and indeed high quality 3C-SiC. This influence was extended to the Raman and PL peaks exhibited by the microstructure defects on the bottom of the SiC membrane, formed which was suspected to originate from the unetched Si<111> during the membrane fabrication.

The optical property of the difference thickness of 3C-SiC was investigated using the visible transmission spectra and shows the degree of transparency of the 3C-SiC membranes. However, from these results, the influence of microstructure defects lowered the transmission percentage of the membranes making them unsuitable for application that require high transparency.

In this project, XPS was used to determine the elements which comprised the surface of 3C-SiC membranes. In this section, the author has confirmed the introduction of fluorine elements resulted from the use of fluorine ion plasma as the etching element for 3C-SiC. In here also, the author showed other processes such as immersing the samples in KOH solution at 70-80°C to etch Si substrate or dipping in hydrofluoric acid to remove native oxide did not introduce any new elements to the 3C-SiC membranes. This is important to understand which fabrication process which could have affected the quality of 3C-SiC as a semiconductor material suitable for electrical and biomedical devices applications.

The adhesion of metals onto the 3C-SiC thin films was tested using the common Thin Film Adhesion Test. The tests enabled the author to choose suitable metals such as Al which have a very good adhesion to make ohmic contacts for further electrical characterization of 3C-SiC.

In the electrical characterization chapter, the influence of fluorinated plasma on metal contacts/3C-SiC behavior was investigated. The author also successfully identify the influence of the contacts geometry to the ohmic behavior of the fluorinated plasma treated 3C-SiC samples. The author presented in detail the characterization of the ohmic contact Transmission Line Model (TLM) test structure parameters made using Al and Pd contacts on and off the 3C-SiC membranes. The effect of fluorinated plasma, heat treatment and the substrate thickness to the metal/3C-SiC specific contact resistance are studied and presented in detail.

Later in the chapter, the substrate effect on the electrical current pathway is studied by means of probing the metal contact/3C-SiC where the substrates were either unetched or etched to investigate the any difference of resistance due to the presence or absence of a substrate path for current. Any difference in resistance would indicate current leakage into the substrate. Further investigation was performed by measuring the sheet resistance,  $R_{sh}$  with linear TLM and comparing the  $R_{sh}$  of the metal/3C-SiC contacts which had no isolation, partial isolation and complete isolation of the substrate underneath.

The final and significant experimental chapter is the assessment of biocompatibility and hemocompatibility of 3C-SiC and the effect of the fabrication processes to them. Biocompatibility of 3C-SiC is studied by means of: 1) assessing the morphology and structure of the cells proliferated which indicates the biocompatibility of 3C-SiC using optical microscopy and Environmental Scanning Electron Microscopy (ESEM), 2) quantifying the amount of cells proliferated on the untreated and treated 3C-SiC samples, and 3) measuring the viability

percentage of the cells proliferated on 3C-SiC samples. Cell counting and cell viability percentage measurements were performed using Trypan Blue exclusion stain technique. Apart from using Trypan Blue assay to assess cell viability, the quantification was also performed using another two assays which are MTT assay and PrestoBlue™ reagent. Hemocompatibility of treated and untreated 3C-SiC (in comparison to Si) was measured by assessing their hemolytic activities.

## 1.3 Author's Achievements

The author in this project has successfully produced important results in the electrically and biocompatibility characterization of 3C-SiC. The effect of the fabrication steps on the 3C-SiC surface character is studied extensively. Throughout the author's PhD program, the following the publications were achieved:

### 1.3.1 Awards

- **N.F. Mohd Nasir**, A.S. Holland and E. Pirogova, "Silicon Carbide Thin Film Devices for Biomedical Applications", **3<sup>rd</sup> Prize** For School of Electrical and Computer Engineering Higher Degree Research (SECE HDR) Poster Competition (RMIT) [5<sup>th</sup> August 2010]
- **N.F. Mohd Nasir**, A.S. Holland, G.K. Reeves, P.W. Leech, A. Collins and P. Tanner "Specific Contact Resistance of Ni/Ti/Au Ohmic Contact to n-Type SiC Membrane", **2<sup>nd</sup> Prize** For School of Electrical and Computer Engineering (SECE) Research Day Poster Presentation (RMIT) [23<sup>rd</sup> June 2011]

### 1.3.2 Peer Reviewed Conference Proceedings Publications

- **N.F. Mohd Nasir**, A.S. Holland, G.K. Reeves, P.W. Leech, A. Collins and P. Tanner (2011). “Specific contact resistance of ohmic contacts to n-type SiC membranes”. Materials Research Society Symposium Proceedings, Volume 1335, pp. 99-104.
- **N.F. Mohd Nasir**, C.M. Shah, P.W. Leech, G.K. Reeves, E. Pirogova, T. Istivan, P. Tanner and A.S. Holland (2012). “Fabrication of 3C-Silicon Carbide Membranes: Towards Development of Novel Microdevices for Biomedical Applications”. 2012 International Conference on Biomedical Engineering (ICoBE 2012) Proceedings, pp. 589-593.
- **N.F. Mohd Nasir**, P.W. Leech, A.S. Holland, G.K. Reeves and P. Tanner (2012). “Properties of Al and Pd Contacts on n-type SiC Membranes”. MRS Online Proceedings Library, 1433 , mrss12-1433-h04-05 doi:10.1557/opl.2012.1145

### 1.3.3 Journal Papers

- **N.F. Mohd Nasir**, P.W. Leech, A.S. Holland, G.K. Reeves and P. Tanner (2012). “Al and Pd Ohmic Contacts on n-type 3C-SiC Membranes”. Applied Surface Science (Submitted).
- **N.F. Mohd Nasir**, P.W. Leech, G.K. Reeves, E. Pirogova, T. Istivan, P. Tanner and A.S. Holland (2012).”Biocompatibility and Hemocompatibility of 3C-SiC Membrane”. Biomedical Microdevices (Submitted).

## 1.4 Thesis Outline

This thesis focuses on the characterization of 3C-SiC thin films and membranes in terms of their electrical, material, biocompatibility and hemocompatibility properties. These are the major chapters listed in this thesis.

Chapter 2 describes the fabrication of 3C-SiC membranes and the material characterization methods involved in this project. The fabrication techniques used to form membranes of the 3C-SiC membranes are presented in detail.

Chapter 3 discusses the characterization of 3C-SiC thin films and membranes using visible transmission spectra, Raman spectroscopy and X-ray photoelectron spectroscopy. The studies on the effect of reactive ion etching and wet etching on the properties of 3C-SiC thin films and membranes are also highlighted here.

Chapter 4 presents the electrical characterization of 3C-SiC thin films. This chapter describes the influence of reactive ion etching influence on the current-voltage (I-V) relation of metal/3C-SiC contacts. The substrate effect on the I-V characteristics of metal/material systems is elaborated further here. The comprehensive study on ohmic contact Transmission Line Model (TLM) test structure parameters such as contact end resistance, sheet resistance and specific contact resistance of metal contacts with 3C-SiC is presented in detail also in this chapter.

Chapter 5 presents the biocompatibility characterization of 3C-SiC which includes the details of the experimental work and the results involved with the cell viability, cytotoxicity and haemocompatibility testing of 3C-SiC. Cell numbers and viability was determined by Trypan blue exclusion staining, Methylthiazolyldiphenyl-tetrazolium bromide (MTT) assay and PrestoBlue™ assay. MTT assay is a typical cytotoxicity assay and the results were compared to

the latest reagent used for cell viability investigation which is PrestoBlue™ in predicting the biocompatibility of the treated and untreated SiC. Finally, the hemolytic activities of the treated and untreated 3C-SiC against human red blood cell (hRBC) was measured by the monitoring of hemoglobin release detected by the absorbance of the supernatant.

Finally, Chapter 6 comes to the summarization of thesis and suggestions for possible future works.

## 1.5 References

- [1] B. D. P. Ee Lim Tan , Brock Horton , Ranyuan Shao , Mohammed Zourob and Keat Ghee Ong "Implantable Biosensors for Real-time Strain and Pressure Monitoring," *Sensors*, vol. 8, pp. 6396-6406, 2008.
- [2] C. Hierold, B. Clasbrumme, D. Behrend, T. Scheiter, M. Steger, K. Oppermann, H. Kapels, E. Landgraf, D. Wenzel, and D. Etuodt, "Implantable low power integrated pressure sensor system for minimal invasive telemetric patient monitoring," in *Micro Electro Mechanical Systems, 1998. MEMS 98. Proceedings., The Eleventh Annual International Workshop on*, 1998, pp. 568-573.
- [3] G. Kotzar, M. Freas, P. Abel, A. Fleischman, S. Roy, C. Zorman, J. M. Moran, and J. Melzak, "Evaluation of MEMS materials of construction for implantable medical devices," *Biomaterials*, vol. 23, pp. 2737-2750, 2002.
- [4] C. A. Zorman, "Silicon carbide as a material for biomedical microsystems," in *Design, Test, Integration & Packaging of MEMS/MOEMS, 2009. MEMS/MOEMS '09. Symposium on*, 2009, pp. 1-7.

- [5] J. Park and R. S. Lakes, *Biomaterials: An Introduction*, 3rd ed. New York: Springer, 2007.
- [6] M. Bosi, B. E. Watts, G. Attolini, C. Ferrari, C. Frigeri, G. Salviati, A. Poggi, F. Mancarella, A. Roncaglia, O. Martínez, and V. Hortelano, "Growth and characterization of 3C-SiC films for Micro Electro Mechanical Systems (MEMS) applications," *Crystal Growth and Design*, vol. 9, pp. 4852-4859, 2009.
- [7] S. Zappe, "Design, Performance and Applications of SiC MEMS," in *Silicon Carbide Microelectromechanical Systems for Harsh Environments*, R. Cheung, Ed., 1st ed London: Imperial College Press, 2006, pp. 128-164.
- [8] C. Dezaudier, N. Becourt, G. Arnaud, S. Contreras, J. L. Ponthenier, J. Camassel, J. L. Robert, J. Pascual, and C. Jaussaud, "Electrical characterization of SiC for high-temperature thermal-sensor applications," *Sensors and Actuators A: Physical*, vol. 46, pp. 71-75, 1995.
- [9] J. B. Casady and R. W. Johnson, "Status of silicon carbide (SiC) as a wide-bandgap semiconductor for high-temperature applications: A review," *Solid-State Electronics*, vol. 39, pp. 1409-1422, 1996.
- [10] W. Reichert, E. Obermeier, and J. Stoemenos, " $\beta$ -SiC films on SOI substrates for high temperature applications," *Diamond and Related Materials*, vol. 6, pp. 1448-1450, 1997.
- [11] M. Mehregany, C. A. Zorman, N. Rajan, and W. Chien Hung, "Silicon carbide MEMS for harsh environments," *Proceedings of the IEEE*, vol. 86, pp. 1594-1609, 1998.
- [12] M. Mehregany and C. A. Zorman, "SiC MEMS: Opportunities and challenges for applications in harsh environments," *Thin Solid Films*, vol. 355, pp. 518-524, 1999.



- [13] R. Cheung, "Introduction to Silicon Carbide Microelectromechanical Systems (MEMS)," in *Silicon Carbide Microelectromechanical Systems for Harsh Environments*, R. Cheung, Ed., 1st ed London: Imperial College Press, 2006, pp. 1-17.
- [14] G.-S. Chung and K.-H. Yoon, "Ohmic contacts to single-crystalline 3C-SiC films for extreme-environment MEMS applications," *Microelectronics Journal*, vol. 39, pp. 1408-1412, 2008.
- [15] L. Kolaklieva and R. Kakanakov, "Ohmic Contacts for High Power and High Temperature Microelectronics," in *Microelectronic and Mechanical Systems*, K. Takahata, Ed., 1st ed: InTech, 2009, pp. 293-318.
- [16] K.-S. Kim and G.-S. Chung, "Growth and characteristics of polycrystalline 3C-SiC films for extreme environment micro/nano-electromechanical systems," *Sensors and Actuators A: Physical*, vol. 155, pp. 125-130, 2009.
- [17] C. H. Wu, C. A. Zorman, and M. Mehregany, "Fabrication and testing of bulk micromachined silicon carbide piezoresistive pressure sensors for high temperature applications," *IEEE Sensors Journal*, vol. 6, pp. 316-323, 2006.
- [18] G. Müller, G. Krötz, and E. Niemann, "SiC for sensors and high-temperature electronics," *Sensors and Actuators A: Physical*, vol. 43, pp. 259-268, 1994.
- [19] J. Zhang, C. Carraro, R. T. Howe, and R. Maboudian, "Electrical, mechanical and metal contact properties of polycrystalline 3C-SiC films for MEMS in harsh environments," *Surface and Coatings Technology*, vol. 201, pp. 8893-8898, 2007.
- [20] T. Sugii, T. Ito, Y. Furumura, M. Doki, F. Mieno, and M. Maeda, "b-SiC/Si heterojunction bipolar transistors with high current gain," *Electron device letters*, vol. 9, pp. 87-89, 1988.

- [21] N. F. Mohd Nasir, A. S. Holland, G. K. Reeves, P. W. Leech, A. Collins, and P. Tanner, "Specific contact resistance of ohmic contacts to n-type SiC membranes," in *MRS Spring Meeting*, San Francisco, CA, 2012, pp. 99-104.
- [22] J. Camassel, "State of the art of 3C-SiC/silicon on insulators," *Journal of Vacuum Science and Technology B: Microelectronics and Nanometer Structures*, vol. 16, pp. 1648-1654, 1998.
- [23] S. Noh, X. Fu, L. Chen, and M. Mehregany, "Deposition and properties of polycrystalline & b-SiC films using LPCVD with different dopant amount," *Electronics Letters*, vol. 42, pp. 775-777, 2006.
- [24] M. B. J. Wijesundara, D. Gao, C. Carraro, R. T. Howe, and R. Maboudian, "Nitrogen doping of polycrystalline 3C-SiC films grown using 1,3-disilabutane in a conventional LPCVD reactor," *Journal of Crystal Growth*, vol. 259, pp. 18-25, 2003.
- [25] A. E. Bazin, J. F. Michaud, F. Cayrel, M. Portail, T. Chassagne, M. Zielinski, E. Collard, and D. Alquier, "High Quality Ohmic Contacts on n-type 3C-SiC Obtained by High and Low Process Temperature," *AIP Conference Proceedings*, vol. 1292, pp. 51-54, 2010.
- [26] C. Jacob, P. Pirouz, H. I. Kuo, and M. Mehregany, "High temperature ohmic contacts to 3C-silicon carbide films," *Solid-State Electronics*, vol. 42, pp. 2329-2334, 1998.
- [27] G. Constantinidis, N. Kornilios, K. Zekentes, J. Stoemenos, and L. di. Cioccio, "High temperature ohmic contacts to 3C-SiC grown on Si substrates by chemical vapor deposition," *Materials Science and Engineering: B*, vol. 46, pp. 176-179, 1997.
- [28] J. Wan, M. A. Capano, and M. R. Melloch, "Formation of low resistivity ohmic contacts to n-type 3C-SiC," *Solid-State Electronics*, vol. 46, pp. 1227-1230, 2002.

- [29] A. J. Rosenbloom, D. M. Sipe, Y. Shishkin, Y. Ke, R. P. Devaty, and W. J. Choyke, "Nanoporous SiC: A candidate semi-permeable material for biomedical applications," *Biomedical Microdevices*, vol. 6, pp. 261-267, 2004.
- [30] R. Gómez, A. Ivorra, R. Villa, P. Godignon, J. Millán, I. Erill, A. Solà, G. Hotter, and L. Palacios, "A SiC microdevice for the minimally invasive monitoring of ischemia in living tissues," *Biomedical Microdevices*, vol. 8, pp. 43-49, 2006.
- [31] G. Gabriel, I. Erill, J. Caro, R. Gómez, D. Riera, R. Villa, and P. Godignon, "Manufacturing and full characterization of silicon carbide-based multi-sensor micro-probes for biomedical applications," *Microelectronics Journal*, vol. 38, pp. 406-415, 2007.
- [32] C. Iliescu, B. Chen, D. P. Poenar, and Y. Y. Lee, "PECVD amorphous silicon carbide membranes for cell culturing," *Sensors and Actuators, B: Chemical*, vol. 129, pp. 404-411, 2008.
- [33] G. Mani, M. D. Feldman, D. Patel, and C. M. Agrawal, "Coronary stents: A materials perspective," *Biomaterials*, vol. 28, pp. 1689-1710, 2007.
- [34] U. Kalnins, A. Erglis, I. Dinne, I. Kumsars, and S. Jegere, "Clinical outcomes of silicon carbide coated stents in patients with coronary artery disease," *Medical Science Monitor*, vol. 8, pp. PI16-PI20, 2002.
- [35] L. F. L. Tanajura, J. E. M. R. Sousa, A. G. M. R. Sousa, A. Abizaid, J. E. T. Paula, M. Albertal, F. Feres, L. A. P. Mattos, R. Staico, and I. M. F. Pinto, "Estudo prospectivo e randomizado de pacientes tratados com e sem stents revestidos com carbeto de silício amorfo para a prevenção da reestenose coronariana. Avaliação ultra-sonográfica," *Arquivos Brasileiros de Cardiologia*, vol. 83, pp. 59-63, 2004.

- [36] J. M. Anderson and J. J. Langone, "Issues and perspectives on the biocompatibility and immunotoxicity evaluation of implanted controlled release systems," *Journal of Controlled Release*, vol. 57, pp. 107-113, 1999.
- [37] C. Coletti, M. J. Jaroszeski, A. M. Hoff, and S. E. Saddow, "Culture of mammalian cells on single crystal SiC substrates," 2006, pp. 46-51.
- [38] C. Coletti, M. J. Jaroszeski, A. Pallaoro, A. M. Hoff, S. Iannotta, and S. E. Saddow, "Biocompatibility and wettability of crystalline SiC and Si surfaces," Lyon, 2007, pp. 5849-5852.
- [39] C. L. Frewin, M. Jaroszeski, E. Weeber, K. E. Muffly, A. Kumar, M. Peters, A. Oliveros, and S. E. Saddow, "Atomic force microscopy analysis of central nervous system cell morphology on silicon carbide and diamond substrates," *Journal of Molecular Recognition*, vol. 22, pp. 380-388, 2009.
- [40] S. E. Saddow, C. L. Frewin, C. Coletti, N. Schettini, E. Weeber, A. Oliveros, and M. Jarosezski, "Single-crystal silicon carbide: A biocompatible and hemocompatible semiconductor for advanced biomedical applications," vol. 679-680, ed. Oslo, 2011, pp. 824-830.
- [41] C. L. Frewin, C. Locke, S. E. Saddow, and E. J. Weeber, "Single-crystal cubic silicon carbide: An in vivo biocompatible semiconductor for brain machine interface devices," in *Engineering in Medicine and Biology Society, EMBC, 2011 Annual International Conference of the IEEE*, 2011, pp. 2957-2960.
- [42] T. Taubner, D. Korobkin, Y. Urzhumov, G. Shvets, and R. Hillenbrand, "Near-field microscopy through a SiC superlens," *Science*, vol. 313, p. 1595, 2006.

- [43] N. Basak, G. L. Harris, J. Griffin, and K. D. Wise, "Bio-compatible micro-sensor for blood pressure measurement using SiC technology," in *2008 MRS Fall Meeting*, Boston, 2009, pp. 193-197.
- [44] M. J. J. Norelli Schettini, Leigh West and Stephen E. Sadow, "Hemocompatibility Assessment of 3C-SiC for Cardiovascular Applications," in *Silicon Carbide Biotechnology: A Biocompatible Semiconductor for Advanced Biomedical Devices and Applications* S. E. Sadow, Ed., ed Amsterdam: Elsevier, 2011, pp. 153-208.
- [45] I. Cimalla, F. Will, K. Tonisch, M. Niebelschütz, V. Cimalla, V. Lebedev, G. Kittler, M. Himmerlich, S. Krischok, J. A. Schaefer, M. Gebinoga, A. Schober, T. Friedrich, and O. Ambacher, "AlGaN/GaN biosensor—effect of device processing steps on the surface properties and biocompatibility," *Sensors and Actuators B: Chemical*, vol. 123, pp. 740-748, 2007.
- [46] T. Doerge, S. Kammer, M. Hanauer, A. Sossalla, and S. Steltenkamp, "Novel method for a flexible double sided microelectrode fabrication process," 2009.
- [47] L. Wang, S. Dimitrijević, J. Han, A. Iacopi, L. Hold, P. Tanner, and H. B. Harrison, "Growth of 3C-SiC on 150-mm Si(100) substrates by alternating supply epitaxy at 1000 °C," *Thin Solid Films*, vol. 519, pp. 6443-6446, 2011.
- [48] L. Wang, S. Dimitrijević, J. Han, P. Tanner, A. Iacopi, and L. Hold, "Demonstration of p-type 3CSiC grown on 150 mm Si(1 0 0) substrates by atomic-layer epitaxy at 1000 °C," *Journal of Crystal Growth*, vol. 329, pp. 67-70, 2011.

# Chapter 2

## Fabrication of 3C-Silicon Carbide Membranes

This chapter reports on the comprehensive fabrication method of 3C-SiC membranes. The epitaxial layers of n-type 3C-SiC films were grown to thicknesses of 0.25 to 1.25  $\mu\text{m}$  on substrates of low doped p-Si  $\langle 100 \rangle$  substrates with a resistivity of 1-20  $\Omega\cdot\text{m}$ . Growth of the SiC was performed using a hot wall low pressure chemical vapour deposition (LPCVD) reactor at the Queensland Microtechnology Facility, Griffith University. The horizontal reactor uses a method of alternating 3 supply epitaxy (ASE) at 1000  $^{\circ}\text{C}$  with pure  $\text{SiH}_4$  and  $\text{C}_2\text{H}_2$  as precursors to produce single crystal films of n-type 3C-SiC [1, 2]. The films of SiC were deposited simultaneously on both sides of a Si wafer (650  $\mu\text{m}$  thick). The resistivity of the films was measured in the range 0.04-0.35  $\Omega\cdot\text{cm}$  for the different wafers by the four-point probe technique. The carrier concentration in the SiC films was measured by hot probe as  $1 \times$

$10^{19}$  to  $7 \times 10^{19} \text{ cm}^{-3}$ . A 3C-SiC suspended membrane on Si has the advantage (compared to a Si membrane) of not requiring an additional layer to act as an etch stop layer when using KOH to etch the Si (membrane carrying substrate) [3]. A standard procedure to produce 3C-SiC membrane would enable a consistent quality and quantity of the SiC membrane material to be investigated materially, electrically and biologically for future applications.

## 2.1 Experimental

### 2.1.1 Photolithography

3C-SiC wafers were diced into rectangular pieces of  $15 \times 20 \text{ mm}^2$  and cleaned with acetone, isopropyl alcohol (or methanol) and deionized water and were dried using a jet stream of nitrogen. Moisture was further removed by baking the samples at  $110^\circ\text{C}$  for 10 minutes. On the backside of each piece of wafer, an array of squares ( $5 \times 5 \text{ mm}^2$ ) and rectangles ( $10 \times 15 \text{ mm}^2$ ) were photolithographically patterned with a layer of AZ4562 (AZ Electronic Materials) photoresist. AZ 4562 was chosen due to its ability to form relatively thick photoresist layers [4].

The photolithography technique established to form the etch pattern for Si removal is described below:

- Hexamethyldisilazane (HMDS) (Sigma-Aldrich) was spin-coated on the wafer backside at the speed of 500 rpm with the acceleration at 100 rpm/s for 5 seconds. HMDS is used to promote better adhesion of photoresist on the substrate by reducing the surface tension of materials [5].

- AZ 4562 photoresist was spin coated after the HMDS was applied. This is initially performed at the speed of 500 rpm with the acceleration at 100 rpm/s for 5 seconds to evenly coat the sample with the photoresist. The actual spinning of AZ 4562 took place with the speed of 2000 rpm, acceleration of 300 rpm/s for 15 s to form an approximately 7  $\mu\text{m}$  thick layer. This thickness could withstand plasma etching as previously reported [6].

Throughout this Ph.D. program, a photoresist layer of  $\sim 7$   $\mu\text{m}$  thickness was constantly formed using AZ 4562 with this recipe. This thickness is suitable for use as the epitaxial 3C-SiC reactive ion etching mask which exposes a window on the backside for Si removal.

After applying the photoresist, the samples were baked in an oven at 90°C for 20 minutes. The photolithographic patterning of the photoresist was performed by exposing the samples to the ultra violet (UV) light for 48 seconds. The development of the pattern was made with AZ400K (AZ Electronic Materials) (1:3 dilution) and the developing time took approximately 1 minute [7]. Then, the samples were post exposure baked in an oven at 110°C for 60 minutes to harden the photoresist and avoid degassing during RIE [8]. The temperature chosen for hardbaking AZ4562 should not exceed 120°C to avoid possible cracking of the photoresist [9]. A series of profilometry traces was conducted to ensure the thickness of the photoresist on the sample was 7  $\mu\text{m}$ . The profilometer system used was an Ambios Technology XP-2 surface profiler and the software version used was *Advanced Stylus Profiling System version 5.5*.



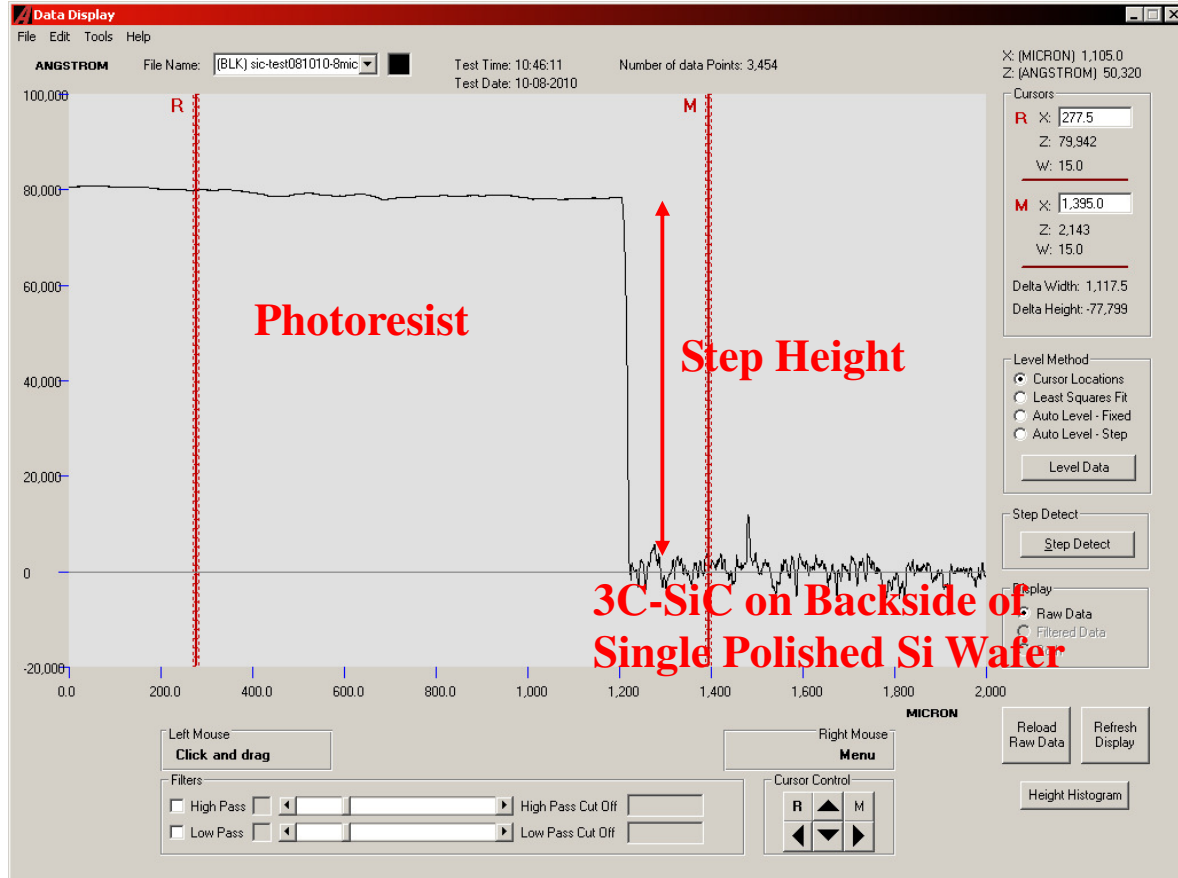


Figure 2.1: A profilometry showing a step height measured from differences of the surface of 3C-SiC and the photoresist. The thickness of the photoresist was about 7.8  $\mu\text{m}$ .

## 2.1.2 Reactive Ion Etching

The etching was carried out on photolithographically patterned samples using a RIE 200W (Plasma Sciences Inc.) etching system. Several other gasses such as  $\text{SF}_6$ ,  $\text{NF}_3$ ,  $\text{CBrF}_3$ , and  $\text{CHF}_3$  had been used effectively to etch SiC [10]. The gas chosen for etching ‘windows’ in the SiC on the backside (in order to allow subsequent wet etching of the Si) in the early stage of the project was pure tetrachloromethane ( $\text{CF}_4$ ). The etching condition used for  $\text{CF}_4$  gas was 22 sccm total flow of with a base pressure ranging from 73 to 86 mTorr and the RF power

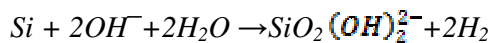
applied was 100W. A series of etching experiments were conducted with durations of 15 to 65 minutes to determine the etch rate.

Later, a mixture of CF<sub>4</sub> and oxygen (O<sub>2</sub>) was used as the etching gas to enhance the etching rate. The reason for using this mixture was due to the deposition of thick fluorocarbon compounds on the 3C-SiC surface using CF<sub>4</sub> as the etching gas by itself [11, 12]. This impurity is suggested to affect the quality of ohmic contacts to 3C-SiC [11, 12]. Thus, by mixing oxygen with CF<sub>4</sub> this would clean the surface from the carbon rich layer [11, 12]. The total flow of CF<sub>4</sub>/O<sub>2</sub> mixture used as the etchant was 14.1/4.7 sccm which was approximately 3 to 1 ratio. Padiyath et al. discovered that the highest etching rate for single crystal 3C-SiC occurred approximately at 33% of O<sub>2</sub> concentration of the CF<sub>4</sub>/O<sub>2</sub> mixture and by using the mixture it could enhance the etching rate of 3C-SiC [13].

### 2.1.3 Wet Etching of Si in KOH

Anisotropic wet etching of Si using potassium hydroxide (KOH) was used to remove Si and finally reveal the 3C-SiC membrane. The SiC coating is an excellent etch mask for KOH etching of Si. SiC is inert to almost all etching solutions except in phosphoric acid at 215°C and alkaline solutions of K<sub>3</sub>Fe(CN)<sub>6</sub> used at temperature higher than 100°C [14].

In this reaction, Si reacts with the hydroxide ions coming from potassium hydroxide and water to produce hydrogen oxides and hydrogen gasses. Thus, the gross chemical reaction of potassium hydroxide and Si can be represented by this formula [15]:



The samples were rinsed and cleaned using acetone to remove the photoresist used in the previous step. A solution of potassium hydroxide (KOH) 45 wt% (at 70°C and later, 80°C) in water was used to etch the silicon (Figure 2.2 (a)). During the wet etching of Si substrates,

vigorous hydrogen bubbles were produced. If the sample was not properly held as it was suspended, the samples had the tendency to flip. This would expose the unetched 3C-SiC to the KOH solution instead the etched side and this had prolonged the etching time. Several improvements in samples fixation techniques in KOH solution were performed to achieve this mean.

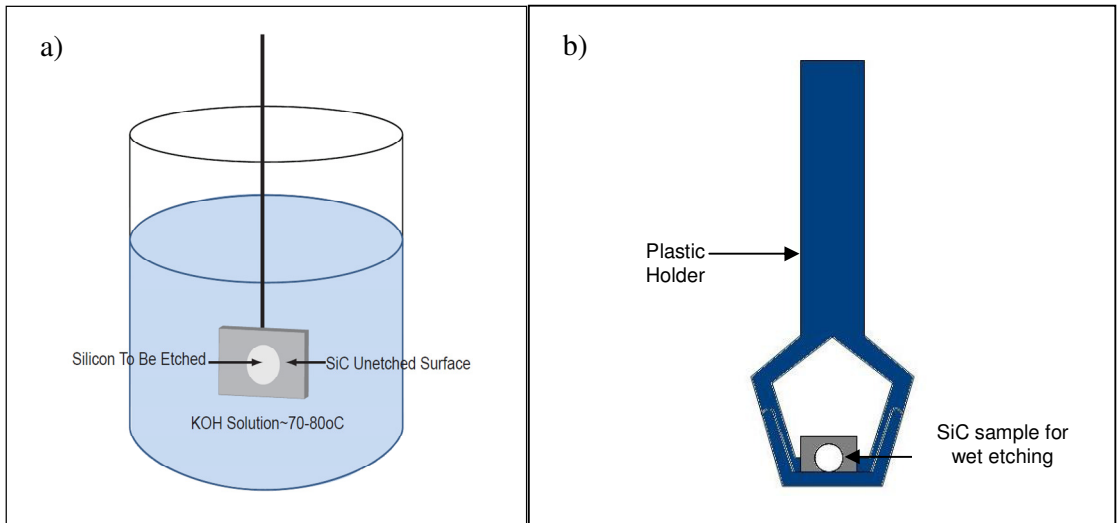


Figure 2.2: a) KOH Etching of a Si substrate coated with SiC. The RIE etched window pattern in the SiC film on the backside of the Si substrate allows etching of the Si in the KOH solution. (SiC is highly resistive to KOH etching and therefore is an excellent etch mask material for silicon etching) b) In this early version of experimental set up, a 3C-SiC etched with RIE was suspended with a plastic holder in the KOH solution for wet etching.

In an early version of the experimental set up (Figure 2.2 (b)) , a 3C-SiC sample etched with RIE was held in the groove of a plastic holder and dipped into a heated KOH solution. The sample was etched without agitation. However, without fixing the sample to the holder, the sample tended to dislocate and flipped to the side of polished side of the sample which was not etched. This contributed to extending the duration of etching time.

A simple solution was used to improve the etching duration. Thus, to fix the sample in steady position for better etching rate, the samples were fixed to the bottom of a beaker or at

the holder by using tape (Figure 2.3). Masking tape was preferred than the duct tape or cellophane since the latters were easily peeled off during wet etching. However, membranes were easily broken while the tape was removed from the samples.

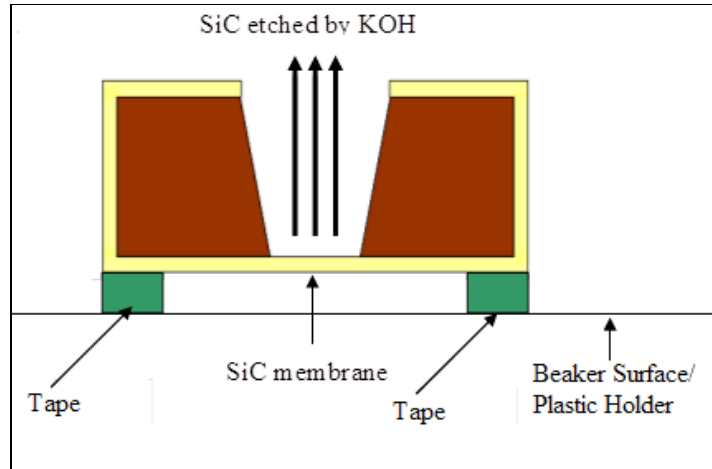


Figure 2.3: 3C-SiC samples were taped at the bottom of the beaker or holder to ensure KOH can react with SiC throughout the etching period.

The final improvement made was by just placing onto a plastic holder and put another plastic holder onto the former and dipped into the KOH solution at 80°C as shown in Figure 2.4. This simple solution was proven to be better than the previous method since the samples were contained and did not flip. The possibility of breaking the membranes was also reduced since no extra force was required to remove the samples from their holders. This method reduced the etching time of Si substrates while ensuring the membrane continued to stay intact on the sample.

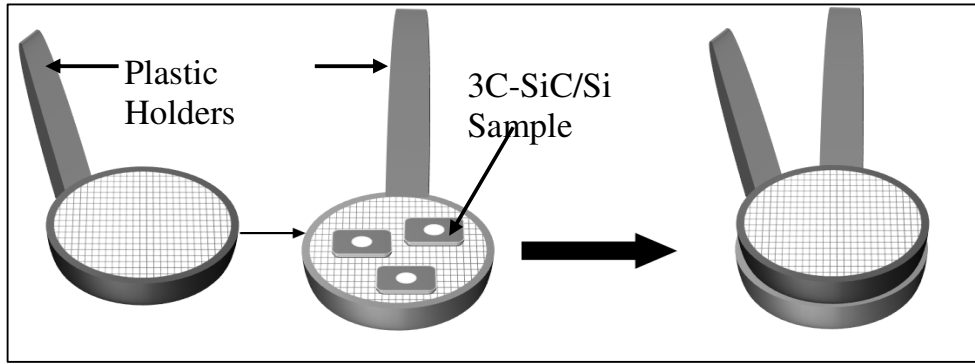


Figure 2.4: Each 3C-SiC sample was put in a plastic holder and covered by another plastic holder to ensure KOH can react with SiC through out the etching period.

Figure 2.5 summarizes the fabrication sequence involved in producing a 3C-SiC membrane that was used for this PhD Program.

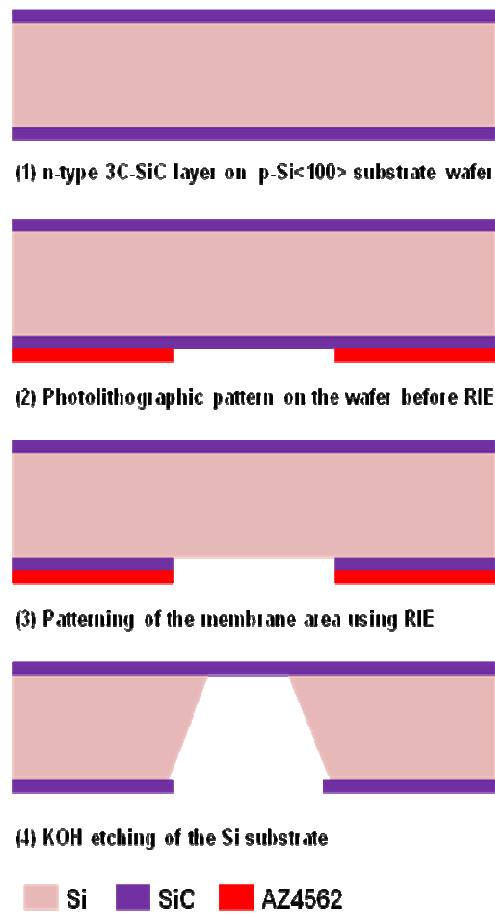


Figure 2.5: Schematic illustration of 3C-SiC membrane fabrication process

## 2.2 Results and Discussions

### 2.2.1 Reactive Ion Etching

Figure 2.6 shows the linear behaviour for the etch rate of the SiC using 22 sccm total flow of tetrachloromethane ( $\text{CF}_4$ ) and an RF power of 100W. It was found that the time used to completely etch the 0.95  $\mu\text{m}$  n-type 3C-SiC layer was 65 minutes. The etching time for the 1.18  $\mu\text{m}$  was 100 minutes but the duration was reduced to 70 minutes by using  $\text{CF}_4/\text{O}_2$  gas mixtures. The reactive ion etching processes were reproducible using the same thickness of 3C-SiC and the RIE conditions.

By using the etch rate established with the 0.95  $\mu\text{m}$  3C-SiC layer, the thinner 3C-SiC layer (0.285  $\mu\text{m}$ ) was etched patterned for 25 minutes either using  $\text{CF}_4$  or  $\text{CF}_4/\text{O}_2$  gasses. Wet etching of the Si using KOH was later performed on the RIE etched samples. The existence of 3C-SiC films served as an excellent mask for the Si etching in KOH solution and the complete etching of the removed area of 3C-SiC shows that reactive ion etching had been successfully implemented for both samples with different 3C-SiC thicknesses.

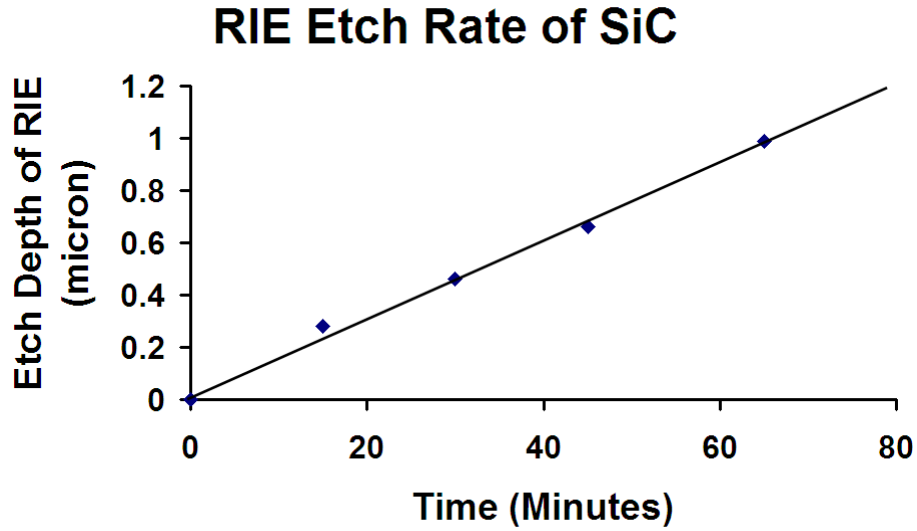


Figure 2.6: The etch rate of 3C-silicon carbide using Reactive Ion Etching ( $\text{CF}_4$ , 22 sccm, 80 mTorr, and 100W)

### 2.2.2 Wet Etching of Si in KOH



Figure 2.7: The final produce of the wet etching using different masks a) double circular mask b) square mask and c) rectangular

In the preliminary stage, 3C-SiC membranes were produced after 63 hours of wet etching of  $650 \mu\text{m}$  ( $0.172 \mu\text{m}/\text{min}$ ) at  $70^\circ\text{C}$  using different shapes of masks. Si substrate exposed to the KOH solution was completely removed leaving a cavity with a 3C-SiC membrane. The etched windows for each of the samples revealed similar pattern compared to the end result predicted by simulation performed by ACES software (Refer Appendix 1). Square and

rectangular shaped membranes as shown in previous study were made through this method. In this study, it is also proven that circular masks do produce square like shapes.

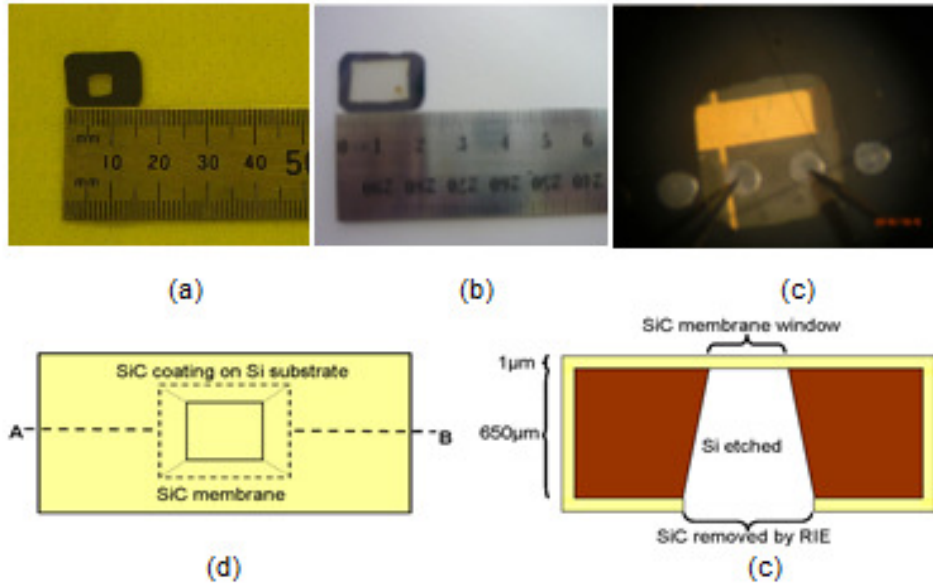


Figure 2.8: (a)  $0.5 \times 0.5 \text{ cm}^2$  3C-SiC membrane ( $0.95 \mu\text{m}$  thick) structure produced after 63 hours of KOH etching of Si ( $650 \mu\text{m}$  thick substrate). (b)  $1.5 \times 1.0 \text{ cm}^2$  3C-SiC membrane ( $0.95 \mu\text{m}$  thick) structure produced after 63 hours of KOH etching of Si ( $650 \mu\text{m}$  thick substrate). (c) Probing of two aluminum contacts on the intact membrane (arbitrary metal tracks can be seen below the SiC membrane). (d) Schematic diagram of SiC membrane structure. (e) Cross section schematic showing the etched Si layer and the SiC membrane window.

In this fabrication step, membranes with area of  $0.5 \times 0.5 \text{ cm}^2$  and  $1.5 \times 1.0 \text{ cm}^2$  were produced using  $0.95 \mu\text{m}$  thick 3C-SiC (Figure 2.8 (a)-(e)). Further work can be performed using this membrane since it was able to withstand standard processes in microfabrication. The  $0.95 \mu\text{m}$  membrane could be cleaned with a stream of nitrogen gas and subsequently, Al ( $300 \text{ nm}$ ) contacts were deposited on the membrane surface using electron beam evaporation without the membranes breaking. Photoresist could be spin coated onto the samples with 3C-SiC membranes at  $2000 \text{ rpm}$  and they could be furnace heated to  $1000^\circ\text{C}$  without any change. The same membranes were able to withstand the small force exerted by a micromanipulator probe and flexed during a standard electrical characterization session (Fig. 2.8 (c)).



Later, the temperature used in the wet etching of Si was increased to 80°C. When the KOH solution was at 70°C, the 650 μm Si substrates took 63 hours to etch. Increasing the temperature to 80°C had enhanced the etching time. However, apart from this factor, the better exposure of the unmasked Si substrate also played an important role to reduce the etching time. Wet etching procedure could be improved by continuously suspending the SiC sample in the KOH solution so the reaction could happen on the etched surface. The sample should not flip due to the bubbles produced during the etching. The etching surface was in a fixed position suspended in the KOH solution throughout the etching process. This factor and the increased KOH temperature contributed to reduce the etching time.

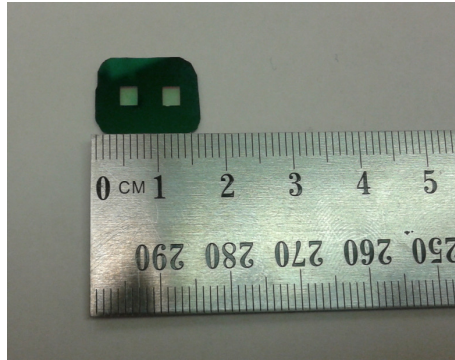


Figure 2.9: A membrane structure in 0.285 μm 3C-SiC produced over an area of 0.5×0.5cm<sup>2</sup> by 28 hours of KOH etching at 80°C.

The optimized conditions for the wet etching was subsequently used to form 0.285 μm 3C-SiC membranes and for the rest of the 3C-SiC membranes fabrication throughout this project. This exercise was intended to observe the ability of the thin membrane to endure typical fabrication techniques. Fabrication of thin 3C-SiC membranes from 20 nm to 400 nm was reported previously [16-18]. However, the area of the membrane produced were far smaller which were in range between 8 μm × 20 μm to 500 μm × 38.5 μm [16-18] compared to the membranes fabricated here which are 5000 μm × 5000 μm.

## 2.3 Conclusion

The fabrication of large membrane structures in 3C-SiC/Si has been reproducibly demonstrated using standard microfabrication techniques such as photolithography, reactive ion etching and chemical wet etching of Si substrate. Simulation was performed before the processes began, and the results from the wet etching were similar to the simulations. The wet etching of circular patterns made on Si substrate produced a square-like shape window. The method which was developed was able to produce 3C-SiC membranes with thicknesses of 1.18  $\mu\text{m}$ , 0.95  $\mu\text{m}$  and 0.285  $\mu\text{m}$ . The membranes were produced over an area of 0.5 $\times$ 0.5  $\text{cm}^2$  and 1.5 $\times$ 1.0  $\text{cm}^2$  without breaking after fabrication. Hence, the possibility of fabricating a thin membrane less than a third of a micron in thickness with relatively larger area was readily achieved. The thicker membranes were capable of being probed and flexed without breaking. Metal deposition, photoresist application and furnace heating were performed with success on these membranes. This finding is of particular importance as it reveals that the studied membrane can withstand small forces, for example, which is an essential element for blood pressure sensing application in blood stream. Deposition of metals and pattern transfer using standard photolithography processes can be achieved with this membrane, hence making it suitable for utilization in biomedical microdevices in the future, e.g. as a working structure for blood pressure sensing applications as propose by Basak et al. [19].

## 2.4 References

- [1] L. Wang, S. Dimitrijević, J. Han, A. Iacopi, L. Hold, P. Tanner, and H. B. Harrison, "Growth of 3C-SiC on 150-mm Si(100) substrates by alternating supply epitaxy at 1000 °C," *Thin Solid Films*, vol. 519, pp. 6443-6446, 2011.
- [2] L. Wang, S. Dimitrijević, J. Han, P. Tanner, A. Iacopi, and L. Hold, "Demonstration of p-type 3C-SiC grown on 150 mm Si(1 0 0) substrates by atomic-layer epitaxy at 1000 °C," *Journal of Crystal Growth*, vol. 329, pp. 67-70, 2011.
- [3] C. A. Zorman and R. J. Parro, "Micro- and nanomechanical structures for silicon carbide MEMS and NEMS," *physica status solidi (b)*, vol. 245, pp. 1404-1424, 2008.
- [4] C. Linder, T. Tschan, and N. F. de Rooij, "Deep dry etching techniques as a new IC compatible tool for silicon micromachining," 1991, pp. 524-527.
- [5] J. Bauer, G. Drescher, and M. Illig, "Surface tension, adhesion and wetting of materials for photolithographic process," *Journal of Vacuum Science & Technology B: Microelectronics and Nanometer Structures*, vol. 14, pp. 2485-2492, 1996.
- [6] T. Akiyama, D. Briand, and N. F. de Rooij, "Piezoresistive n-type 4H-SiC pressure sensor with membrane formed by mechanical milling," in *Sensors, 2011 IEEE*, 2011, pp. 222-225.
- [7] A. v. Pfeil, B. Messerschmidt, V. Blümel, U. Possner, and T. Possner, "Making Fast Cylindrical Gradient-Index Lenses Diffraction Limited by Using a Wave-Front-Correction Element," *Appl. Opt.*, vol. 37, pp. 5211-5215, 1998.
- [8] P. F. Indermühle, S. Roth, L. Dellmann, and N. F. d. Rooij, "Wafer- and piece-wise Si tip transfer technologies for applications in scanning probe microscopy," *Journal of Microelectromechanical Systems*, vol. 8, p. 65, 1999.

- [9] Q. Wenmin, C. Wenzel, A. Jahn, and D. Zeidler, "UV-LIGA: a promising and low-cost variant for microsystem technology," in *Optoelectronic and Microelectronic Materials Devices, 1998. Proceedings. 1998 Conference on*, 1998, pp. 380-383.
- [10] P. H. Yih, V. Saxena, and A. J. Steckl, "A review of SiC reactive ion etching in fluorinated plasmas," *Physica Status Solidi (B) Basic Research*, vol. 202, pp. 605-624, 1997.
- [11] J. W. Palmour, "Dry etching of silicon carbide," United States of America Patent 4981551, 1 January 1991, 1991.
- [12] J. W. Palmour, R. F. Davis, T. M. Walleit, and K. B. Bhasin, "Dry etching of  $\beta$ -SiC in  $\text{CF}_4$  and  $\text{CF}_4+\text{O}_2$  mixtures," *Journal of Vacuum Science & Technology A: Vacuum, Surfaces, and Films*, vol. 4, pp. 590-593, 1986.
- [13] R. Padiyath, R. L. Wright, M. I. Chaudhry, and S. V. Babu, "Reactive ion etching of monocrystalline, polycrystalline, and amorphous silicon carbide in  $\text{CF}_4/\text{O}_2$  mixtures," *Applied Physics Letters*, vol. 58, pp. 1053-1055, 1991.
- [14] D. Zhuang and J. H. Edgar, "Wet etching of GaN, AlN, and SiC: A review," *Materials Science and Engineering R: Reports*, vol. 48, 2005.
- [15] H. Seidel, L. Csepregi, A. Heuberger, and H. Baumgaertel, "Anisotropic etching of crystalline silicon in alkaline solutions. I. Orientation dependence and behavior of passivation layers," *Journal of the Electrochemical Society*, vol. 137, pp. 3612-3626, 1990.
- [16] W. Zhou, J. Yang, G. Sun, X. Liu, F. Yang, and J. Li, "Fracture properties of silicon carbide thin films by bulge test of long rectangular membrane," *Journal of Microelectromechanical Systems*, vol. 17, pp. 453-461, 2008.
- [17] W. Zhou, J. Yang, G. Sun, X. Liu, F. Yang, and J. Li, "Fracture properties of silicon carbide thin films characterized by bulge test of long membranes," 2008, pp. 557-560.

- [18] H. T. M. Pham, C. Fan, G. Pandraud, F. Creemer, P. M. Sarro, N. M. Van der Pers, P. Visser, and K. Kwakernaak, "Very thin SiC membranes for micromachined vacuum sensors," in *Sensors, 2008 IEEE*, 2008, pp. 1143-1146.
- [19] N. Basak, G. L. Harris, J. Griffin, and K. D. Wise, "Bio-compatible micro-sensor for blood pressure measurement using SiC technology," in *2008 MRS Fall Meeting*, Boston, 2009, pp. 193-197.

# **Chapter 3**

## **Material Characterization of 3C-Silicon Carbide Membranes**

This chapter presents results from materials characterization of 3C-SiC (including membranes of 3C-SiC) by Scanning Electron Microscopy, Raman Spectroscopy, Visible Transmission Spectra, X-Ray Photoelectron Spectroscopy techniques and Thin Film Adhesion Test.

## **3.1 Experimental**

### **3.1.1 Scanning Electron Microscopy (SEM)**

SEM micrographs of 3C-SiC membranes and the Si interfaces were taken using a Philips XL30, using 30 kV beam voltage and spot size of 5. 3C-SiC membranes were prepared by standard photolithography, reactive ion etching (RIE) and potassium hydroxide (KOH) etching. Reactive ion etching ( $\text{CF}_4$ , 22 sccm, 80 mTorr, 100W, 65 minutes) was used to remove 3C-SiC. KOH etching (80°C, 28 hours) was performed to removed Si<100> to form 3C-SiC membranes.

### **3.1.2 Raman Spectroscopy**

Raman measurements were performed at room temperature on a Renishaw RM1000 micro-Raman spectrometer with a 514.5 nm line from an argon ion laser excitation source. Measurements were performed with 9 mW of laser power and 20 s integration times. The laser was focused down to a spot size of  $\sim 2 \mu\text{m}$  in diameter. 3C-SiC membranes and 3C-SiC/Si samples used in this experiment were prepared as in section 3.1.1.

### **3.1.3 Visible Transmission Spectra**

The visible transmission spectra of 3C-SiC membranes with thickness of 0.285  $\mu\text{m}$ , 0.95  $\mu\text{m}$  and 1.18  $\mu\text{m}$  were examined using a Micropack DH-2000 UV-VIS-NIR light source and an Oceanoptics HR4000 spectrophotometer connected to a personal computer via a USB cable. The analysis was performed using Spectrasuite 2007 edition software. The transmission spectra of 3C-SiC was compared to air as reference. 3C-SiC membranes used in this experiment were prepared as in section 3.1.1.

### **3.1.4 X-Ray Photoelectron Spectroscopy (XPS)**

X-Ray Photoelectron Spectroscopy on 0.285  $\mu\text{m}$  and 0.95 $\mu\text{m}$  thick 3C-SiC was carried out using a VG Instruments Model 310 Auger/XPS spectrometer. Three types of samples were prepared for this characterization procedure: 1) as-supplied 3C-SiC/Si samples, 2) 3C-SiC samples treated with potassium hydroxide (KOH) for 28 hours at 80°C; 3) 3C-SiC samples treated both with reactive ion etching (RIE) and KOH etching. These samples were etched by RIE with a base pressure at 80 mTorr and the RF power applied was 100W for 5 minutes using 22 sccm of  $\text{CF}_4$ . Later, the samples were immersed in KOH at 80°C for 28 hours. All the samples were dipped in hydrofluoric acid (HF) for 30 seconds to remove any native oxide [1] prior to XPS characterization.

### **3.1.5 Thin Film Adhesion Test**

This is a simple functionality test which is used to determine the quality of the adhesion of metals deposited on the 3C-SiC. It is a good test to determine poor adhesion of a metal contact [2]. This method is also known as the Scotch Tape test [2] because tape is put across the film surface (deposited earlier on 3C-SiC) and it is removed dramatically from the surface. If the metal continues to adhere on the material without sticking to the tape, this means the metal has good adhesion on the material's surface. This test is important since it shows if the metal chosen for the purpose of electrical characterization and future device fabrication is suitable. Prior to metal deposition, 3C-SiC samples were dipped in hydrofluoric acid (HF) for 30 seconds and subsequently cleaned using acetone, isopropanol (IPA) and distilled water and oven dried at 110°C for 5 minutes to remove any remaining moisture.



The metals were deposited on 3C-SiC/Si using electron beam evaporation using Balzers BAK500 electron beam evaporator or Kurt J. Lesker PVD75 electron beam evaporator. The samples were characterized as it is without annealing or any other treatment applied to the metal contacts/substrate.

### 3.2 Scanning Electron Microscopy

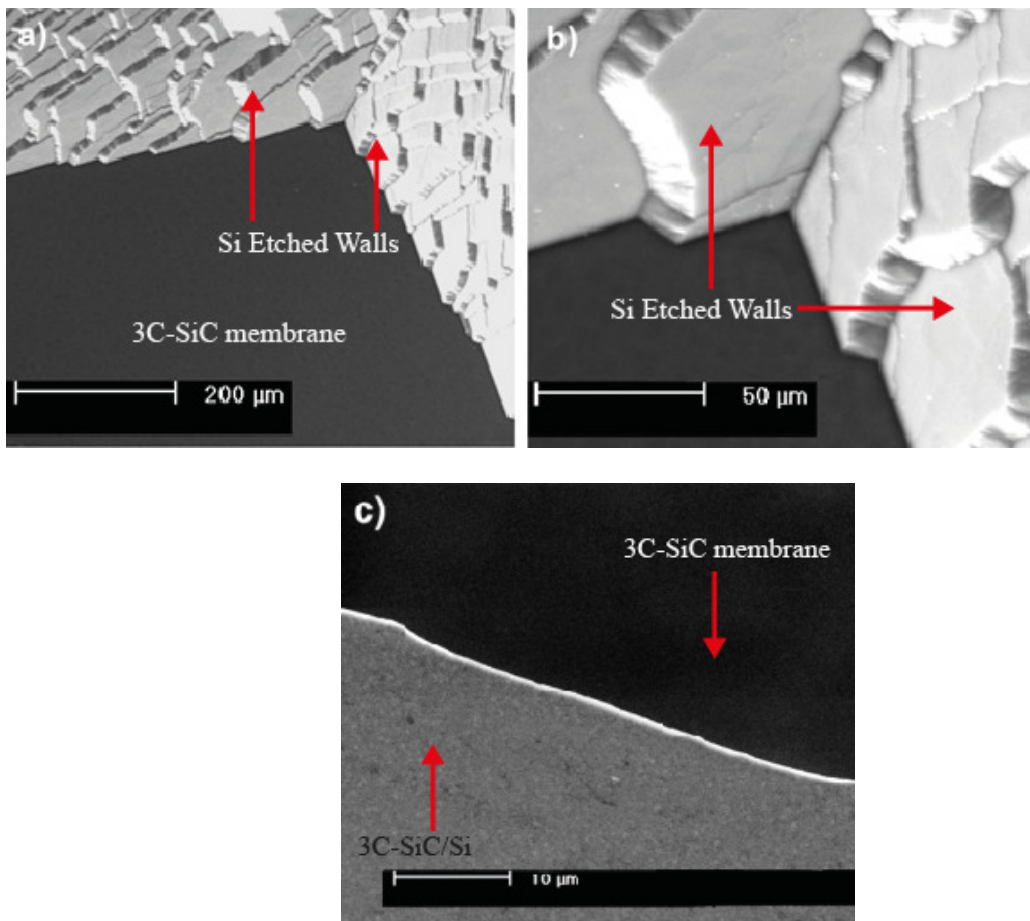


Figure 3.1: Scanning electron micrographs showing the backside of a membrane at a magnification of a) 200× b) 1000× and c) 4000×.

Figure 3.1 (a) (b) and (c) show successively increasing magnification views of the back-surface of a membrane structure after etching in a heated KOH solution. In these SEM

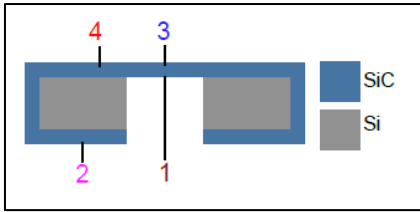
micrographs, the surface of the 3C-SiC layer (dark grey area) was typically very smooth and exhibited an abrupt interface with the etched side-walls of Si which were  $\langle 111 \rangle$  planes.

Etching in KOH solution selectively removed the exposed single crystal Si  $\langle 100 \rangle$  and  $\langle 110 \rangle$  planes within the patterned window region without any roughening of the 3C-SiC film. The KOH etching rate of Si $\langle 111 \rangle$  is hundreds of times slower than the etching rate of other types of planes in single crystal silicon [3, 4]. This enabled the formation of a cavity with well-defined sidewalls while releasing the suspended 3C-SiC membrane structure.

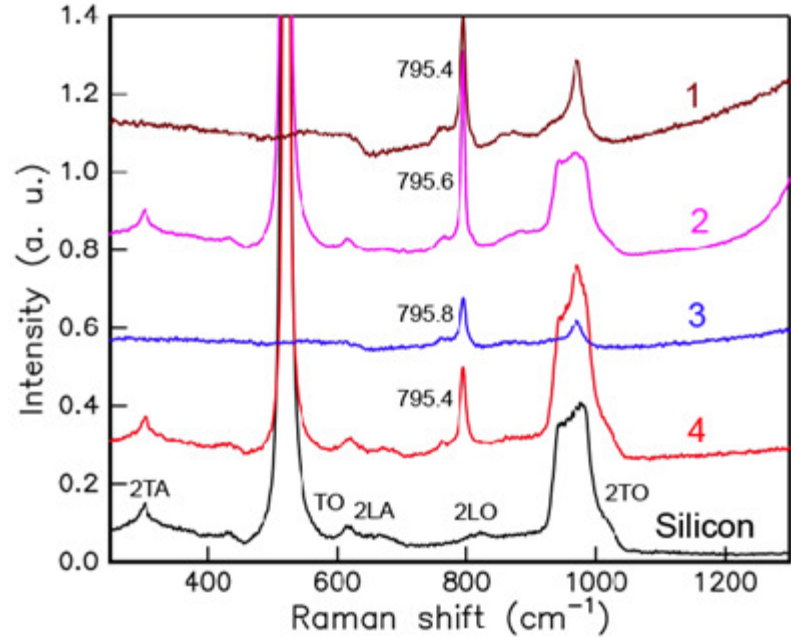
### 3.3 Raman Spectroscopy

Raman spectroscopy and visible room temperature photoluminescence (PL) were conducted on the samples provided by the Queensland Microtechnology Facility, Griffith University. This was used to determine the quality of the 3C-SiC films (and the membranes formed later) before and after the fabrication processes used to form membranes.

Figure 3.2 (a) shows the Raman spectra for various positions on the fabricated 3C-SiC membrane window and its 3C-SiC/Si supporting structure. Most of the Raman lines representing Si are apparent in the spectra for the SiC/Si structures at Position “2” and “4”. Only the 3C-SiC transverse optic (TO) peak is obvious as shown at Position “2” and “4”. A Si TO strong peak is clearly exhibited at Position “1” and “3” indicating the measurements were performed on 3C-SiC/Si. The Raman peaks exhibited by their positions are in accordance with previous reports [5-7].



a)



b)

Figure 3.2: a) Positions of measurements taken on the 3C-SiC/Si sample: Position “1”:Underneath the 3C-SiC membrane, Position “2”:Underneath 3C-SiC/Si, Position “3”:On top of the 3C-SiC membrane and Position “4”:On top of 3C-SiC/Si. b) Raman spectra taken from the positions mapped as in a) where the 3C-SiC transverse optic (TO) peaks is approximately  $795\text{ cm}^{-1}$  and the 3C-SiC longitudinal optic (LO) peak is approximately  $970\text{ cm}^{-1}$ . Silicon spectra is included for reference.

The 3C-SiC longitudinal optic (LO) peak coincides with the Si 2TO peak. 3C-SiC membranes show LO peaks broader and more intense than the 3C-SiC/Si peaks which are sharper but with lesser intensity (as observed by Feng et al. [7]). The SiC TO peak did not shift appreciably as shown in Figure 3.2 (b). This indicates that the strain does not vary.

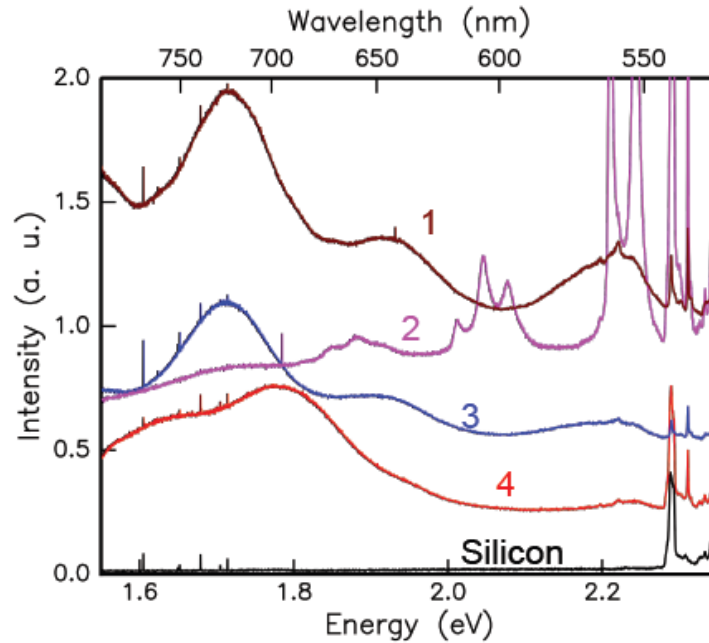


Figure 3.3: PL spectrum of the 3C-SiC free standing membrane and 3C-SiC/Si at room temperature corresponding to positions as mapped in Figure 3.3 (a).

In addition to the Raman peaks, a number of visible photoluminescence peaks are also observed as in Figure 3.3. A broad emission that is associated with phonon density is located between 450 and 600 nm which is attributed to 3C-SiC [8, 9]. This band is clearly observed at Position “1” and “3” but appears to be weaker at Position “4”. The observations made here confirm previous findings where 3C-SiC membranes which were interfacing Si substrate have stronger and more intense lines compared to the front or surface side of 3C-SiC membranes [10]. However, at Position “2” , this broad band is obscured and is replaced with strong and intense peaks. These peaks are attributed to one phonon and two phonon lines at 2.20 to 2.35 eV which are due to nitrogen bound excitation [10].

Other positions exhibiting less intense peaks of two-phonon lines and no one-phonon lines can be observed. At Position “2”, three peaks from 2.0 to 2.5 eV which are unique to this

position are also observed. These triple peaks might be also attributed to three phonon replicas of nitrogen bound excitation which usually appears at 2 to 2.1 eV [10].

In Figure 3.3, PL emission at 1.9 eV is observed at Position “1”, “2” and “3”. This band appears to be missing at Position “4”. This emission band is attributed to dislocations and extended defects [10]. Another emission band is at 2.15 to 2.30 eV and is governed by “defect related features” [10-13]. These bands can be used as a signature band to identify 3C-SiC [8, 9].

3C-SiC membranes were deliberately broken and made into small, medium and large size free standing films. A glass slide spectrum was used as a reference. The peak positions TO and LO Raman peaks of 3C-SiC membrane free standing films were varied slightly between the samples as shown in Table 3.1.

<b>Sample (Free Standing Film Size)</b>	<b>TO (cm<sup>-1</sup>)</b>	<b>LO (cm<sup>-1</sup>)</b>
Small (0.5×0.5 mm <sup>2</sup> )	795.9	971.8
Medium (2×2 mm <sup>2</sup> )	795.1	970.8
Large (6×6 mm <sup>2</sup> )	795.9	971.7

Table 3.1: Transverse optic (TO) and Longitudinal optic (LO) of Raman peaks according to 3C-SiC free standing films sizes.

The TO and LO of Raman peaks of 3C-SiC free standing 3C-SiC films are indicated in the figure below:

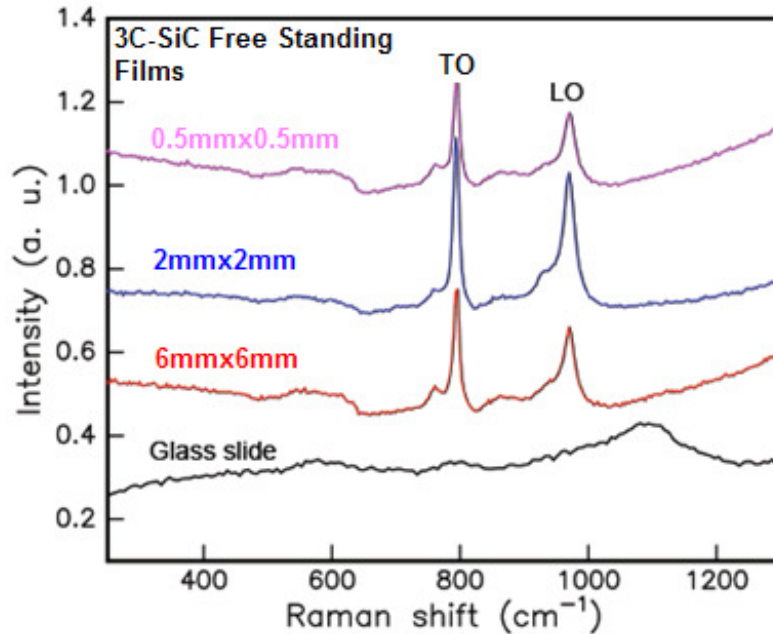


Figure 3.4: The transverse optic (TO) and longitudinal optic (LO) Raman peaks of 3 different sizes of 3C-SiC free standing films.

The positions of the TO and LO peaks for 3C-SiC free standing films were in accordance with the values presented from previous studies [5-7]. One study was conducted on a 1.2  $\mu\text{m}$  thick 3C-SiC membrane and the shape of the peaks presented were similar to those in the Raman spectra in Figure 3.4 [6]. Other thicknesses were also studied, thus, indicating that the thickness of a membrane contributed to their Raman characteristics [6]. PL spectra of all the 3C-SiC free standing films resemble the PL spectra of Position “1” of Figure 3.3. Thus, the measurements were performed on the backside of the membrane which previously interfaced the Si substrate. All of the free standing films’ PL spectra have the 1.9 eV and 2.15-2.3 eV broad emission band.

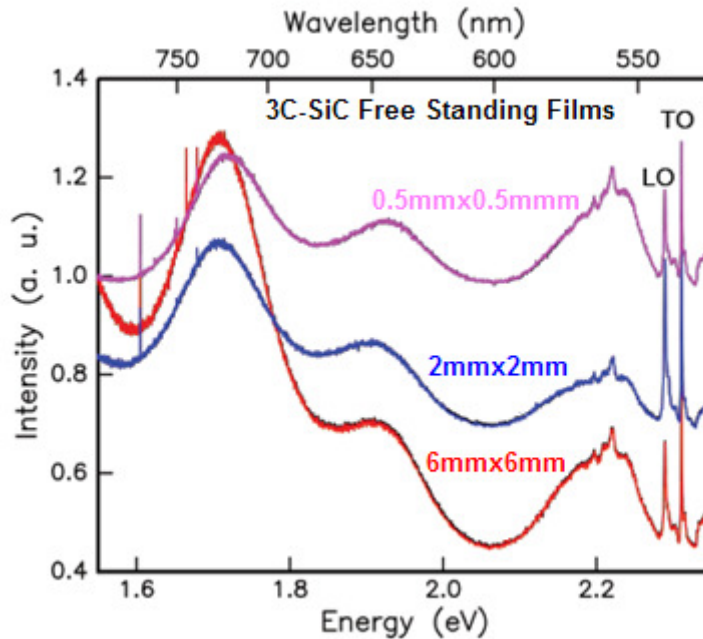


Figure 3.5: PL spectra of 3 different sizes of 3C-SiC free standing films at room temperature.

Two sizes of visual microstructure defects were featured on the 3C-SiC surface (Figure 3.6(a)). The effects have a distinct Raman spectrum and are located at the bottom of the free standing film (previously the SiC/Si interface). With regard to these defects, the SiC surface morphology can be divided into two distinct structures: small circular marks (—) and larger 3D structures (—). These defects appear to exist at the SiC surface that was initially at the SiC/Si interface as in Figure 3.6 (b).. The spectra from this structure are different. It shows 3C-SiC corresponding bands and peaks as well as a large number of other peaks (Figure 3.7). In the region just below  $1000\text{cm}^{-1}$ , there are Si peaks for the defect spectra that are weaker (or non existing) for position 1 peaks. Also the SiC peak at approximately  $2900\text{ cm}^{-1}$  is much weaker for the spectra in the region of the defects.

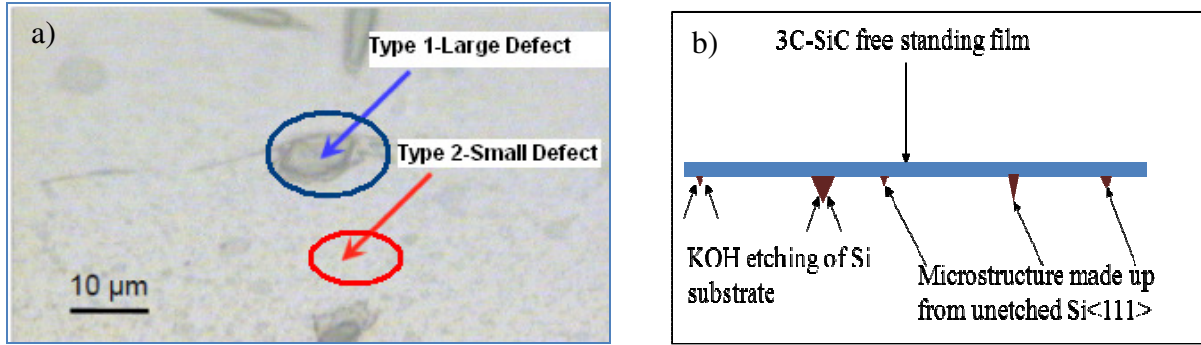


Figure 3.6: a) Optical micrograph showing features on a free standing 3C-SiC membrane at 40× magnifications. Two sizes of visual microstructures defects were apparent on the film. b) The formation of microstructure defects due to the KOH etching of Si substrate leaving Si <111> as the visual microstructure defects.

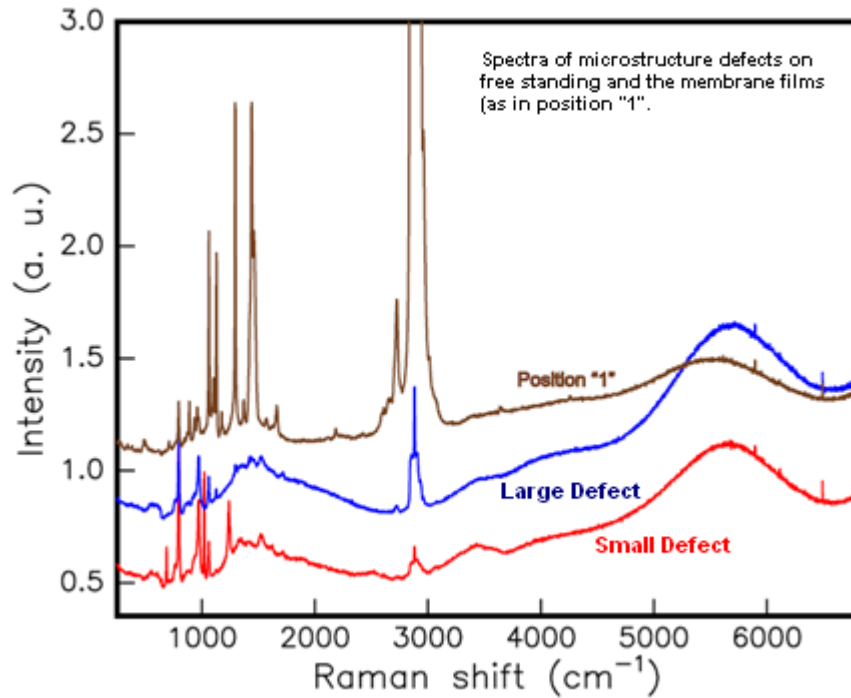


Figure 3.7: Raman spectrum taken from region of the microstructure defects on the free standing films (NOTE: surrounding SiC influences the spectra as the sample region is larger than the defect). Raman Spectra of the microstructures defects in comparison to the spectra at Position “1” (same side of SiC film but away from any defect) which represents 3C-SiC membrane interfacing Si substrate.



### 3.4 Visible Transmission Spectra

Transmission spectra for 0.285  $\mu\text{m}$ , 0.95  $\mu\text{m}$  and 1.18  $\mu\text{m}$  thick 3C-SiC membranes are shown in Figure 3.8, 3.9 and 3.10.

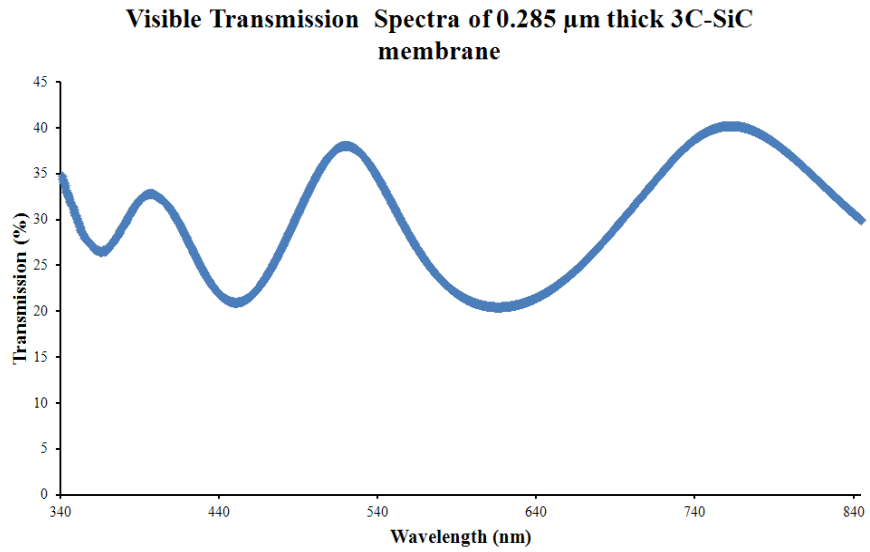


Figure 3.8: Visible transmission spectra of 0.285  $\mu\text{m}$  3C-SiC membrane.

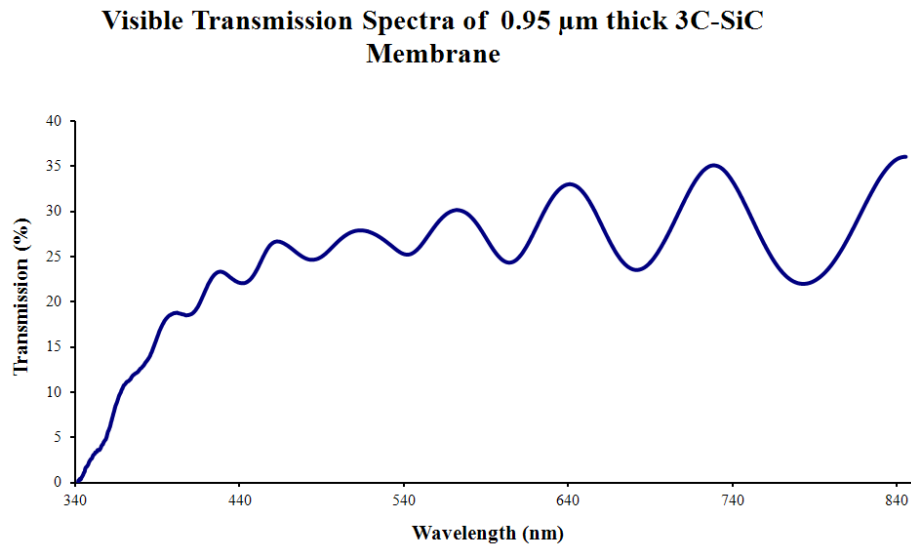


Figure 3.9: Visible transmission spectra of 0.95  $\mu\text{m}$  3C-SiC membrane.

**Visible Transmission Spectra of 1.18  $\mu\text{m}$  thick 3C-SiC membrane**

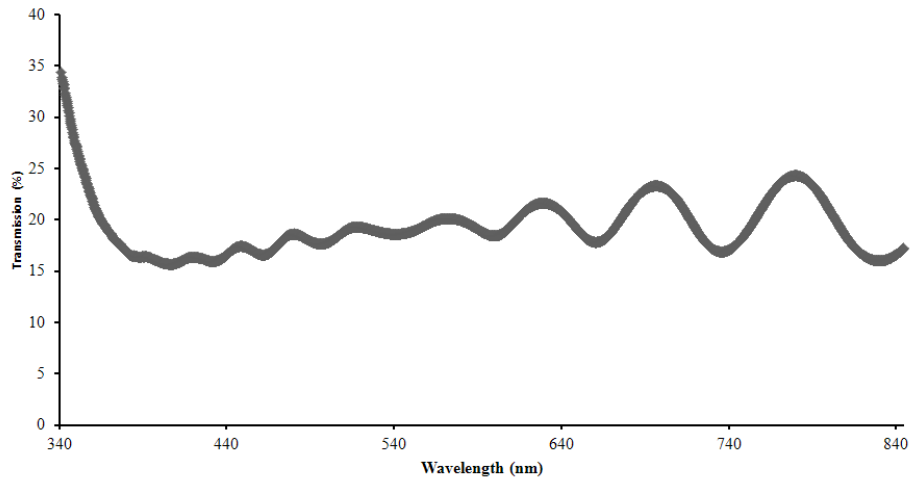


Figure 3.10: Visible transmission spectra of 1.18  $\mu\text{m}$  3C-SiC membrane.

The results for optical transparency against air which were measured at 633 nm are listed in

Table 3.2:

<b>3C-SiC Membrane Thickness</b>	<b>Transmission (%)</b>
0.285 $\mu\text{m}$	21%
0.95 $\mu\text{m}$	32%
1.18 $\mu\text{m}$	21%

Table 3.2: 3C-SiC membranes thicknesses and their corresponding transmission percentage.

The spectra reflect the transparent state of the 3C-SiC membranes. However, the transmission percentage for all the membranes was lower in comparison to previous reports [14-16]. For a 1  $\mu\text{m}$  thick single crystal 3C-SiC membrane, Yamaguchi et al. [14, 15] reported a transmission percentage was about 80%. For 0.4  $\mu\text{m}$  thick sample, Tabata et al. [16] obtained approximately 70% at the spectral wavelength of 633 nm. The low transmission values (21 and 31%) given in Table 3.2 were attributed to the visible light scattering through the membranes due to the

observed microstructure defects. Thus, this 3C-SiC membrane (or this technique for forming such membranes) maybe not be appropriate for applications which require high transparency such as for an X-Ray mask [17, 18]. The transparency value for 0.95  $\mu\text{m}$  thick 3C-SiC was higher may be due to the efficient removal of Si substrate from the membrane, thus, contributing better transmission value compared to the other membranes.

### 3.5 X-Ray Photoelectron Spectroscopy

XPS analysis was performed on an untreated 3C-SiC sample as control and two processed 3C-SiC samples of two different thicknesses as indicated in Figure 3.11 and 3.12. All samples had the finger print peaks for SiC which are C 1s, Si 2s and Si 2p peaks. Both the thick and the thin 3C-SiC films exhibited identical spectra which means there are no elemental composition differences in the samples due to their thickness different or 3C-SiC growth processes as described by Wang et al. [19].

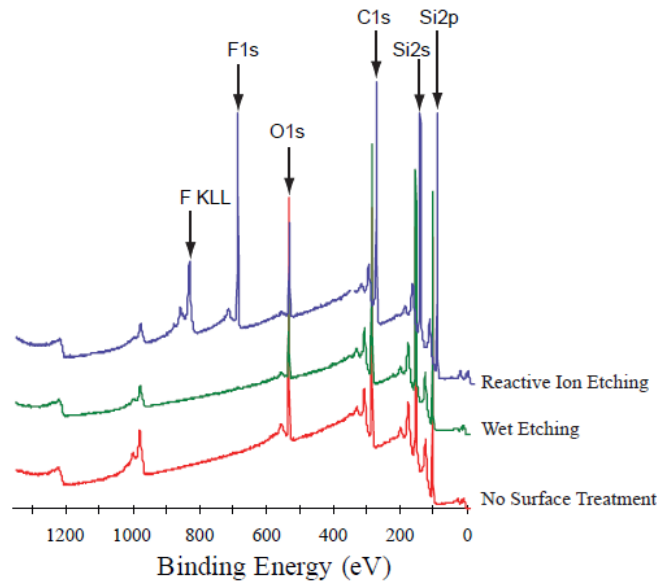


Figure 3.11: Comparison of XPS spectra of 0.285  $\mu\text{m}$  thick 3C-SiC thin film samples which had (i) no surface treatment, (ii) wet etching in KOH and (iii) reactive ion etching with tetrafluoromethane ( $\text{CF}_4$ ).

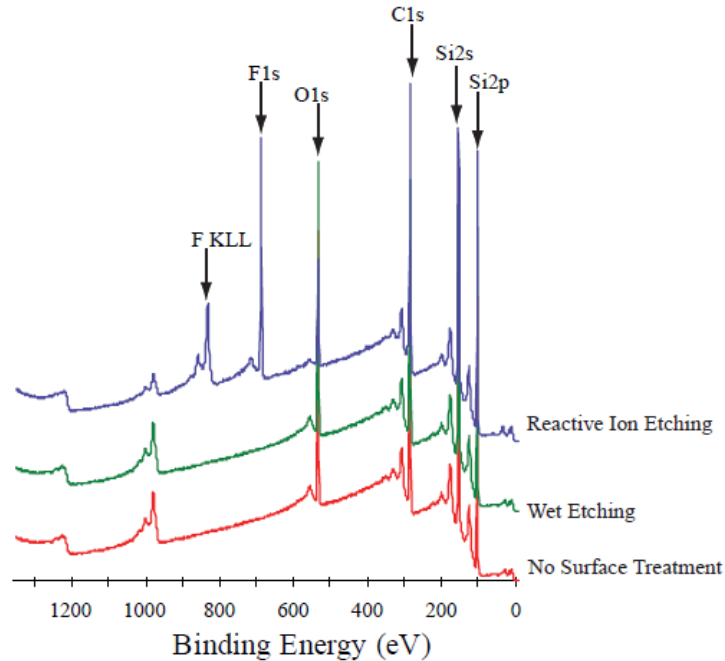


Figure 3.12: Comparison of XPS spectra of 0.95 μm thick 3C-SiC thin film samples which had (i) no surface treatment, (ii) wet etching in KOH and (iii) reactive ion etching with tetrafluoromethane (CF<sub>4</sub>).

All the samples have a sharp peak representing O 1s which indicates the presence of residual native oxide [20] or adsorption of O on the 3C-SiC surface during sample removal from the RIE chamber [21]. Both thicknesses show similar intensity for the Si 2s and Si 2p peaks. C 1s peak for the reactive ion etched 0.95 μm samples are more intense than the thinner version and also the other two similar thickness samples (which were the control and the wet etched only samples) suggesting there was deposition of a C-rich layer on the surface [21]. Thus, carbon from 3C-SiC might redeposited itself together with the residual carbon from the etching gas.

A strong peak attributed to F 1s can be observed only for the reactive ion etched sample. This peak is likely due to a fluorine rich polymer layer which was formed during reactive ion etching [20].

Wet etching either using KOH or HF did not introduce new elements such as potassium or fluorine to the SiC surface. HF solution was used since this method is known to remove organic thin film efficiently comparable to piranha solution. However, the application of HF for similar type of works elsewhere are replaced by piranha solution since HF is very corrosive and can be fatal to users. Here, no significant difference between the control samples and the wet etched samples was observed by XPS. However, the introduction of fluorine into the 3C-SiC surface by means of RIE is apparent. The implantation of fluorine ion or any other halogen elements (such as chlorine which is also commonly used for this process [20]) on the SiC surface due to the reactive ion etching process can be avoided by using alternative method such as micromilling or masking the unetched SiC during etching.

## **3.6 Thin Film Adhesion Test**

Common metals and their combinations used to make various ohmic and schottky contacts on 3C-SiC were tested to observe their adhesion quality. These metals include Nickel (Ni), Platinum (Pt), Aluminum (Al), Palladium (Pd), Gold (Au), Chromium (Cr) and their combinations such as Ni/Au, Pt/Ti and Ti/Au.

The metals and their adhesion quality are listed in Table 3.1. Ni/Au, Pt, Pd and Au showed poor adhesion to 3C-SiC film and were able to be removed easily in this test. Pd, Au and Au are known to be susceptible to peel off from 3C-SiC surface at room temperature [22, 23]. Pt is suggested to behave in such a way due to the stresses imposed by the differences of thermal expansion coefficient of Pt and 3C-SiC [22]. Thus, Pt [24, 25], Pd and Au [25] were usually applied as the overlayer to prevent oxidation rather than an immediate interface with SiC.

<b>Metal</b>	<b>Thickness (nm)</b>	<b>Adhesion</b>
Ni/Au	200:300	Poor
Ni	600	Good*
Pt	25	Poor
Al	600	Good
Pt/Ti	50:5	Good
Ti/Au	50:200	Good
Pd	300	Poor
Au	200	Poor
Cr	200	Good

Table 3.3: The list of the metals deposited on the 3C-SiC thin films and the quality of the adhesion. \*Nickel adhered better if the 3C-SiC/Si samples were plasma etched for surface cleaning (Condition: CF<sub>4</sub>/O<sub>2</sub>, 14/5 sccm, 70mTorr, 100W). Other metals showed the same adhesion quality with or without plasma treatment.

Ni deposition using electron beam is suggested to adhere well on SiC [26]. However, according to this observation, Ni adhered poorly to 3C-SiC surface which was previously not treated with the RIE plasma process. The adhesion of Ni improved for 3C-SiC which was surface treated with the RIE plasma process.

Al and Cr exhibited good adherence on 3C-SiC in this study. Cr is known to have good adhesion to SiC and provide proper mechanical strength for Cr/SiC contacts [27]. A study was conducted to simulate the interaction of SiC and Al layers [28]. It was found that there is a strong bond between Al and SiC layers due to the amount of charge transfer from the Al layer to the C layer, and the equilibrium distance between Al and C atoms which makes strong adhesion of Al contacts to 3C-SiC [28].

## 3.7 Conclusion

The characterization techniques performed were to determine the quality of the SiC material used for this project and to observe the effect of fabrication processes on the material properties of 3C-SiC membranes formed.

Details from SEM micrographs show the smooth morphology of the 3C-SiC membranes and the complete etching of the Si substrate. This work also reveals well defined side walls due to the unetched Si  $\langle 111 \rangle$  which supported the suspended membrane forming a cavity.

Raman Spectroscopy and Visible Photoluminescence Spectra confirms the material supplied from the Queensland Microtechnology Facility, Griffith University and the resulting 3C-SiC product from the fabrication process are high quality 3C-SiC as described in literatures [5-7]. The differences of the Raman Spectra between free standing membrane and 3C-SiC on Si substrate were clear where peaks from Si were apparent on the latter's spectra. Membrane size did not have much influence on the measurements taken whether they were Raman or PL spectra. However, the position on the membrane where the measurement took place played an important role since residual Si at the backside of the free standing membrane appeared to be not fully removed by KOH etching. The effect of fabrication processes on the Raman characteristics could be seen by the formation of microstructures defects at the backside of the 3C-SiC films which gave different readings compared to other measurement performed on the rest of the film which is smooth and free from defects. The microstructures are likely to have originated from unetched Si $\langle 111 \rangle$ . PL spectra from all positions confirmed the fingerprint peaks and bands which are attributed to the defects typically exhibited by 3C-SiC for the samples measured.

Visible Transmission Spectra indicated the optical quality of 3C-SiC membranes produced. The relatively low transmission percentage given made them unsuitable for applications which

require high transparency. Thus, the membrane developed here has more potential as a Micro Electromechanical System (MEMS) structure such as a diaphragm for pressure sensing.

X-Ray Photoelectron Spectroscopy revealed that RIE had introduced fluorine to the 3C-SiC surface. Immersing 3C-SiC in KOH and HF solution had not altered the surface elemental composition. Deposition of a carbon rich layer originating from RIE was prominent in the thicker samples and this layer was suggested to be responsible to induce large amount of leakage current on SiC p-n junctions [21, 29]. However, other studies had suggested that the introduction of halogen group to the surface of 4H-SiC [20] had altered its electrical properties. This effect is also experienced in Gallium Nitride (GaN) [30] based microdevices and it was suggested this also could affect its biocompatibility [31]. From this result, the influence of fluorine on the property of 3C-SiC is suggested to be more significant than the carbon rich layer.

Finally, metals such as Al and Cr are well adhered on 3C-SiC. In the case of Ni, 3C-SiC should be surface treated with RIE to enhance Ni adherence to the 3C-SiC surface. Other metals showed poor adhesion to 3C-SiC. Combination of different layers of metals did improve the adhesion of Pt and Ti. However, no significant improvement was observed for Ni/Au combination layers.



## 3.8 References

- [1] L. S. Hung, S. S. Lau, M. von Allmen, J. W. Mayer, B. M. Ullrich, J. E. Baker, P. Williams, and W. F. Tseng, "Epitaxial growth of Si deposited on (100) Si," *Applied Physics Letters*, vol. 37, pp. 909-911, 1980.
- [2] D. M. Mattox, "Non-Elemental Characterization of Films and Coatings," in *Handbook of Deposition Technologies For Films and Coatings*, R. F. Bunshah, Ed., Second Edition ed New Jersey, United States of America: Noyes Publications, 1994, p. 662.
- [3] C. A. Zorman and R. J. Parro, "Micro- and nanomechanical structures for silicon carbide MEMS and NEMS," *physica status solidi (b)*, vol. 245, pp. 1404-1424, 2008.
- [4] K. E. Bean, "Anisotropic etching of silicon," *Electron Devices, IEEE Transactions on*, vol. 25, pp. 1185-1193, 1978.
- [5] S. Rohmfeld, M. Hundhausen, and L. Ley, "Raman scattering in polycrystalline 3C-SiC:Influence of stacking faults," *Physical Review B*, vol. 58, pp. 9858-9862, 1998.
- [6] J. Zhu, S. Liu, and J. Liang, "Raman study on residual strains in thin 3C-SiC epitaxial layers grown on Si(001)," *Thin Solid Films*, vol. 368, pp. 307-311, 2000.
- [7] Z. C. Feng, W. J. Choyke, and J. A. Powell, "Raman determination of layer stresses and strains for heterostructures and its application to the cubic SiC/Si system," *Journal of Applied Physics*, vol. 64, pp. 6827-6835, 1988.
- [8] L. Zhang, W. Yang, H. Jin, Z. Zheng, Z. Xie, H. Miao, and L. An, "Ultraviolet photoluminescence from 3C-SiC nanorods," *Applied Physics Letters*, vol. 89, pp. 143101-3, 2006.

- [9] X. L. Wu, G. G. Siu, M. J. Stokes, D. L. Fan, Y. Gu, and X. M. Bao, "Blue-emitting beta-SiC fabricated by annealing C<sub>60</sub> coupled on porous silicon," *Applied Physics Letters*, vol. 77, pp. 1292-1294, 2000.
- [10] W. J. Choyke, Z. C. Feng, and J. A. Powell, "Low-temperature photoluminescence studies of chemical-vapor-deposition-grown 3C-SiC on Si," *Journal of Applied Physics*, vol. 64, pp. 3163-3175, 1988.
- [11] F. Giorgis, A. Chiodoni, G. Cicero, S. Ferrero, P. Mandracci, G. Barucca, R. Reitano, and P. Musumeci, "Optical and structural properties of SiC layers grown by an electron cyclotron resonance CVD technique," *Diamond and Related Materials*, vol. 10, pp. 1264-1267, 2001.
- [12] A. Kassiba, M. Makowska-Janusik, J. Bouclé, J. F. Bardeau, A. Bulou, and N. Herlin-Boime, "Photoluminescence features on the Raman spectra of quasistoichiometric SiC nanoparticles: Experimental and numerical simulations," *Physical Review B*, vol. 66, p. 155317, 2002.
- [13] Z. C. Feng, "Optical properties of cubic SiC grown on Si substrate by chemical vapor deposition," *Microelectron. Eng.*, vol. 83, pp. 165-169, 2006.
- [14] Y. Yamaguchi, H. Nagasawa, T. Shoki, and N. Annaka, "Properties Of Heteroepitaxial 3C-SiC Films Grown by LPCVD," in *Solid-State Sensors and Actuators, 1995 and Eurosensors IX.. Transducers '95. The 8th International Conference on*, 1995, pp. 190-193.
- [15] Y.-i. Yamaguchi, H. Nagasawa, T. Shoki, N. Annaka, and H. Mitsui, "Properties of heteroepitaxial 3C-SiC films grown by LPCVD," *Sensors and Actuators A: Physical*, vol. 54, pp. 695-699, 1996.

- [16] A. Tabata and A. Naito, "Structural changes in tungsten wire and their effect on the properties of hydrogenated nanocrystalline cubic silicon carbide thin films," *Thin Solid Films*, vol. 519, pp. 4451-4454, 2011.
- [17] A. Jean, M. Chaker, Y. Diawara, P. K. Leung, E. Gat, P. P. Mercier, H. Pépin, S. Gujrathi, G. G. Ross, and J. C. Kieffer, "Characterization of a-SiC:H films produced in a standard plasma enhanced chemical vapor deposition system for x-ray mask application," *Journal of Applied Physics*, vol. 72, pp. 3110-3115, 1992.
- [18] W. Lin, Z. Min, D. Yohannes, J. Melzak, C. H. Wu, and P. Zhengchun, "A large format membrane-based x-ray mask for microfluidic chip fabrication," *Journal of Micromechanics and Microengineering*, vol. 16, p. 402, 2006.
- [19] L. Wang, S. Dimitrijević, J. Han, A. Iacopi, L. Hold, P. Tanner, and H. B. Harrison, "Growth of 3C-SiC on 150-mm Si(100) substrates by alternating supply epitaxy at 1000 °C," *Thin Solid Films*, vol. 519, pp. 6443-6446, 2011.
- [20] V. Khemka, T. Chow, and R. Gutmann, "Effect of reactive ion etch-induced damage on the performance of 4H-SiC schottky barrier diodes," *Journal of Electronic Materials*, vol. 27, pp. 1128-1135, 1998.
- [21] J. W. Palmour, R. F. Davis, T. M. Wallett, and K. B. Bhasin, "Dry etching of b-SiC in CF<sub>4</sub> and CF<sub>4</sub>+O<sub>2</sub> mixtures," *Journal of Vacuum Science & Technology A: Vacuum, Surfaces, and Films*, vol. 4, pp. 590-593, 1986.
- [22] N. A. Papanicolaou, A. Christou, and M. L. Gipe, "Pt and PtSi<sub>x</sub> Schottky contacts on n-type beta-SiC," *Journal of Applied Physics*, vol. 65, pp. 3526-3530, 1989.

- [23] S. Basu, S. Roy, R. Laha, C. Jacob, and S. Nishino, "Schottky behaviour of Pd/ $\beta$ -SiC junctions," in *Optoelectronic and Microelectronic Materials and Devices, 2000. COMMAD 2000. Proceedings Conference on*, 2000, pp. 328-331.
- [24] R. S. Okojie, D. Lukco, Y. L. Chen, and D. J. Spry, "Reliability assessment of Ti/TaSi<sub>2</sub>/Pt ohmic contacts on SiC after 1000 h at 600 [degree]C," *Journal of Applied Physics*, vol. 91, pp. 6553-6559, 2002.
- [25] L. M. Porter and F. A. Mohammad, "Review of Issues Pertaining To The Development of Contacts To Silicon Carbide," in *Silicon Carbide Microelectromechanical Systems for Harsh Environments*, R. Cheung, Ed., 1st ed London: Imperial College Press, 2006.
- [26] F. Goesmann and R. Schmid-Fetzer, "Metals on 6H-SiC: contact formation from the materials science point of view," *Materials Science and Engineering: B*, vol. 46, pp. 357-362, 1997.
- [27] C. Koliakoudakis, J. Dontas, S. Karakalos, M. Kayambaki, S. Ladas, G. Konstantinidis, K. Zekentes, and S. Kennou, "Cr/4H-SiC Schottky contacts investigated by electrical and photoelectron spectroscopy techniques," *Physica Status Solidi (A) Applications and Materials Science*, vol. 205, pp. 2536-2540, 2008.
- [28] J. Hoekstra and M. Kohyama, "Ab initio calculations of the  $\beta$ -SiC(001)/Al interface," *Physical Review B*, vol. 57, pp. 2334-2341, 1998.
- [29] J. Ryu, H. J. Kim, and R. F. Davis, "Rapid Thermal Annealing of B or N Implanted Monocrystalline 1-SiC Thin Films and its Effect on Electrical Properties and Device Performance," in *MRS Proceedings*, San Francisco, California, USA, 1985, pp. 337-342.
- [30] A. Baharin, R. S. Pinto, U. K. Mishra, B. D. Nener, and G. Parish, "Low contact resistance to plasma-etched p-type GaN," *Electronics Letters*, vol. 47, pp. 342-343, 2011.

- [31] I. Cimalla, F. Will, K. Tonisch, M. Niebelschütz, V. Cimalla, V. Lebedev, G. Kittler, M. Himmerlich, S. Krischok, J. A. Schaefer, M. Gebinoga, A. Schober, T. Friedrich, and O. Ambacher, "AlGaN/GaN biosensor—effect of device processing steps on the surface properties and biocompatibility," *Sensors and Actuators B: Chemical*, vol. 123, pp. 740-748, 2007.

# Chapter 4

## Electrical Characterization of 3C-Silicon Carbide Membranes

In this chapter, comprehensive results from electrical characterizations of metal contacts to 3C-SiC are presented. These include the influence of fluorinated plasma on the electrical behaviour of Al/3C-SiC, electrical characterization of metal/3C-SiC contacts using the ohmic contact transmission line model (TLM) test structures parameters such as contact resistance, sheet resistance, contact end resistance and specific contact resistance and also critical analysis of the substrate influence on the current paths (i.e. whether it crosses the 3C-SiC/Si interface or not).

# 4.1 Influence of Fluorinated Plasma on Metal/Contacts Electrical Behaviour

## 4.1.1 Experimental Methods

In this section, test structures which consisted of a central dot and a concentric ring contact (Figure 4.1) were used to evaluate the effect of fluorinated plasma on the metal/3C-SiC electrical behavior. Al was used as the contact metal since it has good adhesion as described in the previous chapter and it is used widely as an ohmic contact to n-type 3C-SiC without requiring high annealing temperature [1-4]. Cr shows good adhesion on 3C-SiC but Cr/SiC is also known to exhibit Schottky behavior [5-7]. An ohmic contact is a contact that obeys Ohm's law with a linear current-voltage relation although most of the ohmic contacts in semiconductor devices may show some aspect of non-linearity as long as it does not compromise its performance [8, 9].

Arrays of Al patterns were made using standard photolithography techniques onto the samples which were (i) the unetched 3C-SiC, (ii) wet etched only samples and (iii) the samples which were wet KOH etched and reactive ion etched. The non-etched 3C-SiC samples served as control samples. The wet etched samples were treated with potassium hydroxide (KOH) for 28 hours at 80°C. The wet KOH etched and reactive ion etched samples were etched by RIE with base pressure ranging from 73 to 86 mTorr. The RF power applied was 100W for 5 minutes using 14.1/4.7 sccm of CF<sub>4</sub>/O<sub>2</sub>. This mixture was used to remove any possible carbon deposition on the materials' surface [10, 11]. The samples were etched using KOH at 80°C for 28 hours. All the three types of samples were dipped in hydrofluoric (HF) acid for 30 seconds to remove any native oxide. An Al layer (600 nm) was deposited using electron beam evaporation and etched

for the contact patterns. Electrical measurements were made between adjacent circular pads of two aluminium contact patterns and also between a circular dot and an outer ring (Figure 4.1).

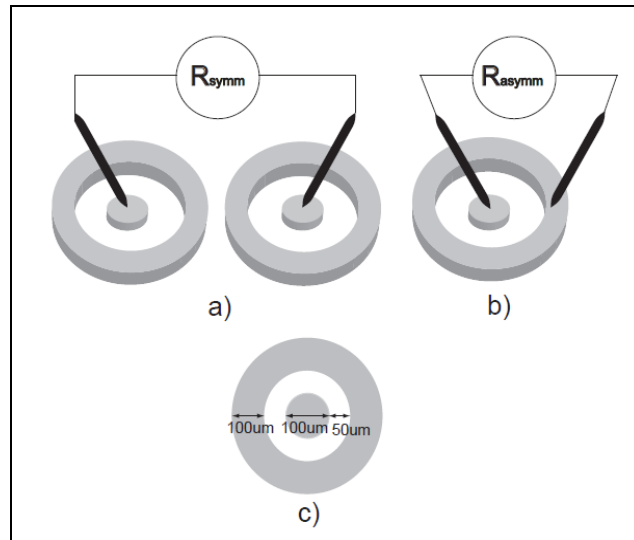


Figure 4.1: Schematic illustration showing the probing of aluminum contact patterns on large area 3C-SiC;

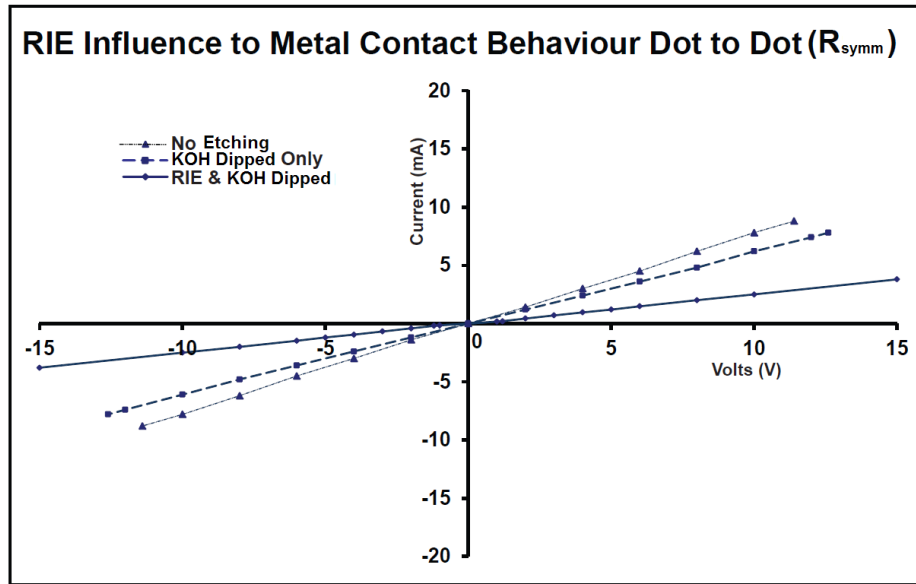
a) Current-voltage measurement from dot to dot contacts. b) Current-voltage measurement from dot to ring contacts.

c) Schematic illustration, geometry and dimensions of the contact electrodes for the electrical measurements.

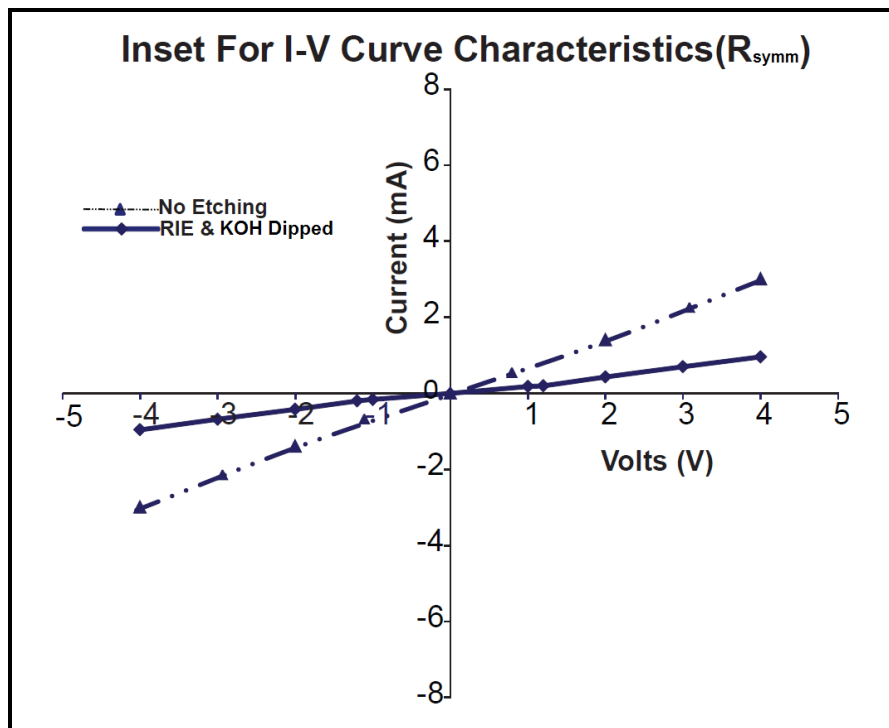
#### 4.1.2 Results and Analysis of The Symmetrical (Dot to Dot) Contacts

In Figure 4.2 (a), the I-V relationship between two adjacent circular dots is shown. The samples which were treated with RIE and the KOH solution showed higher resistance compared to other samples. For the RIE and wet etched 3C-SiC samples, slight non-linear current-voltage response can be observed at lower voltage for both polarities of the applied voltages in comparison to the control samples (Figure 4.2 (b)). This non-linearity phenomenon is unique only for the samples which had been treated with RIE and the KOH solution and was not observed for both the control and KOH dipped only samples I-V characteristics.





(a)



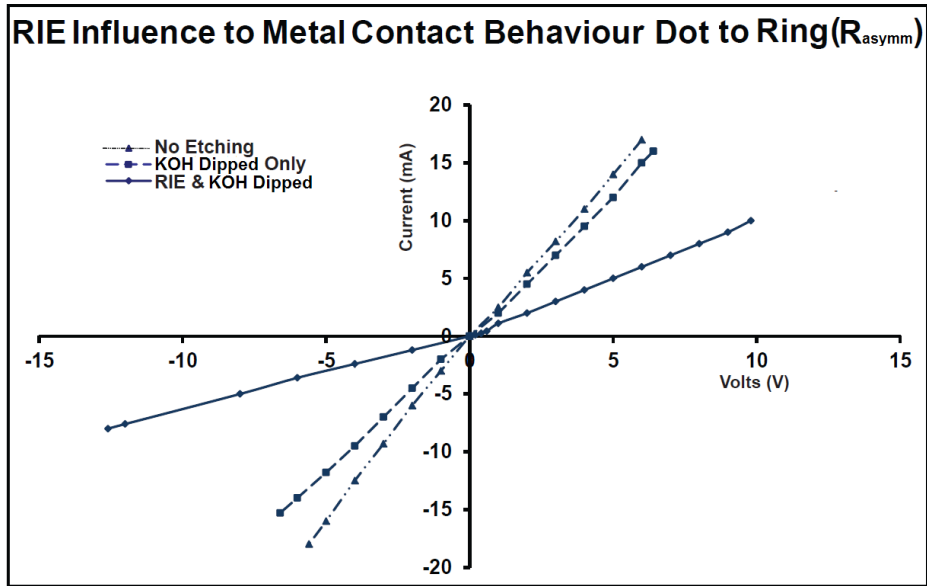
(b)

Figure 4.2: (a) Current-voltage plots from dot to dot metal contacts for (i) the samples that had not been treated, (ii) the samples which were only treated by the KOH and (iii) the samples which were KOH treated and RIE treated. (b) Inset figure shows the comparison between the I-V curves of the untreated samples and the samples influenced by RIE.

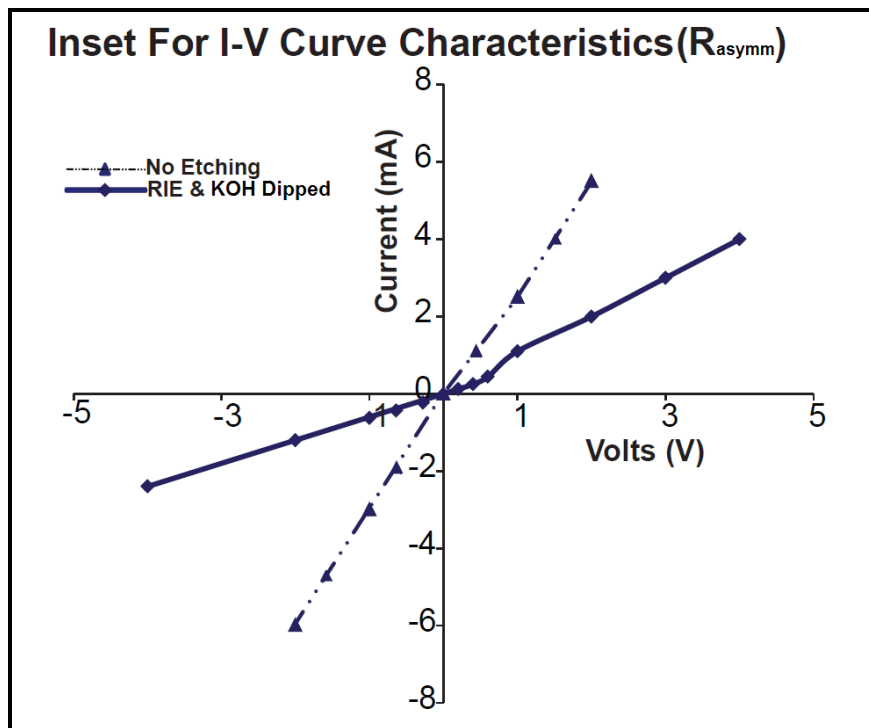
### 4.1.3 Results and Analysis of The Asymmetrical (Dot to Ring) Contacts

Electrical measurement from dot to ring contacts revealed the effects of contact areas. As in the previous results, both untreated sample and KOH treated only samples exhibited linear I-V (ohmic) behavior and relatively lower resistance as in Figure 4.3 (a). However, the samples treated with RIE and KOH showed non-ohmic behavior particularly at the lower reading of the positive applied voltages. The negative applied voltage showed higher resistance which lead to the non-symmetrical current-voltage response of the measurement.

Asymmetry in the I-V curves (e.g. Figure4.3) was likely due to the strong Schottky characteristics of the aluminum-SiC contacts. Asymmetry existed only in the voltage sweep from negative to positive voltage for Schottky contacts of different areas. This is because the reverse bias contact in back-to-back Schottky contacts in a circuit will limit the current in such arrangement. When the large area contact was reverse biased it allowed more current through than the smaller contact at the same reverse bias voltage. (Note; in determining the resistance between the dot and the ring contacts, the dot contact is reverse biased when the ring contact is forward biased and vice versa). This asymmetry in the I-V curves will not happen when the two contacts have the same area or when two contacts (of any areas) are purely ohmic. The plasma etching had altered the ohmic behavior of the Al/3C-SiC contacts and this would have detrimental effect on the electrical performance of the membrane, thus affecting its future use especially in biomedical microdevices. Degradation of ohmic contacts on semiconductor material such as Gallium Nitride due to plasma etching had been studied before [12, 13], but the fluorinated plasma effect on the 3C-SiC is studied here. Carbon layer deposition was suggested to alter electrical characteristics of 3C-SiC, but here, this layer was removed by  $CF_4/O_2$  gas mixture [10]. Thus, fluorinated plasma was the actual reason which is responsible to alter the Al/3C-SiC/Si ohmic behavior.



(a)



(b)

Figure 4.3. a) Current-voltage plots from dot to ring metal contacts for (i) the samples that has not been treated, (ii) the samples which was only treated by the KOH and (iii) the samples which were KOH treated and RIE treated. b) Comparison is made between the I-V curves of the untreated samples and the samples influenced by RIE as shown in the inset figure.

## 4.2 Characterization of Ohmic Contact Transmission Line Model Test Structure Parameters

### 4.2.1 Introduction

Specific contact resistance (also known as contact resistivity or specific contact resistivity),  $\rho_c$ , is the quantification of the resistance posed by the interface regardless to its area [8, 14]. This parameter can be measured using the transmission line model (TLM) pattern. There are two types of TLM pattern used: rectangular and circular. However, the difficulty with the rectangular TLM pattern is the requirement of fabricating mesa structures to isolate the contact pattern from the effect of current flow [15, 16]. The application of circular transmission line model eliminates the mesa etch requirement. Since 3C-SiC is inert to chemical etching [17], another step involving RIE should be performed if the rectangular TLM pattern is used. Circular TLM has another advantage which is the calculation accuracy where the sheet resistance under the metal contact is allowed to be different from the substrate sheet resistance [16].

Reeves [16] modified the resistance equations of the rectangular (TLM) pattern to accommodate the circular version. The circular TLM consists of a central dot, an inner ring and metal surrounding as shown Figure 4.4.  $R_1$  is the resistance measured between the central dot and the inner ring.  $R_2$  is the resistance measured between the two outer contacts as shown in Figure 4.4 (a).

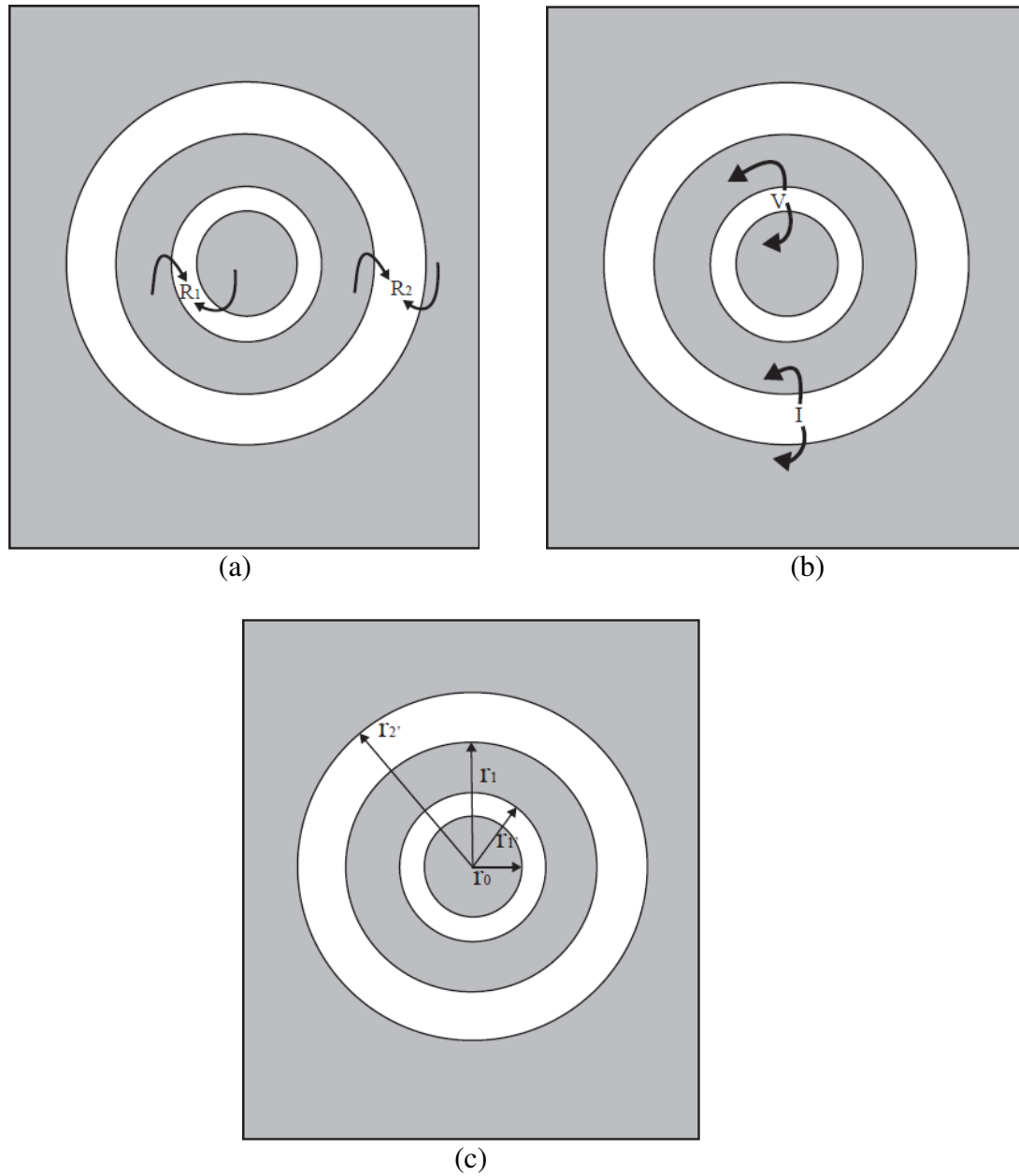


Figure 4.4: Schematic illustrations showing the CTLM contact geometry. a)  $R_1$  is the resistance measured between the central dot and the inner ring.  $R_2$  is the resistance measured between the inner ring and the outer metal surrounding. b) A schematic diagram which shows  $R_c$  measurement. Voltage is measured by probing the centre pad to the second ring. Current is supplied to the second ring and the surrounding metal portion. c)  $r_0$  represents the radius of the central dot,  $r_1$  represents the inner radius of the first ring contact,  $r_1$  represents the outer radius of the first ring contact and  $r_2$  represents the inner radius of the second ring contact. The grey area representing the metal and the white representing the substrate/material.

The contact end resistance,  $R_e$ , is the other additional resistance required to determine  $\rho_c$  and this parameter is obtained by forcing current between the two outer contacts and measuring the voltage between the two inner contacts (refer to Figure 4.4 (b)).

The specific contact resistance,  $\rho_c$ , can be determined from these three parameters ( $R_1, R_2$  and  $R_e$ ) and also the radii of the central dot and the rings ( $r_0, r_1, r_1', r_2'$ ) (as shown in Figure 4.4 (c)) with the expression shown below which has been presented and discussed in details by Reeves in reference [16]:

$$\rho_c = \left( \ln\left(\frac{r_2'}{r_1}\right) \cdot R_1 - \ln\left(\frac{r_1'}{r_0}\right) \cdot R_2 \right) \cdot (r_0)^2 \cdot \Delta \quad (2)$$

where

$$\Delta = \frac{2\pi}{(\alpha r_0)^2 \cdot \phi} \left/ \left\{ \frac{A(r_1, r_1') \cdot B(r_1, r_1')}{C(r_1, r_1')} + D(r_1, r_1') \right\} \right. \quad (3)$$

where

$$\phi = \left( \ln\left(\frac{r_2'}{r_1}\right) \cdot R_1 - \ln\left(\frac{r_1'}{r_0}\right) \cdot R_2 \right) / R_e \quad (5)$$

and

$$\alpha = \sqrt{\frac{R_{sk}}{\rho_c}} \quad (6)$$

where A,B,C and D are combinations of the modified Bessel functions of the first and second kind.  $\alpha$  is related to the sheet resistance beneath the metal contact (which is allowed to be different from the normal sheet resistance) and the specific contact resistance. The calculations of  $\rho_c$  values using CTLM in this project were performed using Matlab Version 7.11.0 (R2010b).

## 4.2.2 Measurements of $\rho_c$ for metal contacts/3C-SiC membranes

### 4.2.2.1 Experimental Methods

Arrays of circular TLM patterns were fabricated on the surface of the 3C-SiC/Si by a standard lift-off process. The array extended across both the membrane and the surrounding wafer. A layer of AZ1512 resist was spin-coated onto the surface of the membrane and lithographically patterned in a circular TLM structure [16]. As illustrated in Figure 4.5, the spacing between electrodes was  $r_1' - r_0 = 60 \mu\text{m}$  and  $r_2' - r_1 = 170 \mu\text{m}$ . A number of different contact systems including Al (300 nm), Pd (300 nm) and Ni (50 nm)/ Ti (50 nm)/ Au (100 nm) were examined as ohmic contacts to 3C-SiC. Al and Pd contacts are preferred over Ni based systems since Ni ohmic contact can only be produced by annealing at temperature higher than 900°C [18]. Prior to the deposition of metal layers by electron beam evaporation; the patterned samples were dipped in buffered HF solution for 60 seconds and rinsed in de-ionised water. The subsequent annealing of the contacts and membranes was performed in a nitrogen atmosphere at temperatures up to 950 °C without any detectable damage to the membranes. Measurements were performed using the CTLM patterns for each of the contact systems.

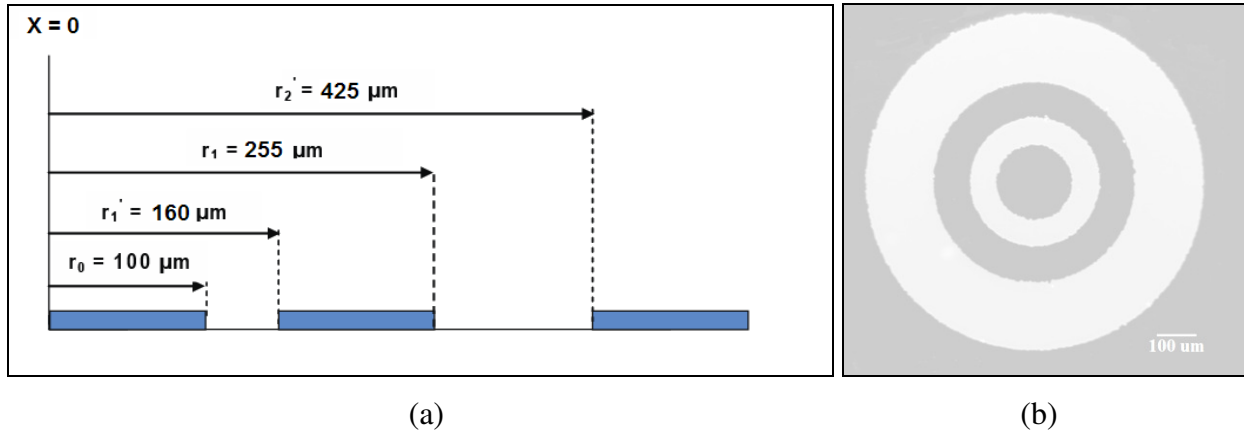


Figure 4.5: a) Geometry and dimensions of electrodes in the Circular TLM pattern used in the measurement of specific contact resistance. b) Optical micrographs of CTLM [16].

A further critical step in the process was the deposition into the etched recess on the backside of the membrane of a layer of resin which was cured at room temperature for 24 hours. The stiffness of the layer of hardened resin enabled the mechanical stabilization of the membrane for subsequent probing on the upper surface. The application of the resin was the last step in the fabrication process and followed directly after either the metal deposition or annealing of the contacts. Another method to enable probing was to leave a certain thickness of the Si substrate. This method was applied in determining the heterojunction (3C-SiC/Si) leakage current to the substrate. Layers of substrate ranging from 80  $\mu\text{m}$  to 260  $\mu\text{m}$  were left unetched to assist subsequent electrical probing of the aluminium contacts as shown in Figure 4.6 (d).



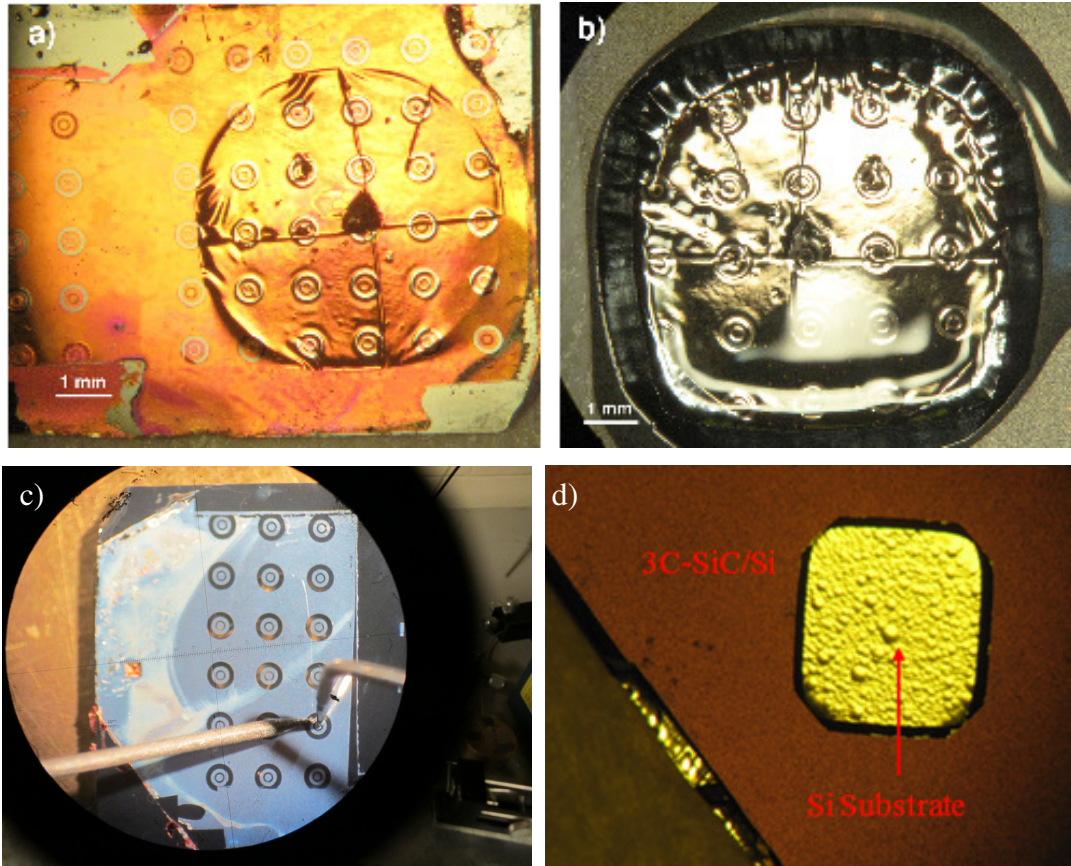


Figure 4.6: a) CTLM patterns fabricated in Ni/Ti/Au metallization on the upper surface of a membrane. b) The underside of a membrane with the etched recess coated with a resin layer. c) Clear resin fills the backside allowing the front surface (Al metallization) to be probed without breaking the membrane. d) The backside of the 3C-SiC thin film in which a thin layer of Si substrate was left unetched to mechanically reinforce the fragile membrane.

#### 4.2.2.2 Results and Analysis of I-V Characteristics of Al, Pd and Ni/Ti/Au on 3C-SiC membranes

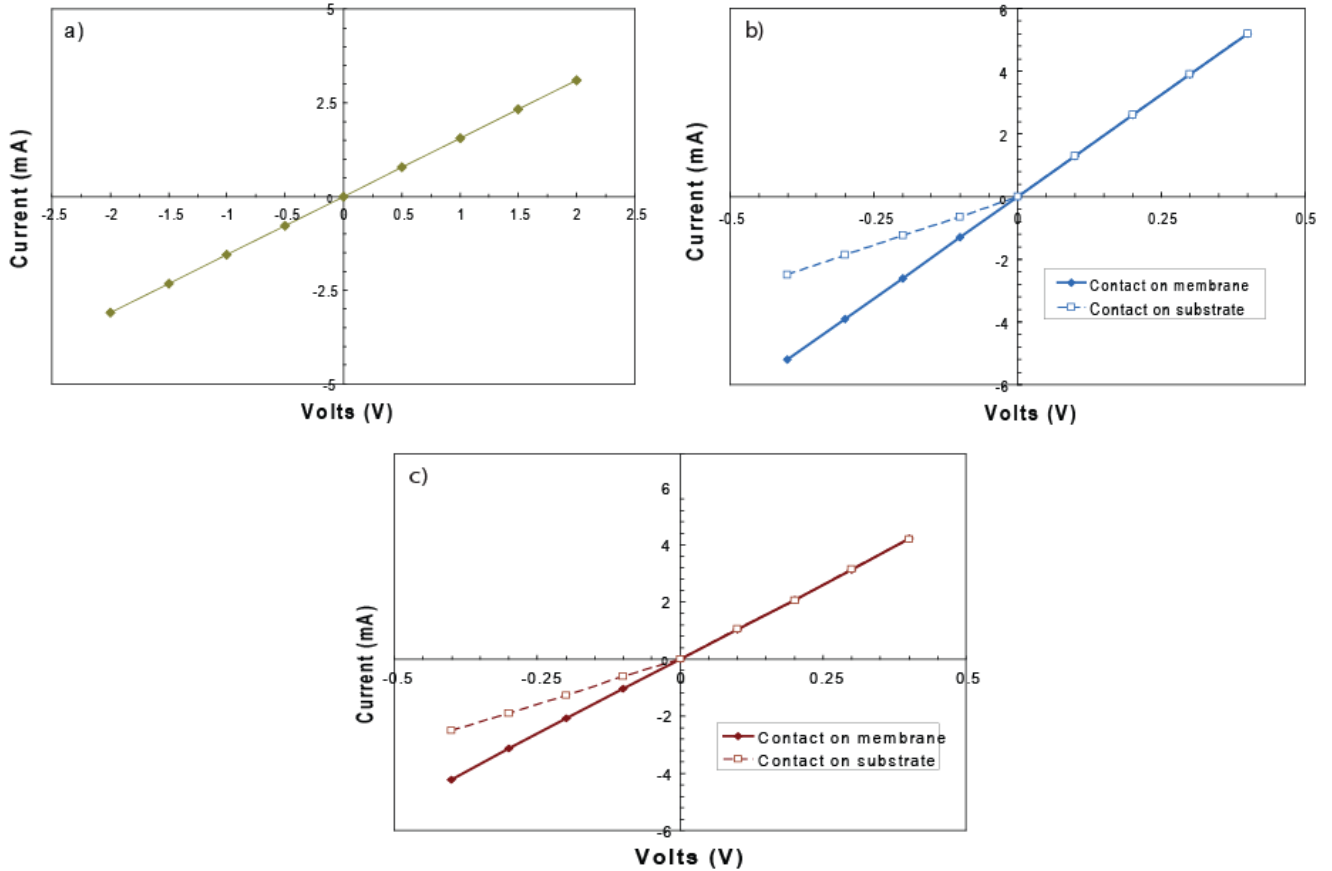


Figure 4.7: Current-voltage plots for a) Al (300 nm) as-deposited on membrane b) Pd (300 nm) annealed at 600 °C, 5 mins on a membrane and substrate and c) Ni (50 nm)/Ti (50 nm)/Au annealed at 950 °C, 5 mins on membrane and on substrate.

In all cases, the as-deposited contacts located on the membranes were ohmic in current/voltage response. Figure 4.7 (a) shows the linear plot for as-deposited Al contacts. Figure 4.7 (b) and (c) compare the current/voltage plots for Pd (annealed at 600 °C, 5 mins) and Ni/Ti/Au contacts (annealed at 950 °C, 5 mins), respectively. The I/V plots were obtained from

CTLM patterns both on a membrane and on the 3C-SiC/Si substrate. For both Pd and Ni/Ti/Au contacts, the CTLM patterns located on the membrane have shown ohmic responses.

The patterns located on the wafer away from the membrane were non-ohmic in current-voltage response with a divergence from linearity which was evident at negative applied voltages. Both the Pd and Ni/Ti/Au contacts have shown a similar divergence from ohmic behaviour outside of the membrane.

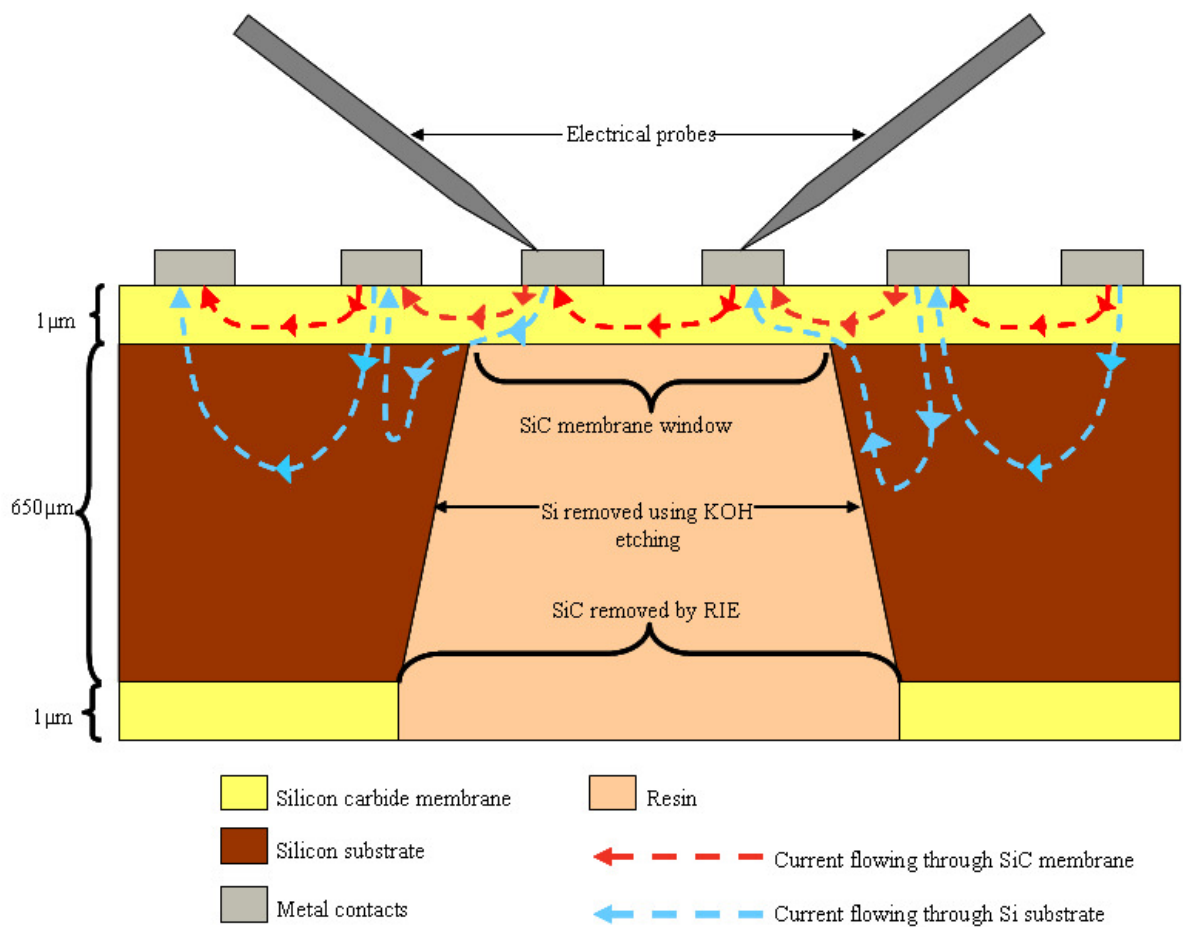


Figure 4.8: Schematic illustration of the membrane showing the alternate current paths for contacts located on the membrane and on the 3C-SiC/Si substrate.

For the CTLM patterns located on the membrane, the current was restricted to flow through the metal/3C-SiC contact interfaces and within the 3C-SiC/ layer as illustrated above in Figure 4.8. For CTLM patterns located away from the membrane, the I/V characteristics have indicated an alternative route for current through the conducting Si substrate. In this case, the current flow through the 3C-SiC/Si heterojunction imposed an additional effect on the resistance measurements. The differences between the current/voltage response for contacts on the membrane and on 3C-SiC/Si was evidently due to current flow through the SiC – Si heterojunction.

#### 4.2.2.3 Results and Analysis of $\rho_c$ for Al, Pd and Ni/Ti/Au on 3C-SiC membranes

$R_1$ ,  $R_2$  and  $R_c$  measurements obtained from the CTLM with Al or Pd or Ni/Ti/Au as the metal contacts on 3C-SiC were used to calculate  $\rho_c$ . The average value of  $\rho_c$  calculated for Ni/Ti/Au contacts on the membranes was  $1.5 \times 10^{-4} \Omega \cdot \text{cm}^2$  and for Pd contacts as  $\rho_c = 2 \times 10^{-4} \Omega \cdot \text{cm}^2$ . This value of  $\rho_c$  for Ni/Ti/Au contacts to 3C-SiC was almost the same as  $\rho_c$  determined by Barda et al. using a linear TLM pattern on a semi-insulating substrate at a doping level of  $1.9 \times 10^{19} \text{ cm}^{-3}$  [19]. Other studies of Ni/3C-SiC contacts have measured  $\rho_c$  within the range  $5 \times 10^{-6} \Omega \cdot \text{cm}^2$  to  $3.47 \times 10^{-3} \Omega \cdot \text{cm}^2$  although these results were obtained for 3C-SiC with 4H and 6H polytype faces [20].

Annealing at temperatures in the range 900-1,000 °C was necessary for formation of ohmic contacts based on Ni [20]. At these temperatures, the predominant interfacial structure has been identified as  $\text{Ni}_2\text{Si}$  and carbon phases [21]. Pd-based contacts have previously been examined as ohmic contacts to p-SiC [20]. Annealing at a temperature of 600 °C has given a minimum in  $\rho_c$  associated with the formation of  $\text{Pd}_3\text{Si}$  interfacial phase [22]. The present results indicate that Pd

contacts also have the ability to form ohmic contacts to 3C-SiC. A distinct advantage of Pd contacts is the lower temperature of annealing (600 °C) than for Ni contacts (900-1,000 °C) required to reduce the value of  $\rho_c$ .

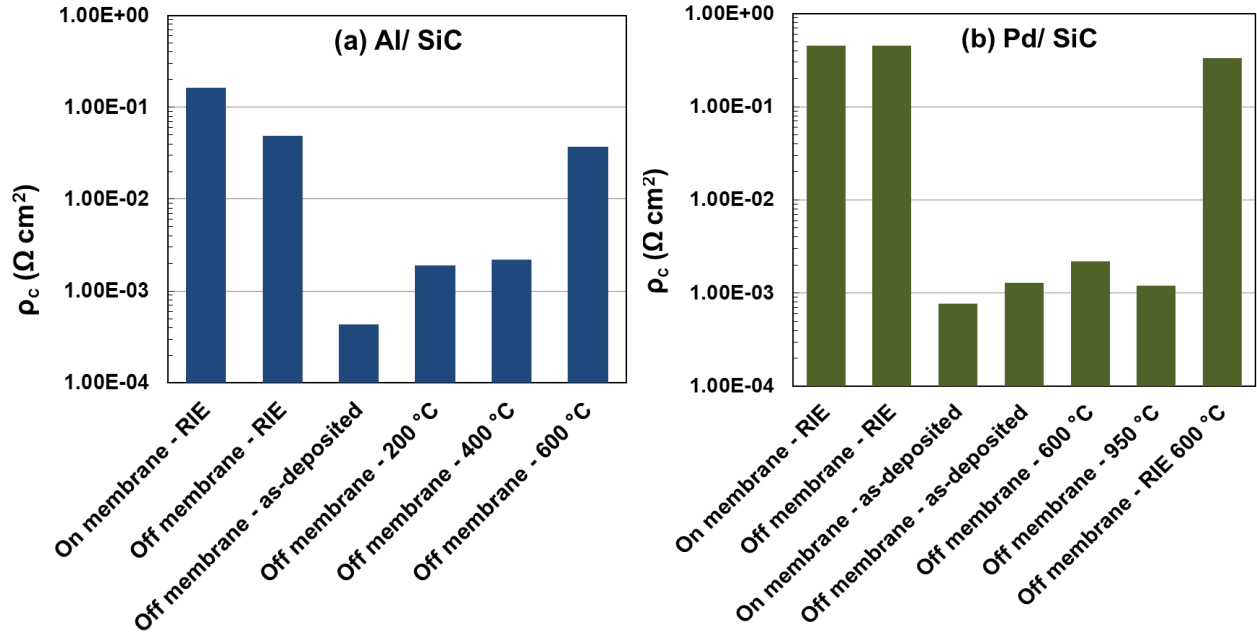


Figure 4.9: Measurements of  $\rho_c$  for a) Al/SiC and b) Pd/3C-SiC contacts located both on and off the membranes, with pre-treatment by RIE or KOH solutions and after annealing.

Figure. 4.9 (a) and (b) summarise the measurements of  $\rho_c$  for a range of Al/SiC and Pd/3C-SiC contacts, respectively. The results in Figure 4.9 (a) show that Al/3C-SiC contacts which were pre-exposed to reactive ion etching in a  $\text{CF}_4$  plasma were significantly higher in  $\rho_c$  than as-grown and KOH etched surfaces of 3C-SiC. This trend was evident for contacts formed both on and off the membrane. For example, the measured value of  $\rho_c$  of  $2 \times 10^{-4} \Omega \text{ cm}^2$  for Pd/3C-SiC contacts on as-deposited SiC off the membrane was  $\sim 3$  orders of magnitude lower than  $\rho_c$  with pre-treatment by RIE ( $3 \times 10^{-1} \Omega \text{ cm}^2$ ). The high value of  $\rho_c$  is consistent with the formation of a fluorocarbon film as previously reported during reactive ion etching of  $\text{SiO}_2$  in  $\text{CF}_4$  plasmas [23].

These results show that the protection of the upper surface of the membrane was a necessary precaution during reactive ion etching of the backside recess by RIE. The implantation of fluorine ion or any other halogen elements (such as chlorine which is also commonly used for this process [24]) on the SiC surface due to the reactive ion etching process can also be avoided by micromilling as an alternative method.

Another feature evident in Figure 4.9 (a) and (b) is the absence of a trend in  $\rho_c$  between contacts which were located on the membrane and off the membrane. In Al/SiC contacts prepared using RIE, Figure 4.9 (a) shows that the value of  $\rho_c$  was lower for contacts off the membrane than on the membrane. In comparison, in Pd/SiC contacts on as-deposited surfaces, the measurements of  $\rho_c$  in Figure 4.9 (b) were lower on the membrane than off the membrane. For the CTLM patterns located on the membrane, the current flow was restricted through the metAl/3C-SiC contact interfaces and within the 3C-SiC layer. For CTLM patterns off the membrane, the potential for current flow through the SiC – Si heterojunction was apparently not a dominant factor in determining  $\rho_c$ .

The measurements in Figure 4.9 (b) for Pd/SiC contacts have shown that annealing of Pd/SiC contacts at 600-950 °C has not appreciably changed the measured value of  $\rho_c$ . Annealing at 600 °C has been previously associated with the formation of the Pd<sub>3</sub>Si phase at the interface [25] while Pd<sub>2</sub>Si was the dominant phase after annealing at 700-900 °C [22]. The value of  $\rho_c$  of  $1.2 \times 10^{-3} \Omega\text{cm}^2$  measured after annealing at 950 °C was slightly lower than the figure of  $6.3 \times 10^{-3} \Omega\text{cm}^2$  reported by Barda et al. for Pd/3C-SiC contacts ( $4.2 \times 10^{18} \text{ cm}^{-3}$ ) annealed at 950°C [26]. A temperature of 1150 °C was required to produce graphite as part of the interfacial reaction in order to achieve a minimum in  $\rho_c$  [22].

The lowest value of  $\rho_c$  measured for the Al/SiC contacts was  $4.3 \times 10^{-5} \Omega\text{cm}^2$  for an as-deposited sample off the membrane. In measurements performed on the as-deposited Al/3C-SiC contacts off the membrane on 5 different types of samples, the magnitude of  $\rho_c$  varied in the range  $4 \times 10^{-5}$  to  $8.9 \times 10^{-4} \Omega\text{cm}^2$  depending on the specific wafer. This range of values in  $\rho_c$  has been attributed to a variation in carrier density between the wafers. The results reported here were consistent with measurements of  $\rho_c = 1.8 \times 10^{-4} \Omega\text{cm}^2$  by Ito et al. for Al/3C-SiC contacts ( $n = 1.3 \times 10^{19} \text{cm}^{-3}$ ) [27]. Figure 4.9 (a) shows that in the Al/3C-SiC contacts, the value of  $\rho_c$  increased after annealing at 200-600 °C. Bazin et al have also previously reported a strong increase in  $\rho_c$  for Al/3C-SiC contacts at an annealing temperature of 600 °C [4]. Although the interface of these contacts was shown to remain relatively abrupt after annealing at 600 °C, the increase in  $\rho_c$  at this temperature was associated with the formation of blisters which developed in the Al metallization (Figure 4.10) [4].

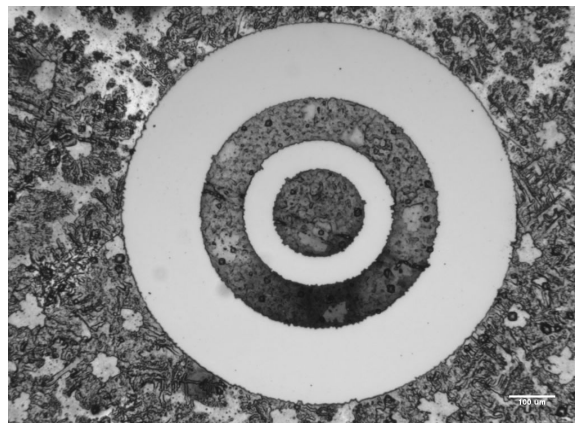


Figure 4.10: a) Formation of blisters after annealing Al at 600°C.

Figure 4.11 shows the specific contact resistance measured on as-deposited Al/3C-SiC contacts with either a partial or no etching of the Si substrate in 3 different wafers. In Figure 4.11, a variation in  $\rho_c$  from wafer to wafer was evident in the measurements. This variation has

been attributed to differences in carrier concentration and resistivity between the wafers. However, the value of  $\rho_c$  was similar for the etched and unetched samples in each wafer. Assuming that current flow occurred through the SiC – Si heterojunction and into the Si substrate, these results have shown that the thickness of the Si substrate below the SiC film was not a significant factor in determining  $\rho_c$ .

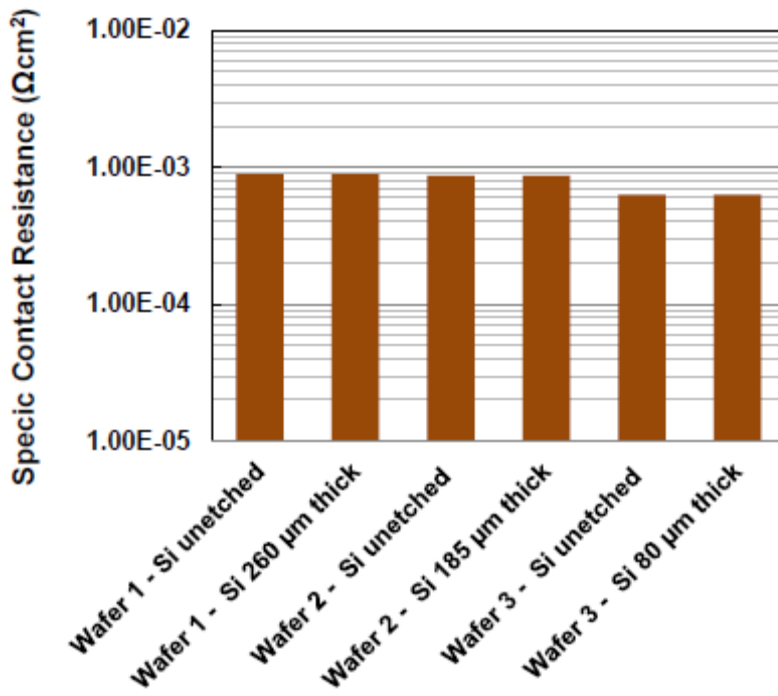


Figure 4.11: Measurements of  $\rho_c$  for as –deposited Al/3C-SiC contacts on wafers 1-3 with a partial etch through the Si substrate.



## 4.3 Analysis of the Substrate Influence on the Current Paths at the 3C-SiC/Si Interface

The effect of the Si substrate in determining  $\rho_c$  values was further investigated using the following two experiments:

- a) Probing the Al contacts on etched and unetched substrates
- b) Measurement of the sheet resistance,  $R_{sh}$  with linear TLM and comparing the  $R_{sh}$  of the Al/3C-SiC contacts which had no isolation, partial isolation and complete isolation. All the experiments were performed at room temperature.

### 4.3.1 Measurements of Two Symmetrical Contacts on Etched and Unetched Substrate

#### 4.3.1.1 Fabrication of Symmetrical Al Contact Patterns

Aluminium (600 nm) was deposited using electron beam evaporation to form metal contacts on the polished side of 3C-SiC/Si. The contacts were made on the surface of partially etched and unetched substrate (Figure 4.12). Arrays of symmetrical circular patterns were photolithographically patterned onto the surface of 3C-SiC/Si. The arrays of the circular pattern were extended across the etched Si substrate and on the surrounding wafer. The excess aluminium was removed by etching.

The distance between the circular contacts was made extra larger than the thickness of both the 3C-SiC layer and the substrate (approximately 650  $\mu\text{m}$ ) so that if there is any substrate effect,

the current would show its preferences to flow into the substrate. The amount of resistance would be equal for measurements on of etched and unetched substrate.

#### 4.3.1.2 Results and Analysis of the Measurements of Two Symmetrical Al Contacts on Etched and Unetched Substrates

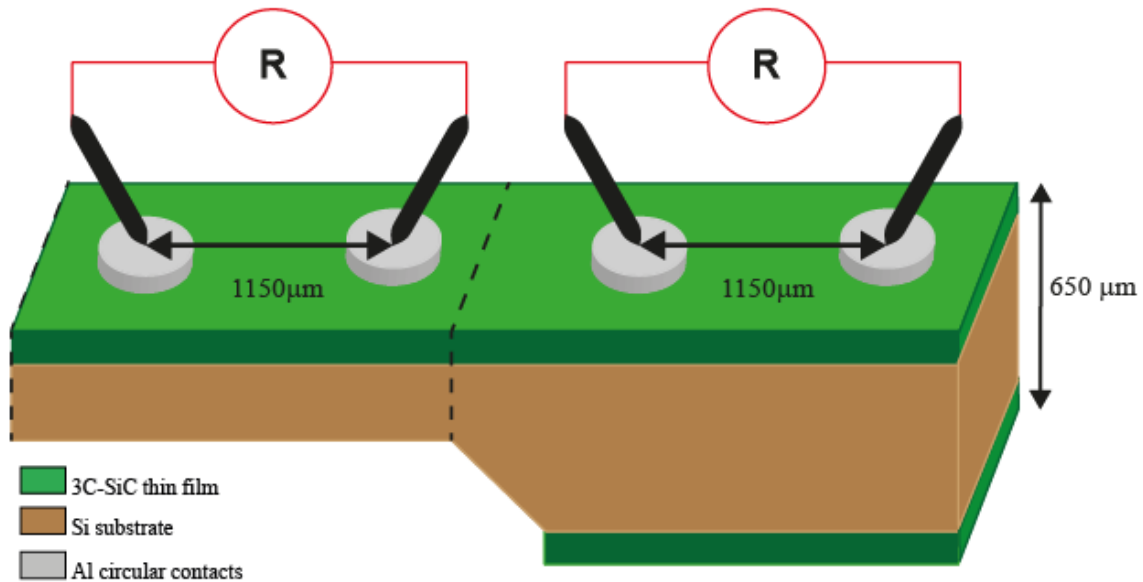


Figure 4.12: Schematic illustration showing the probing of aluminium circular patterns on the etched and unetched Si substrate to determine current leakage.

The current-voltage (I-V) characteristics of the aluminium contact systems were obtained using a Keithley I-V curve tracer. Measurements of resistance were made on the aluminium contacts on the unetched and etched portion of the Si substrate. This preliminary test is used to determine the substrate effect on this system. In each case, the as-deposited aluminium contacts were ohmic in I-V response. Both contacts show the same linearity in the I-V responses and revealed similar resistance values of  $3000 \Omega$  in the  $\pm 0.5V$  region.

The current showed preference to flow through the 3C-SiC layer only even at a very large gap between two metal contacts. Similar behaviours were observed for all the samples of different etched thicknesses and contact distances. This observation confirms that the current flows for both contacts were restricted through the aluminium/3C-SiC contact interfaces and within the 3C-SiC layer. Any current flow through the conducting Si substrate would result in decreasing of the resistance value if substrate affect occurred has a lower resistance.

The measurement of sheet resistance ( $R_{sh}$ ) is used to confirm the I-V curve measurements which were performed. Two methods were used to determine the  $R_{sh}$  and the results of these two methods were compared. Similar values of sheet resistance would confirm that no direct influence of substrate would have an effect on the electrical behaviour of 3C-SiC.

### **4.3.2 Measurements of $R_{sh}$ with Linear TLM**

#### **4.3.2.1 Fabrication of Linear TLM**

In this method, a linear Transmission Line Model (TLM) pattern which consisted of a rectangular mesa and four Al rectangular metal pads with dimensions of 6 mm×2 mm was made photolithographically and etched. Pads spacing (corresponding to  $L_1$ ,  $L_2$  and  $L_3$  in Figure 4.13) were made in between.

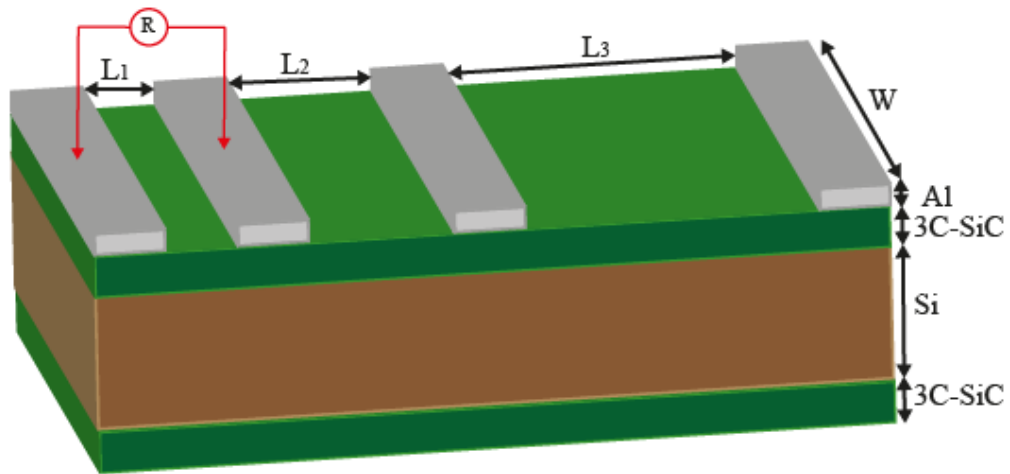


Figure 4.13: 3C-SiC chip with different gaps length of Al pads for measuring the sheet resistance.

For the second method, Al metal pads with 7 mm×2 mm area were made photolithographically at both sides of the mesa. Later, five smaller Al pads with the widths of 4 mm, 2 mm, 1.5 mm, 1 mm and 0.5 mm were formed from the etching of the singular metal pads and its 3C-SiC mesa layer were shallowly diced to create a trench of 10 μm depth. Resistances were measured between the two Al contacts. Complete isolation was made by dicing through the trenches to produce Al pads on 3C-SiC mesa strips. The procedures are shown in detail in Figure 4.14.

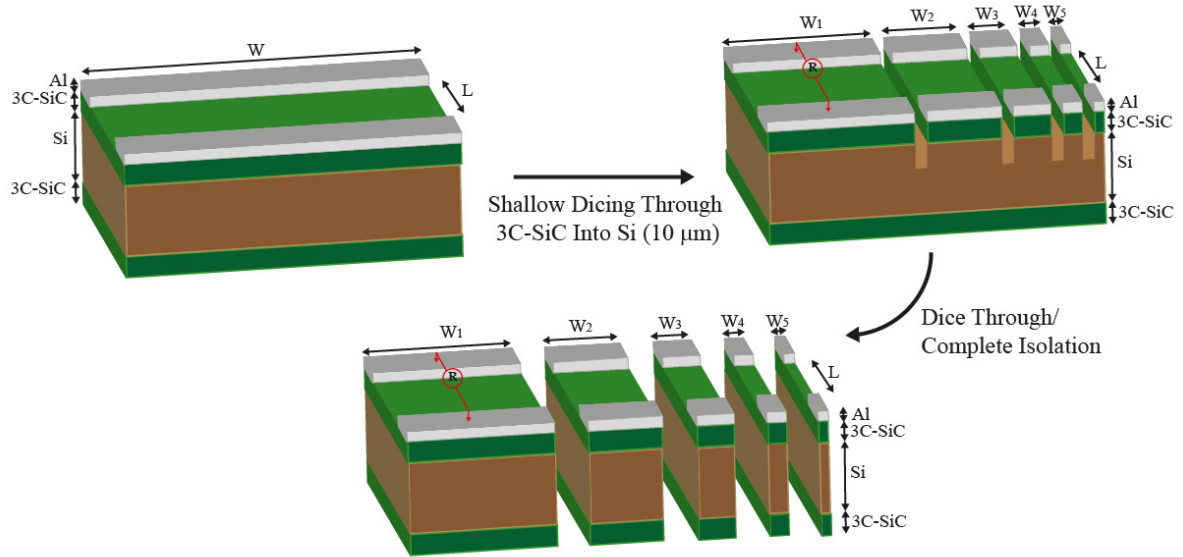


Figure 4.14: Schematic diagram describing the fabrication process of obtaining samples to measure sheet resistance by shallow isolation of the 3C-SiC thin film from the substrate and complete dicing of the samples.

#### 4.3.2.2 Results and Analysis of the $R_{sh}$ Measurements

The  $R_{sh}$  in the first method was determined using the following equation [28]:

$$R_T = 2R_C + R_{sh} \frac{L}{W} \quad (1)$$

where

$R_T$ = Total resistance

$R_C$ = Contact resistance

$L$ =Length

$W$ = Width

$R_T$  which is a function of the pad's spacing was measured between the pads. The contact resistance,  $R_C$ , is obtained from the intercept of the graph and the Y-axis as shown in Figure 4.15.

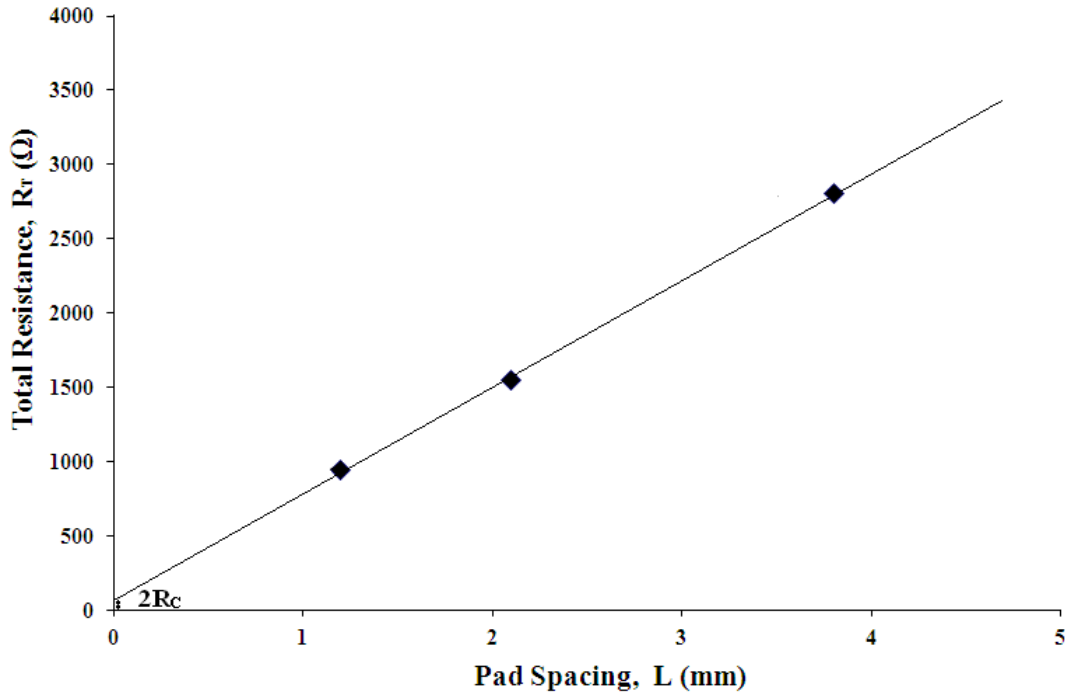


**Figure 4.15:** A linear graph representing a plot of total resistance,  $R_T$ , against pad spacing. The value of  $2R_C$  is obtained from the intercept of the plotting at Y axis.

The  $R_{sh}$  calculated from the measurements of all the pads spacing had given a constant value of  $3000 \Omega/\square$ . This value from the first method was used as a reference.

For the second method, the  $R_{sh}$  of both the shallowly and completely diced 3C-SiC mesa with Al pads was calculated using the following equation:

$$R_T = R_{sh} \frac{L}{W} \quad (2)$$

The values of  $R_{sh}$  for the shallowly diced mesas and the strips with different widths were constant and similar to the previous measurements which were  $3000 \Omega/\square$ . The first method had given the value which might be influenced by the substrate since no isolation was made. Thus, the second method had verified the previous observation where there was no alternative current path through the substrate by first isolating the mesas from the Si and later diced them through

which gave a complete isolation. Lower  $R_{sh}$  was expected for the first method compared to the others if there was any leakage current flowing into the substrate. If the resistance is higher for the 3C-SiC epitaxial layer, the current would show preferences to flow into the substrate. However, the experiments in this cases showed that it was favourable for the current to flow in the 3C-SiC film. Figure 4.16 illustrated the current paths for the metal/3C-SiC where no current leakage occurred during the experimental procedures.

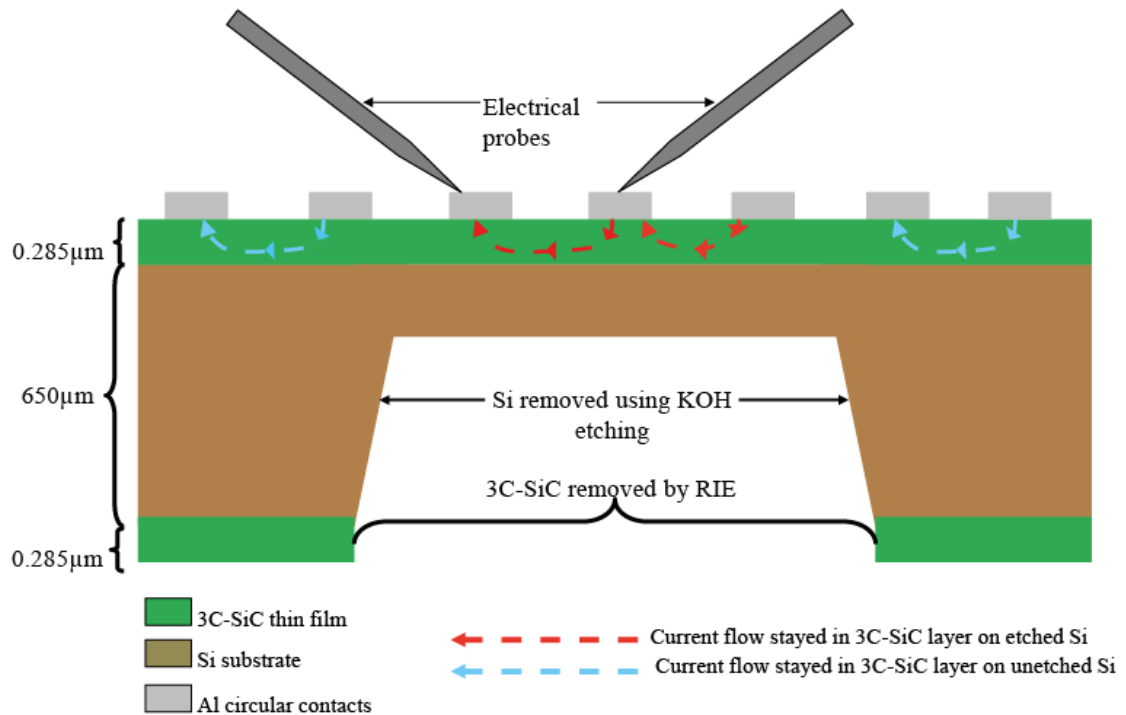


Figure 4.16: Schematic illustration of the membrane showing the current paths for contacts located on the etched and unetched Si substrate. The current shows preference to flow in the epitaxial layer of 3C-SiC rather than leaking into the substrate.

## 4.4 Conclusions

Arrays of dot, ring and circular TLM patterns have been successfully lithographically patterned on the upper surface of 3C-SiC films. Reactive ion etching significantly altered the stoichiometry of the SiC surface and altered the behaviour of the 3C-SiC current-voltage response. Thus, reactive ion etching using fluorinated plasma should be avoided for obtaining metal ohmic contact either by protecting the surface of interest or the use of micromilling to remove portion of 3C-SiC. However, not all material which is fluorinated plasma etched such as Indium Phosphide (InP) showed the same ohmic contact degradation [29]. For both the Al/3C-SiC and Pd/3C-SiC systems, the as-deposited and annealed contacts were ohmic in current/voltage response. However, there was nonlinearity of the I-V characteristics for the contacts off the membrane. The measurements have shown no clear difference in  $\rho_c$  between the contacts located on the membranes and off the membranes. Thus, the presence of the 3C-SiC/Si heterojunction in contacts off the membrane was not a factor in determining  $\rho_c$ . Measurements of  $\rho_c$  for Al/3C-SiC and Pd/3C-SiC contacts with pre-treatment by reactive ion etching in  $\text{CF}_4$  plasma were 3 orders of magnitude higher ( $\rho_c = 2 \times 10^{-1} \Omega\text{cm}^2$ ) than for as-grown SiC or KOH treated surfaces ( $\rho_c = 4 \times 10^{-5} - 8.9 \times 10^{-4} \Omega\text{cm}^2$ ). Annealing of Al/3C-SiC contacts has resulted in a progressive increase in  $\rho_c$  with increase in temperature to 600 °C.



As a summary the resistivity measured in this thesis is tabulated against the resistivity measurements in literatures:

<b>Resistivity Values from Literature</b>	<b>Resistivity Values Measured</b>	<b>Deposited Metal</b>	<b>Annealing Temperature</b>
$1.5 \times 10^{-4} \Omega \cdot \text{cm}^2$	$1.5 \times 10^{-4} \Omega \cdot \text{cm}^2$ <sup>[19]</sup>	Ni/Ti	950°C
$1.2 \times 10^{-3} \Omega \text{cm}^2$	$6.3 \times 10^{-3} \Omega \text{cm}^2$ <sup>[26]</sup>	Pd	950°C
$4.3 \times 10^{-5} \Omega \text{cm}^2$	$1.8 \times 10^{-4} \Omega \text{cm}^2$ <sup>[27]</sup>	Al	0°C

Table 4.1 Resistivity values measured compared to the resistivity values in literatures

The substrate effect on the electrical characteristic properties of 3C-SiC/Si can be neglected at room temperature. The current flow was restricted at the metal contact/3C-SiC junction and the epitaxial layer of 3C-SiC without leaking into the Si substrate. Constant resistance values for the resistance measurements for the I-V responses on etched and unetched substrate and the same values of  $R_{sh}$  for various samples indicates the current preference to flow in the 3C-SiC layer. This finding verifies previous electrical characterization results [4, 30-34] obtained from the ohmic contacts on the 3C-SiC/Si system which undermined the influence of the Si substrate. However, the application 3C-SiC membrane to determine its electrical characteristics (especially the ohmic contact Transmission Line Model (TLM) test structure parameters) is the best way to eliminate any possibility of leakage current into the substrate for this type of system.

## 4.5 References

- [1] L. M. Porter and R. F. Davis, "A critical review of ohmic and rectifying contacts for silicon carbide," *Materials Science and Engineering B*, vol. 34, pp. 83-105, 1995.
- [2] L. Chen, "Silicon Carbide Pressure Sensors and Infra-Red Emitters," Doctor of Philosophy Dissertation, Department of Materials Science and Engineering, Case Western University, 2008.
- [3] Y. Kondo, T. Takahashi, K. Ishii, Y. Hayashi, E. Sakuma, S. Misawa, H. Daimon, M. Yamanaka, and S. Yoshida, "Experimental 3C-SiC MOSFET," *Electron Device Letters, IEEE*, vol. 7, pp. 404-406, 1986.
- [4] A. E. Bazin, J. F. Michaud, F. Cayrel, M. Portail, T. Chassagne, M. Zielinski, E. Collard, and D. Alquier, "High Quality Ohmic Contacts on n-type 3C-SiC Obtained by High and Low Process Temperature," *AIP Conference Proceedings*, vol. 1292, pp. 51-54, 2010.
- [5] C. Koliakoudakis, J. Dontas, S. Karakalos, M. Kayambaki, S. Ladas, G. Konstantinidis, S. Kennou, and K. Zekentes, "Fabrication and characterization of Cr-based Schottky Diode on n-type 4H-SiC," vol. 615 617, ed. Barcelona, 2009, pp. 651-654.
- [6] C. Koliakoudakis, J. Dontas, S. Karakalos, M. Kayambaki, S. Ladas, G. Konstantinidis, K. Zekentes, and S. Kennou, "Cr/4H-SiC Schottky contacts investigated by electrical and photoelectron spectroscopy techniques," *Physica Status Solidi (A) Applications and Materials Science*, vol. 205, pp. 2536-2540, 2008.
- [7] R. Yakimova, C. Hemmingsson, M. F. Macmillan, T. Yakimov, and E. Janzén, "Barrier height determination for n-type 4H-SiC Schottky contacts made using various metals," *Journal of Electronic Materials*, vol. 27, pp. 871-875, 1998.

- [8] D. K. Schroder, "Semiconductor Material and Device Characterization," 3rd ed New Jersey, USA: John Wiley & Sons, 2006, pp. 127-184.
- [9] G. K. Reeves, "A New Technique for the Measurement of Specific Contact Resistance," Telecom Australia, Clayton, Victoria, Australia 14 February 1980.
- [10] J. W. Palmour, R. F. Davis, T. M. Wallett, and K. B. Bhasin, "Dry etching of  $\beta$ -SiC in  $\text{CF}_4$  and  $\text{CF}_4+\text{O}_2$  mixtures," *Journal of Vacuum Science & Technology A: Vacuum, Surfaces, and Films*, vol. 4, pp. 590-593, 1986.
- [11] J. W. Palmour, "Dry etching of silicon carbide," United States of America Patent 4981551, 1 January 1991, 1991.
- [12] A. Baharin, R. S. Pinto, U. K. Mishra, B. D. Nener, and G. Parish, "Low contact resistance to plasma-etched p-type GaN," *Electronics Letters*, vol. 47, pp. 342-343, 2011.
- [13] A. Baharin, R. S. Pinto, U. K. Mishra, B. D. Nener, and G. Parish, "Low resistivity contacts to plasma etched Mg-doped GaN using very low power inductively coupled plasma etching," *Thin Solid Films*, vol. 519, pp. 3686-3689, 2011.
- [14] M. Bhaskaran, "Synthesis and Characterisation of Silicide Thin Films for Evaluation of Specific Contact Resistivity of Multi-layered Silicon-based Ohmic Contacts," Doctor of Philosophy, School of Electrical and Computer Engineering, RMIT University, Melbourne, Australia, 2009.
- [15] G. S. Marlow and M. B. Das, "The effects of contact size and non-zero metal resistance on the determination of specific contact resistance," *Solid-State Electronics*, vol. 25, pp. 91-94, 1982.
- [16] G. K. Reeves, "Specific contact resistance using a circular transmission line model," *Solid State Electronics*, vol. 23, pp. 487-490, 1980.

- [17] D. Zhuang and J. H. Edgar, "Wet etching of GaN, AlN, and SiC: A review," *Materials Science and Engineering R: Reports*, vol. 48, 2005.
- [18] L. M. Porter and F. A. Mohammad, "Review of Issues Pertaining To The Development of Contacts To Silicon Carbide," in *Silicon Carbide Microelectromechanical Systems for Harsh Environments*, R. Cheung, Ed., 1st ed London: Imperial College Press, 2006.
- [19] B. Barda, P. Macháč, M. Hubičková, and J. Náhlík, "Comparison of Ni/Ti and Ni ohmic contacts on n-type 6H-SiC," *Journal of Materials Science: Materials in Electronics*, vol. 19, pp. 1039-1044, 2008.
- [20] W. Lu, W. E. Collins, and W. C. Mitchel, "Material Selection and Interfacial Reaction in Ohmic-Contact Formation on SiC," in *SiC Power Materials*, Z. C. Chen, Ed., ed, 2004, pp. 303-338.
- [21] L. Kassamakova, R. D. Kakanakov, I. V. Kassamakov, N. Nordell, S. Savage, B. Hjörvarsson, E. B. Svedberg, L. Abom, and L. D. Madsen, "Temperature stable Pd ohmic contacts to p-type 4H-SiC formed at low temperatures," *IEEE Transactions on Electron Devices*, vol. 46, pp. 605-611, 1999.
- [22] C. S. Pai, C. M. Hanson, and S. S. Lau, "X-ray diffraction and ion backscattering study of thermally annealed Pd/SiC and Ni/SiC," *Journal of Applied Physics*, vol. 57, pp. 618-619, 1985.
- [23] G. S. Oehrlein, Y. Zhang, D. Vender, and O. Joubert, "Fluorocarbon high density plasmas II silicon dioxide and silicon etching using CF<sub>4</sub> and CHF<sub>3</sub>," *Journal of Vacuum Science & Technology A: Vacuum, Surfaces, and Films*, vol. 12, pp. 333-344, 1994.

- [24] V. Khemka, T. Chow, and R. Gutmann, "Effect of reactive ion etch-induced damage on the performance of 4H-SiC schottky barrier diodes," *Journal of Electronic Materials*, vol. 27, pp. 1128-1135, 1998.
- [25] E. V. Kalinina, G. F. Kholuyanov, A. V. Shchukarev, N. S. Savkina, A. I. Babanin, M. A. Yagovkina, and N. I. Kuznetsov, "Pd ohmic contacts to p-SiC 4H, 6H and 15R polytypes," *Diamond and Related Materials*, vol. 8, pp. 1114-1117, 1999.
- [26] B. Barda, P. Machac, S. Cichon, V. Machovic, M. Kudrnova, A. Michalcova, J. Siegel, "Origin of ohmic behavior in Ni, N<sub>2</sub>Si and Pd contacts on n-type SiC", *Applied Surface Scienc*, vol. 257 pp. 414-422, 2010.
- [27] K. Ito, T. Onishi, H. Takeda, K. Kohama, S. Tsukimoto, M. Konno, Y. Suzuki, and M. Murakami, "The simultaneous formation of Ni/Al ohmic contacts to both n- and p-type 4H-SiC," *Journal of Electronic Materials*, vol. 37, pp. 1674-1680, 2008.
- [28] G. K. Reeves and H. B. Harrison, "Obtaining the specific contact resistance from transmission line model measurements," *Electron Device Letters, IEEE*, vol. 3, pp. 111-113, 1982.
- [29] S. Kim and I. Adesida, "0.15- $\mu$ m-Gate InAlAs/InGaAs/InP E-HEMTs utilizing Ir/Ti/Pt/Au gate structure," *IEEE Electron Device Letters*, vol. 27, pp. 873-876, 2006.
- [30] J. Wan, M. A. Capano, and M. R. Melloch, "Formation of low resistivity ohmic contacts to n-type 3C-SiC," *Solid-State Electronics*, vol. 46, pp. 1227-1230, 2002.
- [31] G. Constantinidis, N. Kornilios, K. Zekentes, J. Stoemenos, and L. di Cioccio, "High temperature ohmic contacts to 3C-SiC grown on Si substrates by chemical vapor deposition," *Materials Science and Engineering: B*, vol. 46, pp. 176-179, 1997.

- [32] C. Jacob, P. Pirouz, H. I. Kuo, and M. Mehregany, "High temperature ohmic contacts to 3C-silicon carbide films," *Solid-State Electronics*, vol. 42, pp. 2329-2334, 1998.
- [33] O. Chang-Min and C. Gwiy-Sang, "Ohmic Contacts of Polycrystalline 3C-SiC Thin-Films Grown on Si (100) Wafers for Microsensors of Vehicle Engines," in *Strategic Technology, The 1st International Forum on*, 2006, pp. 301-304.
- [34] J. I. Noh, K. S. Nahm, K. C. Kim, and M. A. Capano, "Effect of surface preparation on Ni ohmic contact to 3C-SiC," *Solid-State Electronics*, vol. 46, pp. 2273-2279, 2002.

# Chapter 5

## **Biocompatibility and Hemocompatibility Assessment of 3C-Silicon Carbide Thin Films**

BioMEMS devices are required to be made with materials that are biocompatible and hemocompatible. In this chapter, the biocompatibility of i) as grown 3C-SiC thin films, ii) treated with KOH solution and iii) treated both with plasma gasses and KOH solution were investigated by means of optical micrographs and Electron Scanning Electron Microscopy (SEM) of the cell's morphological structure, cell counting and cell viability assessment using Trypan Blue exclusion assay, MTT assay and PrestoBlue™ reagent. Hemolytic activity of

human red blood cells (hRBC) with 3C-SiC was used to assess 3C-SiC thin films' hemocompatibility.

## 5.1 Introduction

The assessment of 3C-SiC (treated and non-treated) performed in this chapter is based on internationally accepted standards. The definitions of biocompatibility set by The Medical Device Directive (MDD) and the Active Implantable MDD (AIMDD) of the European Commission are used. To meet those standards the material should be free from imposing toxicity to the cells, from irritating the surrounding tissue in which it has been implanted and from inducing carcinogenic effects [1]. Hemocompatibility is generally defined as the suitability of the material to be used for blood contacting applications [2].

Apart from investigating live cells by observing cells structure and morphology through observation of micrographs, biocompatibility is investigated by using assays commonly used in life science studies such as Trypan Blue exclusion assay, MTT assay and PrestoBlue assay. Trypan blue determines cell viability by utilizing the ability of living cell membranes to exclude trypan blue dye, as opposed to a dead cell which has no such ability [3].

Yellow tetrazolium salt 3-(4, 5-dimethylthiazol-2-yl)-2, 5-diphenyltetrazolium bromide (MTT) (Invitrogen) assay is a conventional assay that is widely used to detect cell viability and cell cytotoxicity on the basis of detecting the conversion of yellow tetrazolium salt of the reagent by the viable cell into insoluble purple formazan [4-7]. In order to solubilize the formazan, dimethyl sulfoxide (DMSO) or isopropan-2-ol (IPA) is added to determine the absorbance of the solutions spectrophotometrically [4, 5]. PrestoBlue<sup>TM</sup> reagent is a resazurin based solution used



to quantitatively measure cell viability by determining the level of cellular metabolic activity of living cells [8-10]. It is a state of the art cell viability reagent which has less protocol, much rapid than MTT assay and the most important aspect, it has limited side effect on the tested cells [11]. PrestoBlue™ is a new type of cell viability assay, which has been introduced recently where no scientific publication published as the state of the art assay used to be used for cell viability quantitative measurement. In this chapter, the author reports the finding obtained (using the MTT and PrestoBlue™ assays) for cell viability studies.

The hemocompatibility assessment was conducted by adapting protocol outlined by Chanda et al. [12], where the samples of interest were exposed directly to the suspended human red blood cells. Thus, the hemocompatibility quality of 3C-SiC in comparison to Si is determined.

## **5.2 Experimental**

### **5.2.1 Basic Cell Culture Technique**

The mammalian cell lines used in this work are the Chinese hamster ovary (CHO) cells. CHO cell line was chosen due to its robustness and easiness to culture [13]. Stocks of CHO cell lines were cultivated in sufficient amount required to conduct the experimental investigation. The cells which were kept under liquid nitrogen (-273°C), were resuscitated by subculturing them in a mixture of medium, buffer, serum and antibiotics in accordance to the American tissue-type culture collection (ATTC) standard.

The medium used in experiments was Dulbecco's Modified Eagle Medium (Gibco®) added with 2% HEPES (4-(2-hydroxyethyl)-1-piperazineethanesulfonic acid) which is a zwitterionic sulfonic acid buffer. The addition of HEPES was meant to assist in providing maximum buffering at the typical range of physiological pH [14, 15]. The media was also supplemented

with filtered 10% Fetal Bovine Serum (FBS) (Interpath), which is essential for promotion of animal cells' growth and proliferation [16]. Antibiotic (Penicillin/ Streptomycin) (Invitrogen) was added last to the cell and mixtures to prevent bacterial contamination of the culture [15]. The CHO cell lines were cultured in 75 cm<sup>2</sup> cell culture flasks for 24 hours at 37°C in the atmosphere containing 5% CO<sub>2</sub> and 95% relative humidity. After 24 hours of culture, the cell lines were studied using optical microscopy. Only the cells reached a confluency of 90% in their growth, can be used for further experimentation. Later, optical microscopy was used to provide qualitative assessment of the proliferation and adhesion of the cells on the materials. The ability of the cells to continuously proliferate after detachment from the materials was also observed in this experimental evaluation.

### 5.2.2 Cell Counting

These are the details of the materials used for the cell counting and cell viability tests:

1. Rectangular Thermanox<sup>TM</sup> coverslips with external dimensions, 10.5×22mm, (pretreated for tissue culture application) as positive control
2. Thermanox<sup>TM</sup> coverslips treated with Bovine Serum Albumin (BSA) as negative control
3. <100> Silicon (Si) samples
4. 3C-SiC grown epitaxially on Si<100> (3C-SiC/Si) samples
5. 3C-SiC/Si samples treated by dipping in potassium hydroxide (KOH) solution for 28 hours at 80°C
6. 3C-SiC/Si samples treated with reactive ion etching (RIE) and KOH dipping. These samples were plasma etched by RIE with base pressure ranging from 73 to 86 mTorr and the RF power applied was 100W for 5 minutes using 14.1/4.7 sccm of

tetrafluoromethane/oxygen (CF<sub>4</sub>/O<sub>2</sub>). Later, the samples were immersed in KOH at 80°C for 28 hours. These procedures were used previously to fabricate 3C-SiC membranes.

Before any treatment, all the samples were rinsed with acetone, IPA and deionized (DI) water and later dipped in hydrofluoric (HF) acid for 30 seconds to remove natural oxide. The samples were diced into 10.5mm ×22mm similar to Thermanox™ coverslips shape and size. The samples were sterilized by double autoclaved (121°C) and treated with ultraviolet light (UV) radiation for 15-20 minutes prior to work.

All the samples were tested in triplicates and each experiment was repeated three times. The cells were subcultured on the materials placed in 6 well cell culture plates (Greiner, # 657 185). Approximately 2 ml of stock solution of media together with 1.0 ×10<sup>5</sup> cells/ml were seeded to each well containing the materials. Prior to the seeding, the amount of cells was determined by Trypan blue exclusion staining technique. The cells (10 μl) were stain with Trypan blue dye (10 μl) and subsequently the CHO cells were counted using Countess® Automated Cell Counter (Invitrogen). The seeded cell culture plates were then incubated at 37°C and 5% CO<sub>2</sub> overnight.

After incubation, the cells were studied using optical microscope. This procedure provides the qualitative data assessment of cells' behavior prior to the quantitative testing such as cell counting and viability tests. The cells from each well with different materials were trypsinized (100 μl) for detachment and later were subcultured in 6 well plates for overnight. The cells growth and proliferation were observed by optical microscopy. The live cells were counted to determine their viability after detachment from the materials. These cells were cultured later for 24 hours to measure their viability using MTT (Invitrogen) assay and Prestoblu<sup>TM</sup> Cell Viability reagent (Invitrogen, USA) assay.

### **5.2.3 Cell Viability Studies**

In cell viability studies, 100  $\mu\text{l}$  of solution consisted of media and antibiotics with approximately  $1.0 \times 10^3$  CHO cells from the previous cell counting test were seeded to the wells of 96 well cell culture plates (Greiner, # 655 180) and incubated at  $37^\circ\text{C}$  and 5%  $\text{CO}_2$  overnight. Two 96 well culture plates were prepared for MTT assay test and Prestoblu<sup>TM</sup> Cell Viability reagent (Invitrogen, USA) test. These cells were earlier cultured on different materials as described in the previous section.

#### **5.2.3.1 MTT Assay Test**

MTT assay was prepared prior to the experiment by adding 1 ml of PBS to 5 mg of MTT powder in a vial and mixed uniformly by vortexing for 2 minutes to dissolve the particles. The remaining undissolved particles were removed by filtering with microfilters (pore size  $22\mu\text{m}$  diameter). The MTT assay was used immediately after preparation or stored at  $-20^\circ\text{C}$  before experiment. Due to its light sensitivity, MTT assay vial or tube was wrapped with aluminum foil and kept away from light source [4].

The plated cells, previously incubated overnight at  $37^\circ\text{C}$  and 5%  $\text{CO}_2$ , were added with 20  $\mu\text{l}$  of MTT assay. The plate was covered with the aluminum foil to protect MTT from light and it was agitated with the plate shaker for 5 minutes to ensure the MTT mixed uniformly with the cells mixture. Subsequently, it was incubated for 4 hours at  $37^\circ\text{C}$  and 5%  $\text{CO}_2$  and later, 25  $\mu\text{l}$  of the mixtures were removed from the plated cells. Insoluble purple formazan were formed and then dissolved by adding 50  $\mu\text{l}$  of DMSO on each plated cell.

After that cells were incubated at 37°C and 5% CO<sub>2</sub> for 10 minutes. The absorbances or the optical density, OD of the dissolved formazan were taken at 595 nm. Experiments were performed in triplicates with each experiment repeated three times.

Cellular viability can be measured by equation (1):

$$\frac{(OD_{595} \text{ Sample} - OD_{595} \text{ Background})}{(OD_{595} \text{ Control Sample} - OD_{595} \text{ Background})} \times 100 \quad (1)$$

Cytotoxicity can be measured from the same data by modifying equation (1):

$$\left( 1 - \left( \frac{(OD_{402} \text{ Average (RBC in Water)} - OD_{402} \text{ (RBC with materials)})}{(OD_{402} \text{ (RBC in Water)} - OD_{402} \text{ (RBC in PBS)})} \right) \right) \times 100 \quad (2)$$

### 5.2.3.2 PrestoBlue™ Reagent Test

After overnight incubation, Prestoblue™ Cell Viability reagent (Invitrogen, USA) assay (10 µl) as supplied were added to the mixture and uniformly mixed by using the plate shaker for 5 minutes. The plate was incubated for 2 hours at 37°C and 5% CO<sub>2</sub> before measuring the absorbance at 595 nm and 630 nm. Each experiment was made in triplicates and the experiments were repeated three times. Cellular viability was measured by expression (1). The procedure and measurement was conducted according to the manufacturer's protocol (refer Appendix C).

### 5.2.4 Hemolysis Assay

Human red blood cell (hRBC) (2 ml) was collected from a healthy, female donor and Ethylene diaminetetraacetic acid (EDTA) was used as the anticoagulant. The blood was kept at 4°C prior to the experiment. In this experiment, 8 ml of Phosphate Buffer Saline (PBS) was added to 2 ml of human blood. Similar to the blood sample, the buffer was also refrigerated at 4°C. The mixture was centrifuged at 4°C and 1970 rpm until clear supernatant was produced.

Hemolysis was monitored by measuring the absorbance of the released hemoglobin at 405 nm by the plate reader. A solution of hRBC in water which produces 100% hemolysis was made and used as a reference. The solution was diluted until the optical density, (OD) of the hemolytic hRBC was equal to 1. The same concentration of hRBC in PBS was also made based on assumption that there is no hemolysis should occur. This solution subsequently was added to the studied materials before hemolytic activity is monitored. All of the buffers and solutions were kept in ice or refrigerated at 4°C.

Six pieces of materials, which included Si, untreated 3C-SiC/Si, KOH treated 3C-SiC/Si and 3C-SiC/Si treated with both KOH and reactive ion etched with CF<sub>4</sub>/O<sub>2</sub> were placed in 24 well cell culture plates. The tests were also performed in triplicates. 1 ml of RBC diluted in PBS was added to each well and incubated at 37°C and 5% CO<sub>2</sub> for 3 hours. Triplicates of 200 ul of solutions from each well were added to 96 well cell culture plate and the OD of each wells were read by the plate reader.

The hemocompatibility of the materials were calculated based on this formula:

$$\frac{(OD_{405} \text{ Average (RBC in Water)} - OD_{405} \text{ (RBC with materials)})}{(OD_{405} \text{ (RBC in Water)} - OD_{405} \text{ (RBC in PBS)})} \times 100 \quad (3)$$

### 5.2.5 Environmental Scanning Electron Microscopy (ESEM)

CHO cells cultured on the materials were investigated by using Environmental Scanning Electron Microscope (ESEM) (FEI Quanta 200 ESEM). Most of the observations were carried out at 30kV, spot size 5 except for the untreated 3C-SiC sample where the spot size used was 4.5. The magnifications were performed at 400× and 1200× to observe the cells morphology and structure.

Before using the ESEM, the cells must be fixed first. The reagents used were 4% paraformaldehyde (PFA) in water, 0.1 M phosphate-buffered saline (PBS) at pH 7.3 and graded series of ethanol (30%, 50%, 70%, 90% and 100%). These graded series of ethanol were made for cells dehydration. All the reagents and solution were kept at room temperature.

The procedure was modified from the protocol outlined by Carol et al. [17]. Firstly, the media was removed from the cell culture wells containing materials of interest. The cells attached to the materials were rinsed with PBS twice before 2 ml of 4% PFA fixative was added. The cells were left in the fixative for 20-30 minutes and after that, they were rinsed with PBS three times. A session of dehydrating the cells using series of ethanol grade was performed. This started with 30% and changed to solutions of 50%, 70% and 90%. Final dehydration sessions were made three times with 100% ethanol solution. Each session took about 15 minutes. The samples were air dried. Before using the ESEM, the samples were sputter coated with platinum (40 Å thick).

## 5.3 Results and Discussions

### 5.3.1 Basic Cell Culture Technique



Figure 5.1: Optical micrograph of CHO cells grown for 24 hours and reached 90% confluent at 4× magnifications. The cells were ready to be used for cell counting and cell viability tests.

CHO cells were incubated for 24 hours in the atmosphere containing 5% CO<sub>2</sub> with 95% relative humidity. In these conditions, the cells' growth can reach 90-95% of confluency. As shown in Figure 5.1, CHO cells proliferated and attached well to the surface of the tissue culture flask.

This indicated the healthy growth of the cells without stressing out. However, there were cells that were detached which can be seen as luminating spherical cells floating in the medium as shown in Figure 5.1. Fungal and bacterial contamination should be avoided during the cell culturing which will affect the cell proliferation through competition of the nutrients uptake.



## 5.3.2 Optical Microscopy

### 5.3.2.1 Cell Lines Cultured on Materials

Figure 5.2 shows a good proliferation of CHO cells on the positive control. Most of the control's surface was covered by cells. In comparison, the cells showed preferences to grow on the coverslip than on the well's surface. The cells were flattened and spread with high confluency on the coverslip. Here, there were cells which were detached from the surface and floating in the medium.

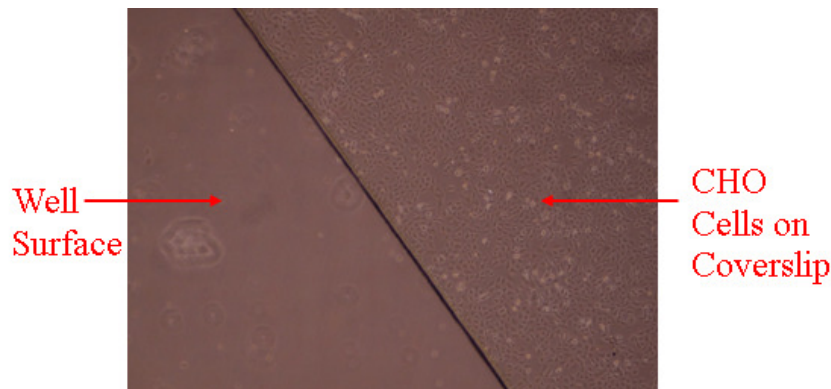


Figure 5.2: Optical micrograph of CHO cells cultured overnight on Thermanox™ Coverslip (positive control) at 4 × magnifications.

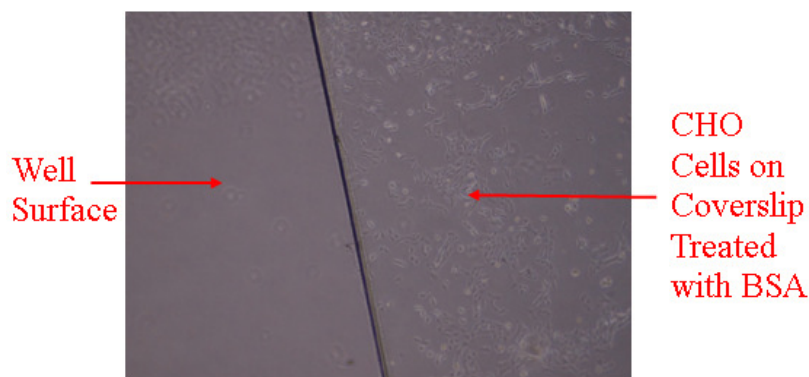


Figure 5.3: Optical micrograph of CHO cells cultured overnight on Thermanox™ Coverslip treated with Bovine Serum Albumin (BSA) (negative control) at 4× magnifications.

Fewer cells proliferated on the negative control coverslip as in Figure 5.3. Although, the cells were flattened on the negative control's surface, but, more cells observed to be more elongated in

appearance. The cells grown on the negative control were more stressed out compared to the cells cultured on the positive control.

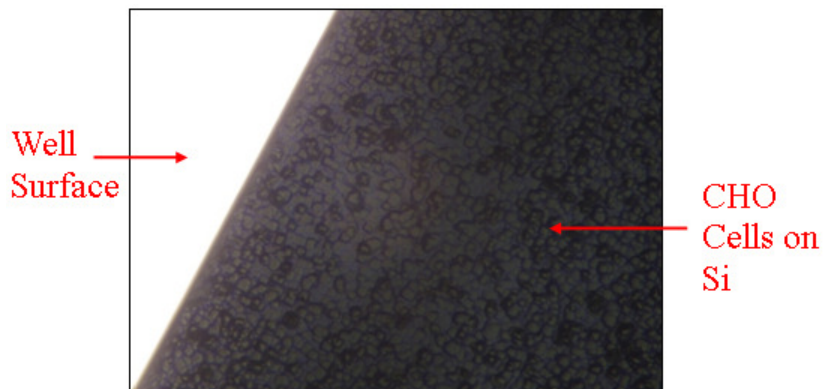


Figure 5.4: Optical micrograph of CHO cells cultured overnight on Si at 20× magnifications.

Here, the cells were more spherical in comparison to the cells on controls. A good proliferation and adhesion is indicated usually by stellar shape of the cells rather than spherical [5, 18, 19]. Thus, there were less contact area between the cells and Si which indicate lower biocompatibility quality of Si [5, 18, 19].



Figure 5.5: Optical micrograph of CHO cells cultured overnight on 3C-SiC/Si untreated at 20× magnifications.

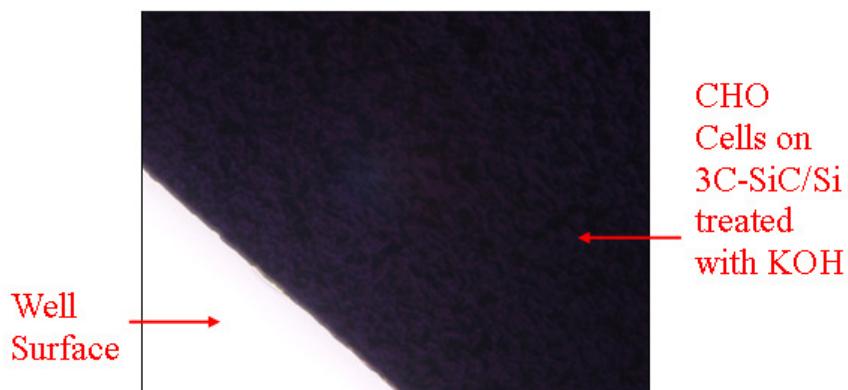


Figure 5.6: Optical micrograph of CHO cells cultured overnight on 3C-SiC/Si treated with KOH solution at 20× magnifications.

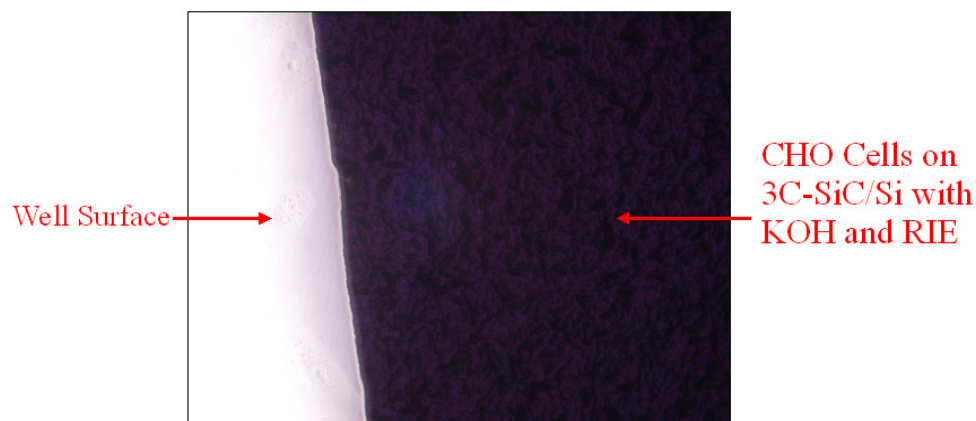


Figure 5.7: Optical micrograph of CHO cells cultured overnight on 3C-SiC/Si treated with KOH solution and reactive ion etching at 20× magnifications.

The cells subcultured on the 3C-SiC/Si samples (the untreated sample, KOH treated and reactive ion etched sample) were exhibiting similar morphology. The CHO cells were stellular and flattened while spreading radially over the material's surface. This morphology maximizes their contact area with the substrate as shown in the figures and indicates good proliferation and adhesion to the samples' surface [5, 18, 19]. This means the cells indiscriminately proliferated well and had similar shapes on all three type of 3C-SiC samples. It is important to note, that in all the cases, 3C-SiC/Si samples whether untreated or treated (chemically or physically) showed better biocompatibility than Si substrate.

### 5.3.2.2 Cell Lines Cultured on Plate Well Surface

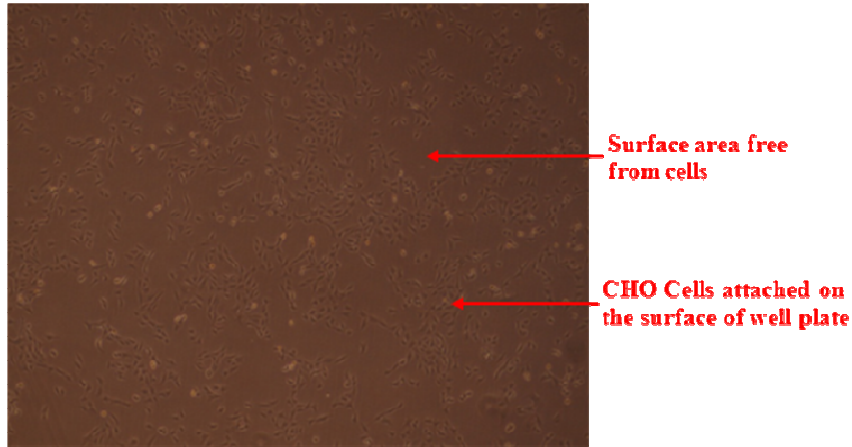


Figure 5.8: Optical micrograph of CHO cells cultured overnight on the 6 well plate surface previously subcultured on Thermanox™ Coverslip (positive control) at 4× magnifications.

Here, the CHO cells were removed from the coverslip and cultured on cell culture plates. In these experiments, the morphology and the structure of the cells in Figure 5.8 were used as positive control in comparison to other cells cultured subsequently after removal on the well. The cells were viable and showed similar structure as on the coverslip. The cells were elongated, spread radially, and flattened showing a good adhesion to the 6 well cell culture plates' surface. The cells proliferation was fast, that such high confluency level was achieved overnight.

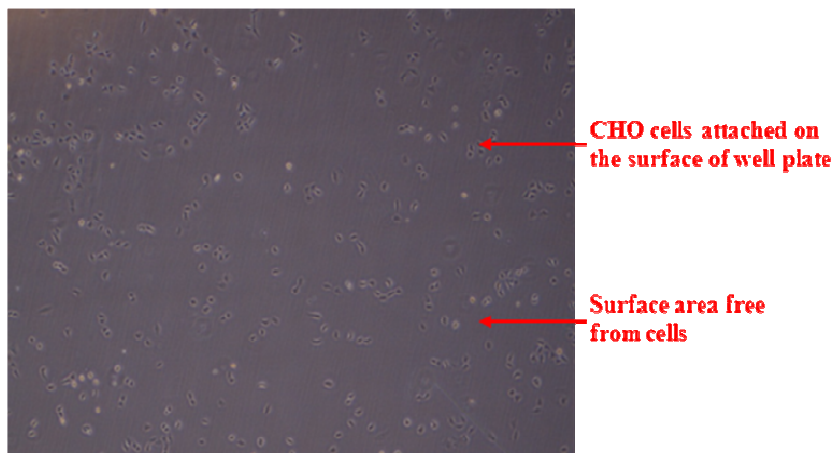


Figure 5.9: Optical micrograph of CHO cells cultured overnight on the 6 well plate's surface previously subcultured on Thermanox™ Coverslip treated with BSA (negative control) at 4× magnifications.

Here, CHO cells originally from BSA treated coverslip served as negative control. As can be seen from Figure 5.9, the cells proliferated lesser than the positive control exhibited by lesser amount of the surface covered by the cells. The cells were structurally more spherical indicating lesser tendency of them to adhere on the surface. In comparison to Figure 5.8, more floating luminating cells which represent dead cells can be seen in Figure 5.9. This agrees well with the dominating structures showed by the CHO cells in the optical micrograph.

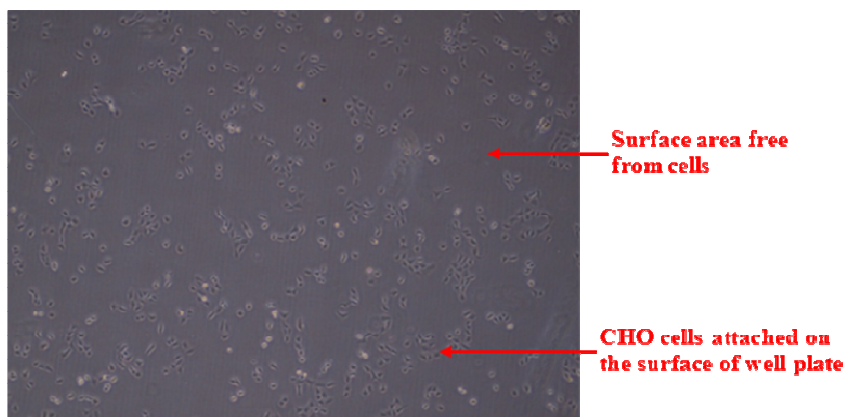


Figure 5.10: Optical micrograph of CHO cells cultured overnight on the 6 well plate's surface previously subcultured on Si at 4× magnifications.

CHO cells previously cultured on Si showed better amount and morphology than the cells originally from the negative control. Higher density of cells is apparent here (Figure 5.10) in comparison to Figure 5.9. More stellular cells are observed here, although significant amount of spherical cells were clearly visible.

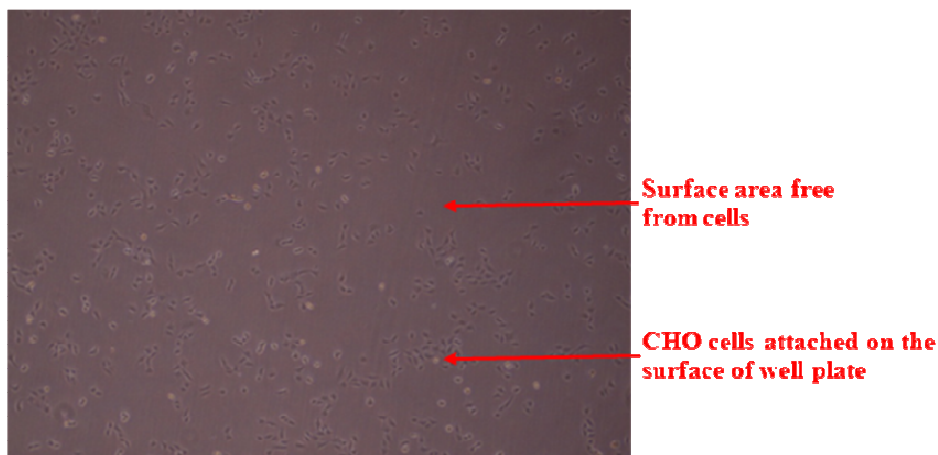


Figure 5.11: Optical micrograph of CHO cells cultured overnight on the 6 well plate's surface previously subcultured on 3C-SiC/Si untreated at 4× magnifications.

The cells subcultured from the untreated 3C-SiC/Si were more stellated and this type of cells predominated more than the spherical cells. Dead cells were apparently slightly lesser in comparison. However, no clear difference in cell density between cells originally from Si (Figure 5.10) and untreated 3C-SiC/Si (Figure 5.11) can be observed.

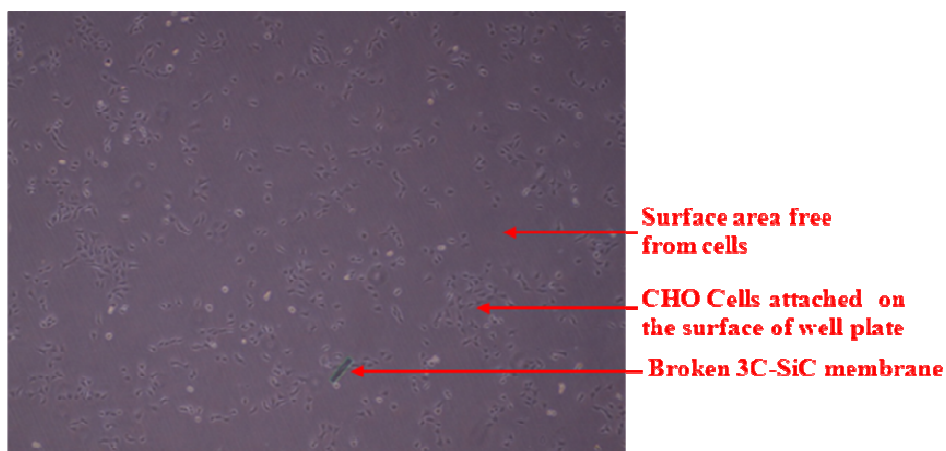


Figure 5.12: Optical micrograph of CHO cells cultured overnight on the 6 well plate's surface previously subcultured on 3C-SiC treated with KOH solution at 4× magnifications.

In Figure 5.12, higher cell density is observed in comparison to the cells from untreated 3C-SiC/Si (Figure 5.11) which indicates proliferation of cells were more prominent on the KOH treated 3C-SiC/Si samples. The cells also showed similar morphology and viability with the cells originally grown on untreated 3C-SiC/Si.

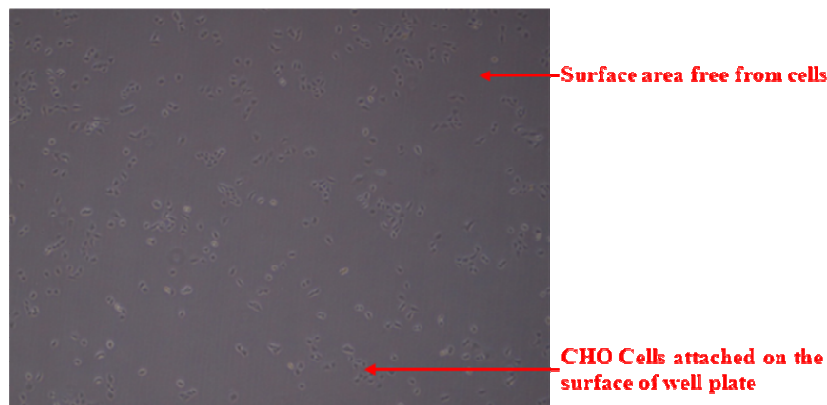


Figure 5.13: Optical micrograph of CHO cells cultured overnight on the 6 well plate's surface previously subcultured on 3C-SiC treated with KOH solution and reactive ion etching at 4× magnifications.

Cell density were lesser and comparable to the negative control (Figure 5.9). This indication corresponded well with the cells morphology which was more spherical (as shown in Figure 5.13).

All the cells, upon removal from the materials were able to proliferate on the surface of the tissue culture plate wells with different capabilities due to the materials' biocompatibility. Cells from positive control showed the highest density of adherent cells. The cells were in a very healthy condition even after trypsination which occasionally caused damage or injured the cells [20, 21]. Therefore, the inability of the cells to live or proliferate could be attributed to the non-biocompatibility characteristic of the materials not to the experimental procedures.

The observation of the cell morphology after culturing without the substrate was easier. Cells from the negative control showed low population density and exhibited lower adhesion as indicated by the cell morphology. The cells' population has high correspondence with the

morphology. If the cells were more stellate and flattened in shape, the counts of the cells would be higher.

The cells originally cultured from Si appeared to be rounded and showed lesser proliferation. More dead cells represented by floating luminating cells were more apparent. These three characteristics indicate slightly lower biocompatibility of Si in comparison to SiC. More CHO cells with stellar morphology and higher population were observed for the untreated 3C-SiC/Si and the KOH treated 3C-SiC/Si cells. Thus from this observation, untreated and chemically treated 3C-SiC are more biocompatible relatively to Si and did not show cytotoxicity behavior to animal cells.

Low cell density and spherical morphology were the trait exhibited by the cells subsequently cultured from the reactive ion etched 3C-SiC/Si. This finding showed that plasma etched 3C-SiC is not as biocompatible as the untreated 3C-SiC and chemically treated 3C-SiC. However, this observation must be confirmed with other techniques to measure cell viability with the materials of interest before any final conclusion can be drawn.



### 5.3.3 Environmental Scanning Electron Microscopy (ESEM)

The ESEM micrographs show the morphology of the cells which were fixed on the substrate.

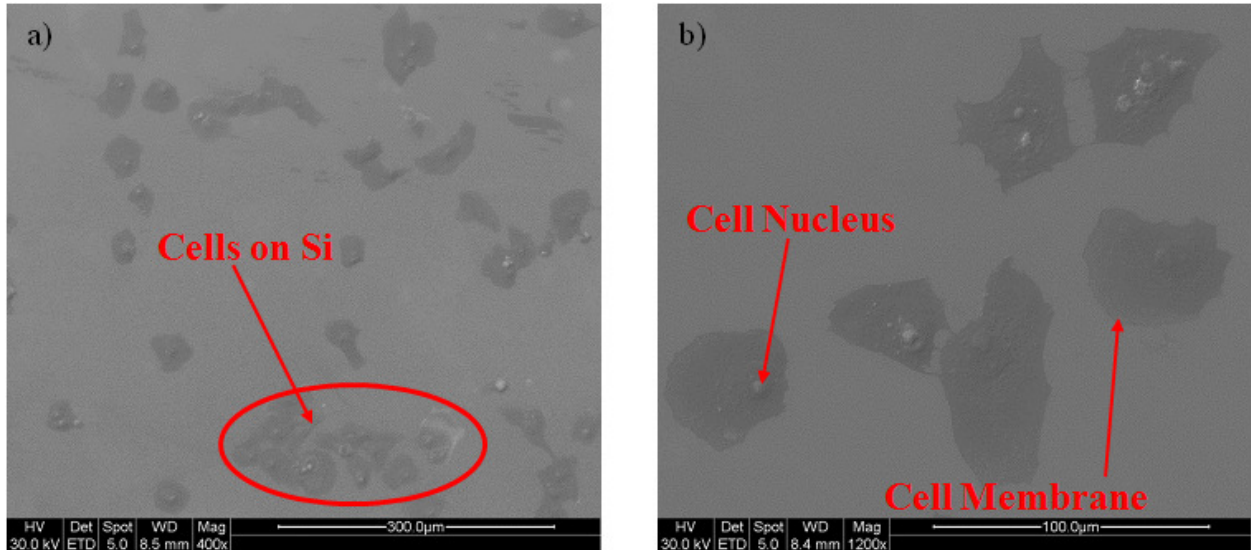


Figure 5.14: ESEM micrographs showing CHO cells cultured on Si a) 400x and b) 1200x.

The ESEM micrographs showed the morphology and the structure of the cells cultured on Si samples. In Figure 5.14 (a), the cells seem to grow and proliferate although not in high density. Here, the cells appeared to be flat and the nucleus can be clearly seen from the micrographs.

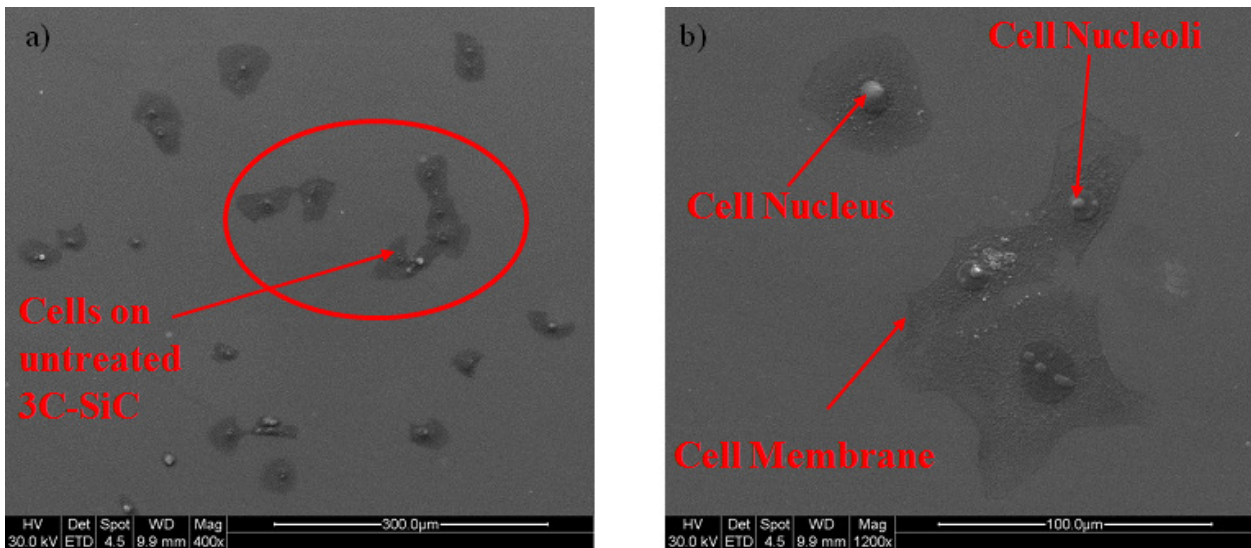


Figure 5.15: ESEM micrographs showing CHO cells cultured on untreated 3C-SiC a) 400x and b) 1200x.

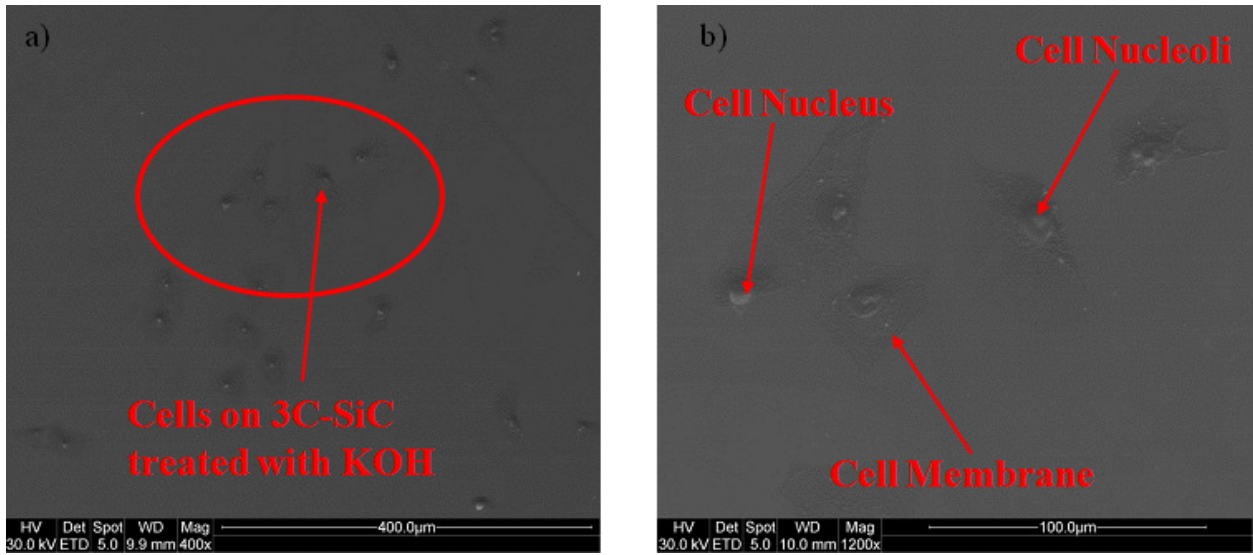


Figure 5.16: ESEM micrographs showing CHO cells cultured on 3C-SiC treated with KOH solution a) 400x and b) 1200x.

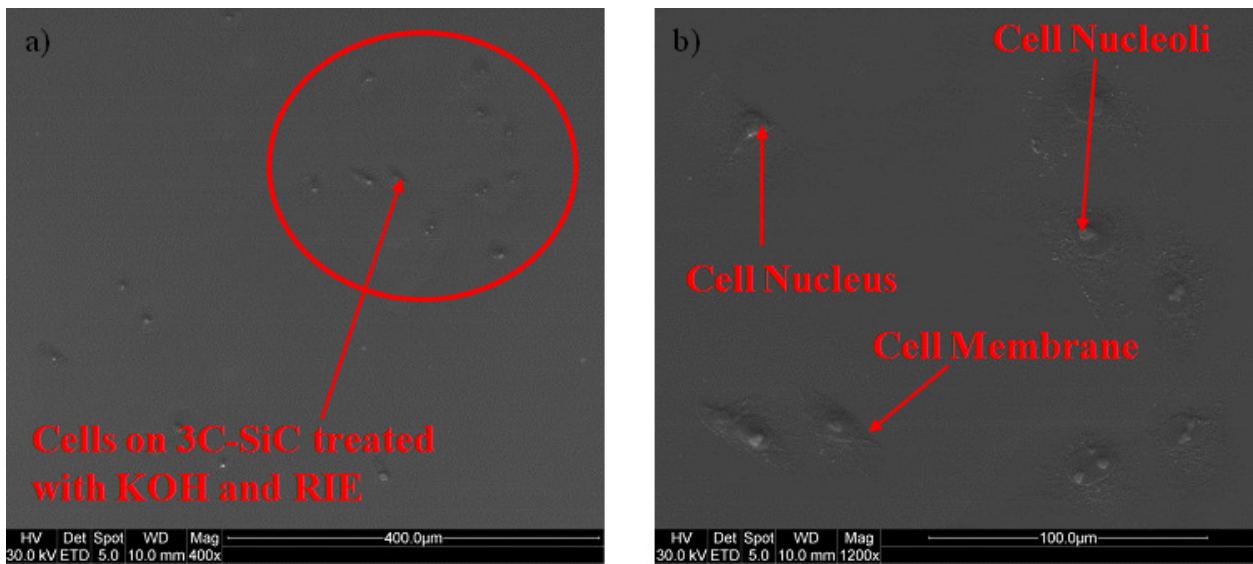


Figure 5.17: ESEM micrographs showing CHO cells cultured on 3C-SiC treated with KOH solution and reactive ion etching a) 400x and b) 1200x.

All the cells cultured on 3C-SiC showed similar morphology and structure. They proliferated randomly on 3C-SiC samples and Si without any particular trends, thus, the cell activity seems was non uniform all over the surface. No distinct feature could be observed for all the three types of 3C-SiC and even with cells on Si. Thus, at microscopic level, no clear indication of non-biocompatibility characteristic can be observed.

## 5.3.4 Cell Counting

### 5.3.4.1 Total Cells Counting

Trypan blue stain exclusion technique was used to determine the total cell counts, the amount of viable cell and the viable percentage of CHO cells cultured on the materials.

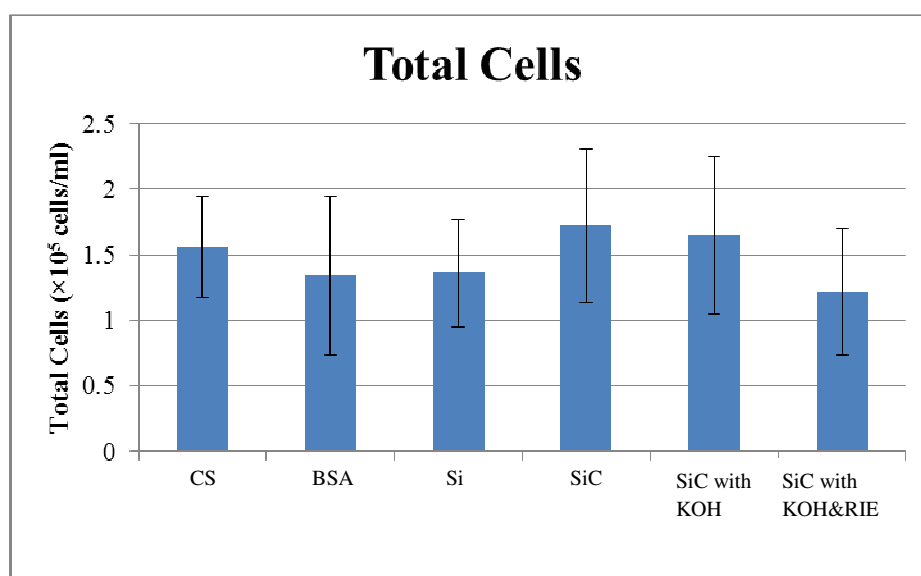


Figure 5.18: The number of total cells cultured on the materials after incubated overnight, stained by Trypan blue dye and counted using Countess® Automated Cell Counter (Invitrogen). The cells cultured on Thermanox™ coverslip were used as positive control and the cells cultured on Thermanox™ coverslip treated with Bovine Serum Albumin (BSA) were used as negative control. The total cells counted include living cells and dead cells.

Here, the trypan blue stain exclusion assay has confirmed quantitatively that the cells were able to proliferate on the materials. The number of total cells counted represents both the living and the dead cell. The amount of the total cells on the biocompatible coverslip after overnight incubation has exceeded 150,000 per ml. The total cell counts for the CHO cells on untreated and KOH treated 3C-SiC/Si were relatively higher than the positive control, where the former is

approximately 10% and the latter is 5% higher. The amount of cells counted for Si are comparable to the result from the negative control which is approximately 15% lesser than the positive control. The least amount of cells is the RIE and KOH treated 3C-SiC/Si which is about 20% less than the positive control. This finding is consistent with the observation made in section 5.2.2.2 where the morphology and the cell population density gave preliminary insight to the cells viability.

### 5.3.4.2 Living Cells Counting

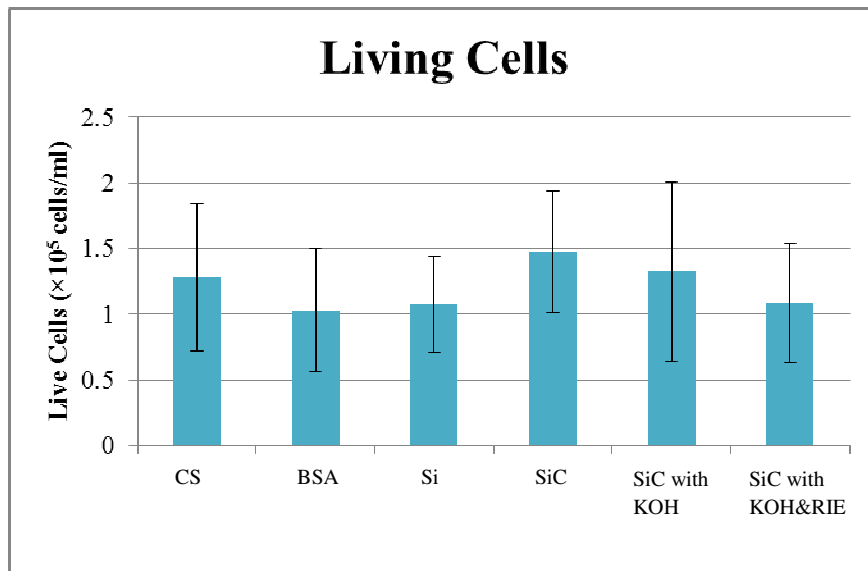


Figure 5.19: The amount of living cells cultured on the materials after incubated overnight, stained by Trypan blue dye and counted using Countess® Automated Cell Counter (Invitrogen). The cells cultured on Thermanox™ coverslip were used as positive control and the cells cultured on Thermanox™ coverslip treated with Bovine Serum Albumin (BSA) were used as negative control.

Previous results shown in Figure 5.18 do not distinguish between the living cells and the dead cells counted for CHO cells cultured on the materials. However, the trypan blue exclusion assay is capable to provide the number of living cells. As can be seen from Figure 5.19, the amount of

living CHO cells for the untreated 3C-SiC/Si is the highest, which is 15% more than the positive control and the cells previously cultured on the KOH treated 3C-SiC/Si is comparable to the positive control. The amount of the cells from the RIE and KOH treated 3C-SiC/Si and Si are comparable to the negative control which are 15% lesser than the positive control. From the cell counting, cell multiplied the highest on the untreated 3C-SiC and the KOH treated 3C-SiC samples. Both samples also have a higher number of total living cells. Lesser amount of cells proliferated on the Si and the 3C-SiC treated with RIE and KOH. There was a lower number of living cells on these samples.

#### **5.3.4.3 Cell Viability Percentage**

Trypan blue stain exclusion technique is a very powerful tool since it is not only able to provide information on the amount of cells (living or dead) but also capable in providing preliminary result about cell viability. Here, the cell viability percentage is assessed indirectly based on the CHO cell membrane integrity [22].

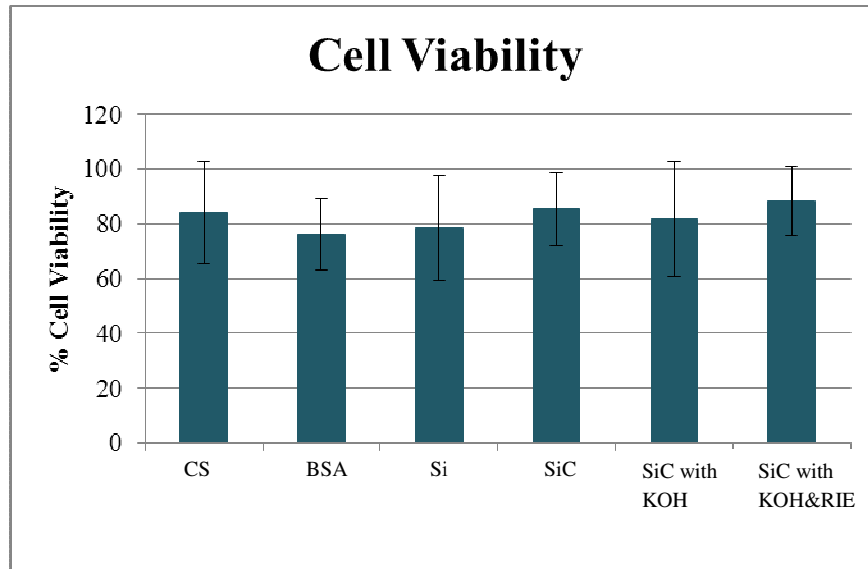


Figure 5.20: The viability percentage of the cells after had been cultured on the materials and incubated overnight and stained by Trypan blue dye. The cell viability percentage was obtained using Countess® Automated Cell Counter (Invitrogen). The cells cultured on Thermanox™ coverslip were used as positive control and the cells cultured on Thermanox™ coverslip treated with Bovine Serum Albumin (BSA) were used as negative control.

Contrary to the cell counting finding, the cell viability result shows the highest percentage of viable cell was from the RIE and KOH treated 3C-SiC/Si samples and the untreated 3C-SiC/Si samples. All the 3C-SiC/Si based samples showed a higher cell viability (in percentage) compared to Si samples. The results obtained for the cell viability percentage (refer Figure 5.20) contradicted the total cell count results (refer Figure 5.18) and the living cell count results (refer Figure 5.19) where the highest percentage of cell viability is for the KOH and RIE treated samples which is approximately 88%. This is due to the high ratio of the amount of the living cells to the total cells of the RIE and KOH treated 3C-SiC samples and the difference of this ratio is only about 10%. Meanwhile, the differences for other samples (for the positive control, negative control, Si, untreated 3C-SiC and KOH only treated samples) ranges from 25-33% which explained lower cell viability percentage obtained for these samples.

Although this technique is able to measure cell membranes integrity but on the other hand this technique compromised the ability of cells to continue their proliferation [22]. Consequently, the accuracy of this technique for determining cell viability is questionable. Thus, I would like to conclude that other assays capable of measuring cell viability are required for accurate verification the cell viability on the materials of interest.

### 5.3.5 Cell Viability Tests

#### 5.3.5.1 MTT Assay

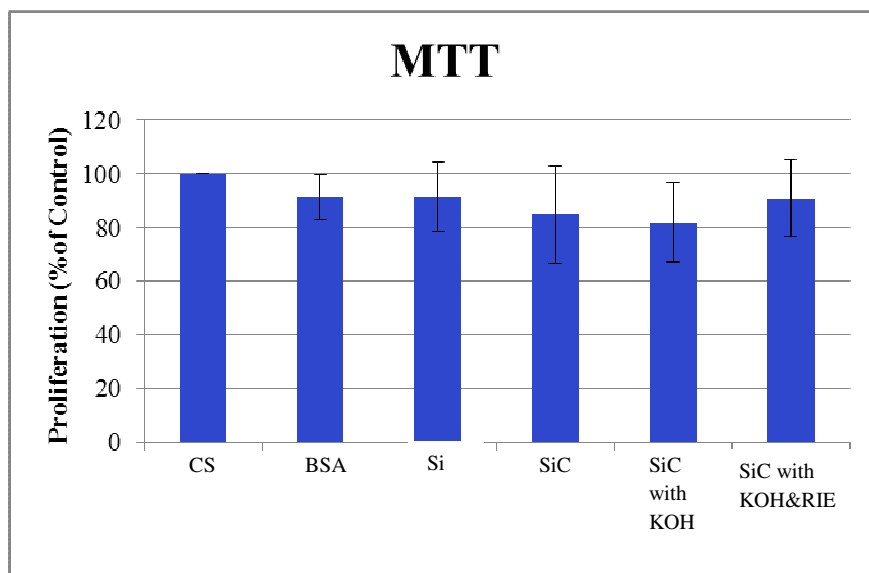


Figure 5.21: CHO cells viability percentage on the materials against control using MTT assay (Invitrogen, USA) assay. The tests were performed in triplicates and the reported values are expressed as  $\bar{x} \pm \sigma_m$ . The cells cultured on Thermanox™ coverslip were used as positive control and the cells cultured on Thermanox™ coverslip treated with Bovine Serum Albumin (BSA) were used as negative control.

A histogram of measured MTT assay proliferation percentage for Si, untreated 3C-SiC/Si, KOH treated 3C-SiC/Si and RIE and KOH treated 3C-SiC/Si in comparison to the positive control is expressed in mean  $\pm$  standard deviation. Here, the result for the RIE and KOH treated 3C-SiC/Si samples are in agreement with the result presented in 5.2.4.3 where CHO cells showed higher viability level on the plasma etched and KOH treated 3C-SiC/Si samples which is approximately 91%. Viability percentage of CHO cells on both Si and negative control are better using MTT assay viability test (which are approximately 91%) in comparison to untreated 3C-SiC and KOH treated 3C-SiC (which are 85% and 80%). These results from MTT assay (for negative control, Si, untreated 3C-SiC and KOH only treated samples) not only contradicted with the trypan blue exclusion assay results but also with the optical microscopy observations before. This contradiction is not surprising since, MTT assay, despite known as convenient and economic [4], but sometimes provides confusing and inaccurate result [23]. This is indicated in Figure 5.22 by high standard deviation error bars where non-living cells are also able to reduce tetrazolium salt into soluble formazan [24]. Thus, as precaution, an extra care is needed if using this assay. In this case, these contradicting results should be accompanied and verified by another independent cell viability assay.



### 5.3.5.2 PrestoBlue™ Assay

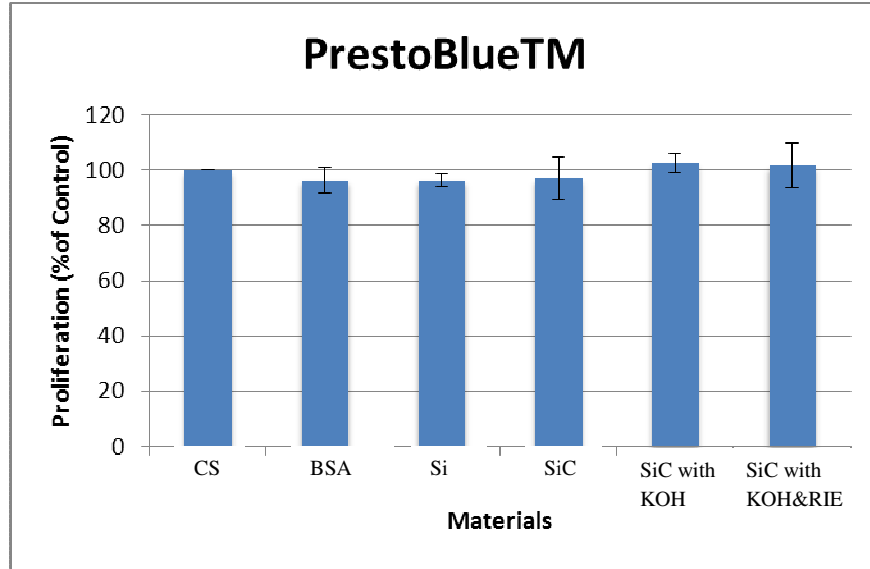


Figure 5.22: CHO cells viability percentage on the materials against control using Prestoblu<sup>™</sup> Cell Viability reagent (Invitrogen, USA) assay. The tests were performed in triplicates and the result is expressed as  $\bar{x} \pm \sigma_m$ . The cells cultured on Thermanox<sup>™</sup> coverslip were used as positive control and the cells cultured on Thermanox<sup>™</sup> coverslip treated with Bovine Serum Albumin (BSA) were used as negative control.

A histogram of measured PrestoBlue<sup>™</sup> assay proliferation percentage for Si, untreated 3C-SiC/Si, KOH treated 3C-SiC/Si and RIE and KOH treated 3C-SiC/Si in comparison to the positive control is expressed in mean  $\pm$  standard deviation. The result here has confirmed the positive effect of RIE on 3C-SiC. However, PrestoBlue<sup>™</sup> indicates that KOH treated 3C-SiC/Si samples were also favored by the cells to rapidly grow. CHO cells were more viable on these types of samples. Therefore, it can be suggested that surface treatment of SiC surface might positively altered for a better cell growth or at least not to be toxic and thus, biocompatible. As can be seen from Figure 5.22, untreated 3C-SiC showed a proliferation rate similar to Si and the negative control. The results obtained were also relatively more reproducible in comparison to

the MTT assay based on the small standard deviation error, which indicates the higher accuracy of the used reagent that supports the claim by Newman et al. [11].

### 5.3.6 Hemolysis Assay

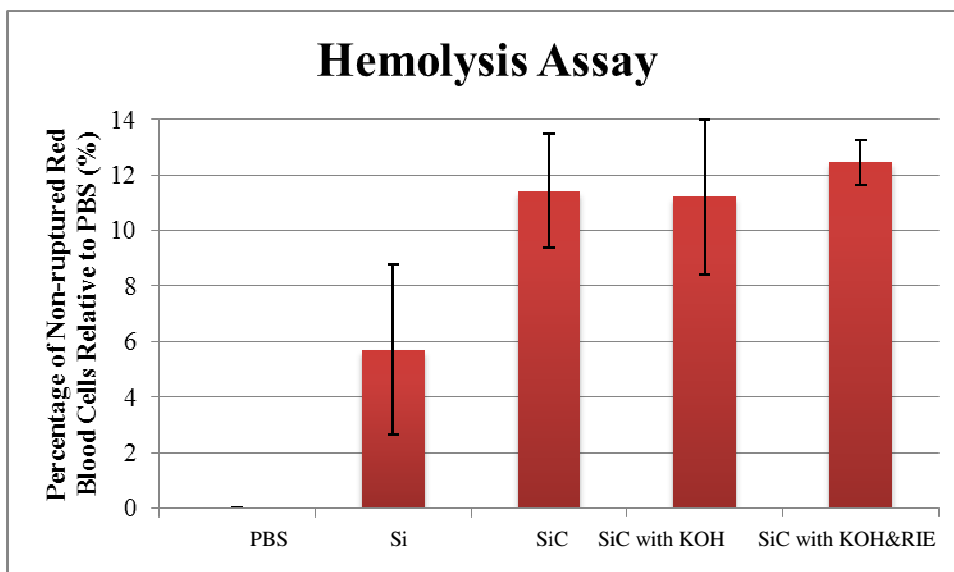


Figure 5.23: Hemolytic activity of hRBC with the materials. The tests were performed in triplicates and the reported values are expressed as  $\bar{x} \pm \sigma_{ST}$ . Results from PBS (where no hemolysis should occur) is set to zero and compared to the hemolysis results from other materials interacting with hRBC.

A histogram of hemolysis assay percentage for the non-ruptured red blood cells reacting with Si, untreated 3C-SiC/Si, KOH treated 3C-SiC/Si and RIE and KOH treated 3C-SiC/Si against PBS is expressed in mean  $\pm$  standard deviation. Here, the results were based on the assumption that no red blood cells should rupture in a buffer solution, where it is set to zero for easy comprehension. Thus, if a material, which interacts with red blood cells, provides a comparatively positive result against PBS, this means that the material is hemocompatible (shown as the absence of hemolytic activity).

All the materials tested here showed a positive hemocompatibility ranging from 6% to 12.5% in comparison to PBS. Interestingly, 3C-SiC samples showed a superior hemocompatibility (at least 5% more hemocompatible) than Si. Untreated 3C-SiC/Si and KOH treated 3C-SiC showed similar data. RIE and KOH treated 3C-SiC exhibited better hemocompatibility to any other samples with low standard deviation error. Thus, plasma etching could improve the hemocompatibility of 3C-SiC.

## 5.4 Conclusion

The assessment and comparison of the analyzed samples such as: Si, untreated 3C-SiC/Si, KOH treated 3C-SiC/Si and RIE and KOH treated 3C-SiC/Si of their biocompatibility and hemocompatibility characteristics has reveals important discoveries in this subject. From the optical micrographs showing the cultured CHO cells on the materials, CHO cells with spherical structure were dominating the Si surface. This represents lower contact areas and adhesion of the cells to the substrate. Meanwhile, all the cells on the 3C-SiC/Si samples were flattened and stellular which indicate a high contact and adhesion between the cells and 3C-SiC. This is the first indication of the biocompatibility of 3C-SiC.

The CHO cells were later removed and cultured on the 6 well cell culture plates where their viability were assessed visually and chemically using trypan blue exclusion assay, MTT assay and PrestoBlue™ reagents. The cells were able to proliferate even after removal during overnight period on all the materials tested. By removing the cells from the substrate, this had helped the observation on the cells. The cells seemed to favor untreated 3C-SiC/Si and KOH treated 3C-SiC/Si. As expected, spherical CHO cells formed the majority population for the Si origin cells with lower cell density. However, lesser cells with spherical structure were observed

from the RIE and KOH treated 3C-SiC/Si origin cells. Thus, the discrepancy could be attributed to the technique during the cell culture, and this was verified later by the positive results from the cell viability assay and reagent. The cells here were later counted using trypan blue exclusion assay. ESEM micrographs showed no distinct feature which could relate non-biocompatibility at micro level. All the samples showed similar structure and cell population density.

The quantification of both total and living cells showed interesting results where cell counts for untreated and KOH treated 3C-SiC/Si samples were much higher than the positive control. A similar result obtained qualitatively from the optical microscopy seems to be confirmed with these results where the cell counts for Si and RIE and KOH treated 3C-SiC/Si were low. However, despite unpromising counting and visual observation performed, the viability percentage of the cells for the RIE and KOH treated 3C-SiC/Si was the highest. This is attributed to the high ratio of living cells to the total cells counted.

Two viability tests were conducted to further verify the results. The viability of the cells previously cultured on RIE and KOH treated 3C-SiC/Si was high in both tests. However, lower results were obtained with MTT assay for untreated and KOH treated 3C-SiC, but this discrepancy can be attributed to the accuracy of the assay. KOH treated 3C-SiC also showed high cell viability with PrestoBlue™ test.

In most results, 3C-SiC has better biocompatibility quality in comparison to Si. This reaffirmed the biocompatibility of SiC against Si in literatures [5, 18, 19, 25]. Chemical treatment such as immersing 3C-SiC in KOH or HF solution did not alter 3C-SiC biocompatibility. This case was different with plasma treated 3C-SiC. The alteration of 3C-SiC surface had showed impact on its biocompatibility. Mixed results were obtained; however, based on the viability tests, plasma treatment of the 3C-SiC surface had improved the biocompatibility

quality of 3C-SiC. Plasma treatment might deposited C-rich layer on the 3C-SiC surface [26] and it is suggested carbon as a biomedical material showed good electrochemical potential comparable to living cells which lead to better quality of cell attachment [27]. Previous studied showed lower biocompatibility was corresponded to the decreased of carbon concentration on the 3C-SiC [19].

Previously, a study was conducted on the effect of device fabrication steps such as wet etching (KOH, HF and HCl) and plasma etching using SF<sub>6</sub> and chlorine on the sheet carrier concentration property and biocompatibility of AlGaIn/GaN based high-electron-mobility transistor (HEMT) [28]. The study revealed that these processing steps posed little effect on the biocompatibility of AlGaIn/GaN devices. Polyimide is commonly used to passivate sensor devices [28] and in another study [29], a cytotoxicity test was performed on polyimide samples (treated and untreated with CF<sub>4</sub>). It is showed the there was no cytotoxicity due to RIE. Thus, treating 3C-SiC with plasma gasses such CF<sub>4</sub> would improve the biocompatibility of 3C-SiC.

The hemocompatibility result based on the hemolytic activity of the cell-material was conclusive. Previous hemocompatibility studies on 3C-SiC revealed that SiC is more hemocompatible than Si [30, 31] and 3C-SiC showed better hemocompatible in comparison to other SiC polytypes [31]. Here, 3C-SiC samples showed superior hemocompatibility quality more than Si based on the hemolytic activity. Plasma etched samples showed the highest hemocompatibility and without any doubt, plasma etching with fluorinated plasma had enhanced the hemocompatibility of 3C-SiC.

## 5.5 References

- [1] P. U. Abel and T. von Woedtke, "Biosensors for in vivo glucose measurement: can we cross the experimental stage," *Biosensors and Bioelectronics*, vol. 17, pp. 1059-1070, 2002.
- [2] M. J. J. Norelli Schettini, Leigh West and Stephen E. Sadow, "Hemocompatibility Assessment of 3C-SiC for Cardiovascular Applications," in *Silicon Carbide Biotechnology: A Biocompatible Semiconductor for Advanced Biomedical Devices and Applications* S. E. Sadow, Ed., ed Amsterdam: Elsevier, 2011, pp. 153-208.
- [3] W. Strober, "Trypan Blue Exclusion Test of Cell Viability," in *Current Protocols in Immunology*, ed: John Wiley & Sons, Inc., 2001.
- [4] J. M. Edmondson, L. S. Armstrong, and A. O. Martinez, "A rapid and simple MTT-based spectrophotometric assay for determining drug sensitivity in monolayer cultures," *Methods in Cell Science*, vol. 11, pp. 15-17, 1988.
- [5] C. Coletti, M. J. Jaroszeski, A. M. Hoff, and S. E. Sadow, "Culture of mammalian cells on single crystal SiC substrates," 2006, pp. 46-51.
- [6] N. J. Marshall, C. J. Goodwin, and S. J. Holt, "A critical assessment of the use of microculture tetrazolium assays to measure cell growth and function," *Growth Regulation*, vol. 5, pp. 69-84, 1995.
- [7] T. Mosmann, "Rapid colorimetric assay for cellular growth and survival: Application to proliferation and cytotoxicity assays," *Journal of Immunological Methods*, vol. 65, pp. 55-63, 1983.

- [8] A. C. Reisetter, L. V. Stebounova, J. Baltrusaitis, L. Powers, A. Gupta, V. H. Grassian, and M. M. Monick, "Induction of inflammasome-dependent pyroptosis by carbon black nanoparticles," *Journal of Biological Chemistry*, vol. 286, pp. 21844-21852, 2011.
- [9] R. J. Tynan, J. Weidenhofer, M. Hinwood, M. J. Cairns, T. A. Day, and F. R. Walker, "A comparative examination of the anti-inflammatory effects of SSRI and SNRI antidepressants on LPS stimulated microglia," *Brain, Behavior, and Immunity*, vol. 26, pp. 469-479, 2012.
- [10] T. Machleidt, M. B. Robers, S. B. Hermanson, J. M. Dudek, and K. Bi, "TR-FRET Cellular Assays for Interrogating Posttranslational Modifications of Histone H3," *Journal of Biomolecular Screening*, vol. 16, pp. 1236-1246, December 1, 2011 2011.
- [11] R. A. Newman, S. Gopinath, and D. Kuninger, "Multiplexing with PrestoBlue (TM) Reagent: Providing Accurate Viability Assessment of Primary Cells Following Treatment with Toxicological Compounds & Enabling Downstream Functional Assays," *In Vitro Cellular & Developmental Biology-Animal*, vol. 47, pp. S32-S33, Jun 2011.
- [12] N. Chanda, P. Kan, L. D. Watkinson, R. Shukla, A. Zambre, T. L. Carmack, H. Engelbrecht, J. R. Lever, K. Katti, G. M. Fent, S. W. Casteel, C. J. Smith, W. H. Miller, S. Jurisson, E. Boote, J. D. Robertson, C. Cutler, M. Dobrovolskaia, R. Kannan, and K. V. Katti, "Radioactive gold nanoparticles in cancer therapy: therapeutic efficacy studies of GA-198AuNP nanoconstruct in prostate tumor-bearing mice," *Nanomedicine: Nanotechnology, Biology and Medicine*, vol. 6, pp. 201-209, 2010.
- [13] T. T. Puck, S. J. Cieciura, and A. Robinson, "Genetics of somatic mammalian cells," *The Journal of Experimental Medicine*, vol. 108, pp. 945-956, 1958.

- [14] S. C. Baicu and M. J. Taylor, "Acid–base buffering in organ preservation solutions as a function of temperature: new parameters for comparing buffer capacity and efficiency," *Cryobiology*, vol. 45, pp. 33-48, 2002.
- [15] R. I. Freshney. (2011, 17 June 2012). *Culture of Animal Cells : A Manual of Basic Technique and Specialized Applications (6 ed.)*.
- [16] G. Gstraunthaler, "Alternatives to the use of fetal bovine serum: serum-free cell culture," *ALTEX : Alternativen zu Tierexperimenten*, vol. 20, pp. 275-281, 2003.
- [17] H. Carol, P. Jong, C. Marilyn, and K. Sucheta, "Preparation of cultured cells for scanning electron microscope," 2007.
- [18] C. L. Frewin, C. Locke, S. E. Sadow, and E. J. Weeber, "Single-crystal cubic silicon carbide: An in vivo biocompatible semiconductor for brain machine interface devices," in *Engineering in Medicine and Biology Society, EMBC, 2011 Annual International Conference of the IEEE*, 2011, pp. 2957-2960.
- [19] C. Coletti, M. J. Jaroszeski, A. Pallaoro, A. M. Hoff, S. Iannotta, and S. E. Sadow, "Biocompatibility and wettability of crystalline SiC and Si surfaces," Lyon, 2007, pp. 5849-5852.
- [20] J. Collett, A. Crawford, P. V. Hatton, M. Geoghegan, and S. Rimmer, "Thermally responsive polymeric hydrogel brushes: synthesis, physical properties and use for the culture of chondrocytes," *Journal of The Royal Society Interface*, vol. 4, pp. 117-126, February 22, 2007 2007.
- [21] J. P. Sutradhar BC, G Hong, SH Choi and G Kim, "Effects of Trypsinization on Viability of Equine Chondrocytes in Cell Culture," *Pakistan Veterinary Journal*, vol. 30, pp. 232-238, 2010.



- [22] N. H. Masoodzadehgan, "Superparamagnetic iron oxide nanoparticles development, characterization, copper-64 labeling and cellular tracking," Master of Science in Medical Physics, Department of Biomedical Engineering, Georgia Institute of Technology, Georgia, USA, 2012.
- [23] H. Wan, R. Williams, P. Doherty, and D. F. Williams, "A study of the reproducibility of the MTT test," *Journal of Materials Science: Materials in Medicine*, vol. 5, pp. 154-159, 1994.
- [24] M. Pagé, N. Bejaoui, B. Cinq-Mars, and P. Lemieux, "Optimization of the tetrazolium-based colorimetric assay for the measurement of cell number and cytotoxicity," *International Journal of Immunopharmacology*, vol. 10, pp. 785-793, 1988.
- [25] G. Gabriel, I. Erill, J. Caro, R. Gómez, D. Riera, R. Villa, and P. Godignon, "Manufacturing and full characterization of silicon carbide-based multi-sensor micro-probes for biomedical applications," *Microelectronics Journal*, vol. 38, pp. 406-415, 2007.
- [26] J. W. Palmour, R. F. Davis, T. M. Wallett, and K. B. Bhasin, "Dry etching of b-SiC in CF<sub>4</sub> and CF<sub>4</sub>+O<sub>2</sub> mixtures," *Journal of Vacuum Science & Technology A: Vacuum, Surfaces, and Films*, vol. 4, pp. 590-593, 1986.
- [27] A. Angelescu, I. Kleps, M. Mihaela, M. Simion, T. Neghina, S. Petrescu, N. Moldovan, C. Paduraru, and A. Raducanu, "Porous silicon matrix for applications in biology," *Reviews on Advanced Materials Science*, vol. 5, pp. 440-449, 2003.
- [28] I. Cimalla, F. Will, K. Tonisch, M. Niebelschütz, V. Cimalla, V. Lebedev, G. Kittler, M. Himmerlich, S. Krischok, J. A. Schaefer, M. Gebinoga, A. Schober, T. Friedrich, and O. Ambacher, "AlGaN/GaN biosensor—effect of device processing steps on the surface

- properties and biocompatibility," *Sensors and Actuators B: Chemical*, vol. 123, pp. 740-748, 2007.
- [29] T. Doerge, S. Kammer, M. Hanauer, A. Sossalla, and S. Steltenkamp, "Novel method for a flexible double sided microelectrode fabrication process," 2009.
- [30] N. Nurdin, P. François, Y. Mugnier, J. Krumeich, M. Moret, B. O. Aronsson, P. Descouts, R. Barbucci, C. Bacquey, and L. Koole, "Haemocompatibility evaluation of DLC- and SiC-coated surfaces," *European Cells and Materials*, vol. 5, pp. 17-28, 2003.
- [31] S. E. Sadow, C. L. Frewin, C. Coletti, N. Schettini, E. Weeber, A. Oliveros, and M. Jarosezski, "Single-crystal silicon carbide: A biocompatible and hemocompatible semiconductor for advanced biomedical applications," vol. 679-680, ed. Oslo, 2011, pp. 824-830.

# Chapter 6

## Conclusion and Future Works

### 6.1 Conclusion

During the course of this program, the author established reproducible techniques and obtained significant scientific results regarding to the 3C-SiC membranes fabrication processes and properties. This thesis covers the optimal conditions required to fabricate 3C-SiC membranes. Extensive characterization results on the material and electrical properties of 3C-SiC

membranes and the effect of the fabrication processes on the 3C-SiC properties are presented. Biocompatibility and hemocompatibility results of 3C-SiC are covered in detail in this study.

In every chapter, a detailed conclusion was made at the end of the respective chapters. In this chapter, brief conclusions of the results obtained throughout the PhD. program are presented and this highlights the opportunity for more investigation to be carry out on investigating the properties of 3C-SiC membranes and future applications of this newly developed material especially in BioMEMS.

### **6.1.1 Fabrication of 3C-SiC Membranes**

3C-SiC membranes have been produced successfully using standard microfabrication techniques such as photolithography, reactive ion etching and chemical wet etching of Si substrate. The fabrication method was proven to be reproducible and was used to produce 3C-SiC membranes with thicknesses of 1.18  $\mu\text{m}$ , 0.95  $\mu\text{m}$  and 0.285  $\mu\text{m}$ .. Several membranes with different areas were produced but the largest version was about 1.5 $\times$ 1.0  $\text{cm}^2$ . (Much larger membranes could have been made but this was not an objective in this thesis). The shape of membranes produced corresponded to the etching of the Si substrate crystalline plane and the mask applied during photolithography which in accordance to the simulation. Optimization of 3C-SiC membranes' fabrication technique is one of the main issue in this chapter where the RIE etch rate for 3C-SiC is established and the Si substrate etching using KOH solution was reduced and optimized. The membranes produced were able to withstand forces from a stream of nitrogen gas (during drying), probing sessions, metal deposition, photoresist application and furnace heating were performed without breaking.

### 6.1.2 Material Characterization of 3C-SiC Silicon Carbide Membranes

SEM micrographs show well-defined side walls due to the unetched Si <111> which support the suspended membrane (with smooth morphology) forming a cavity. Raman Spectroscopy and Visible Photoluminescence Spectra showed peaks originating from Si substrate were apparent for the spectra taken from the backside of the free standing membrane. This suggests that remains of the Si substrate were not fully removed by KOH etching and likely due to the <111> plane which has hundreds of times slower etching rate. These (<111> only Si features) existed visually as microstructure defects. The front side of the 3C-SiC membrane did not show such influence from the defects confirming the high quality 3C-SiC provided by the Griffith University. The influence of these microstructure defects extended to the Visible Transmission Spectra where lower transmission percentages were obtained. The author suggests that the membrane is more suitable as a BioMEMS structure such a diaphragm membrane or cantilever rather than in application which required high transparency property such as an X-ray mask. XPS revealed that RIE with fluorinated plasma had introduced significant amount of fluorine to the 3C-SiC surface. However, 3C-SiC immersion in KOH and HF solution whether to remove Si or native oxide had proven not to alter the surface elemental composition. The author also addressed the influence of the fluorinated surface which is more detrimental than the carbon rich layer redeposited from RIE in affecting the 3C-SiC electrical contacts.

### 6.1.3 Electrical Characterization of 3C-Silicon Carbide Membranes

The influence of fluorinated plasma treatment on the electrical properties of 3C-SiC is first demonstrated in the opening of the 4<sup>th</sup> chapter. The samples without plasma treatment showed good ohmic characteristics. The effect of fluorinated plasma was demonstrated where nonlinearity of the current-voltage characteristics is obvious and further elaborated for the contacts with different area.

This finding is further investigated by measuring the specific contact resistance,  $\rho_c$ , using circular transmission line model (CTLM) on the Al/3C-SiC and Pd/3C-SiC systems. Measurements of  $\rho_c$  for Al/3C-SiC and Pd/3C-SiC contacts with pre-treatment by reactive ion etching in CF<sub>4</sub> plasma were three orders of magnitude higher ( $\rho_c = 2 \times 10^{-1} \Omega\text{cm}^2$ ) than for as-grown SiC or KOH treated surfaces ( $\rho_c = 4 \times 10^{-5} - 8.9 \times 10^{-4} \Omega\text{cm}^2$ ). Annealing of Al/3C-SiC contacts has resulted in a progressive increase in  $\rho_c$  with increase in temperature to 600 °C. The presence of the 3C-SiC/Si heterojunction in contacts off the membrane was not a factor in determining  $\rho_c$  since the measurements have shown no clear difference in  $\rho_c$  between the contacts located on the membranes and off the membranes.

The substrate effect on the electrical characteristic properties of 3C-SiC/Si can be neglected at room temperature since the current flow was restricted at the metal contact/3C-SiC junction and the epitaxial layer of 3C-SiC without leaking into the Si substrate. However, the use of 3C-SiC membranes to determine its electrical characteristics (especially the ohmic contact Transmission Line Model (TLM) test structure parameters) is the best way to eliminate any possibility of leakage current into the substrate for this type of system.

## **6.1.4 Biocompatibility and Hemocompatibility Assessment of 3C-Silicon Carbide Thin Films**

Comparison was made between the cells grown on the Thermanox™ coverslips (positive control), Thermanox™ coverslips treated with Bovine Serum Albumin (BSA) (negative control), Si, untreated 3C-SiC/Si, 3C-SiC/Si treated only with KOH solution and 3C-SiC/Si treated with KOH solution and CF<sub>4</sub> plasma in an RIE system. Optical micrographs showed the cells preference to adhere and proliferate on the positive and all the 3C-SiC/Si samples in comparison to the negative control and Si samples. This qualitative result indicates the biocompatibility of 3C-SiC. Further qualitative results, showed the ability of the cell to continue proliferation after removal from the materials using trypsinization.

Untreated 3C-SiC/Si and KOH treated 3C-SiC samples showed a high number of cells both qualitatively (optical micrographs observation) and quantitatively (using trypan blue exclusion technique) in comparison to Si samples. Contradicting results were obtained for the KOH and RIE treated 3C-SiC/Si samples where a smaller number of cells was observed through the optical microscope and the cell count was low. However, the same trypan blue exclusion stain technique indicated the high cell viability percentage for the KOH and RIE treated 3C-SiC/Si samples. MTT assay and PrestoBlue™ reagents reaffirmed this finding and the author can conclude that 3C-SiC has better biocompatibility than Si and surface treating 3C-SiC may assist to increase its biocompatibility.

The hemocompatibility result based on the hemolytic activity of the cell-material was conclusive. Here, 3C-SiC samples showed superior hemocompatibility quality more than Si

based on the hemolytic activity. Plasma treated samples showed the highest hemocompatibility and without any doubt, plasma treatment with a fluorinated plasma had enhanced the hemocompatibility of 3C-SiC.

#### **6.1.5 Author's Conclusion Statement**

From the results presented here, the author concluded that fabrication processes of 3C-SiC membrane had altered the properties of 3C-SiC. In order to have a good quality of ohmic characteristic, RIE which uses fluorinated plasma should be avoided. Protecting the surface that would be deposited with metal or using alternative method such as micromilling to remove 3C-SiC is suggested to in order for processing not to degrade the electrical property of 3C-SiC. On the other hand, fluorinated plasma improved both biocompatibility and hemocompatibility of 3C-SiC. Thus, the alteration of electrical property or biocompatibility/hemocompatibility quality of 3C-SiC due to the utilization of RIE should compromise the effect outlined by the author.



## **6.2 Future Work**

The scopes of this work can be extended further into other dimensions. Few interesting topics based on the authors' work are listed below:

### **6.2.1 Fabrication and Finite Element Modeling of MEMS Structures Based on 3C-SiC Membranes**

Extra features can be fabricated using the epilayer 3C-SiC on Si substrate. These interesting structures may include (but not limited to) holes in the membranes, cantilevers and bridges. Finite element modelling of the mechanical characteristics of the membranes and structures mentioned above could provide interesting data for future MEMS application.

### **6.2.2 Mechanical Characterization of 3C-SiC Membranes**

The fabrication of 3C-SiC membranes lead to the possibility of quantifying its mechanical properties. At the RMIT Microscopy and Microanalysis Facility, School of Applied Science, Hysitron Nano-indenter which is nano-indentation equipment is recently purchased and available for research. Nano-indentation and nano-mechanical properties of the membrane can be examined. The tribological study of the membrane can be also conducted using the same equipment.

### **6.2.3 Investigation of Schottky Behavior and Other Electrical Properties of Metal/3C-SiC Contacts**

Schottky contact on 3C-SiC can be made using Cr or Au. However, as shown in Chapter 3, Au showed poor adhesion to 3C-SiC, thus, Cr is a better choice for this investigation. The effect of fluorinated plasma to the Schottky behavior of 3C-SiC would complement the finding obtained in this thesis. Hall Effect characterization of metal/3C-SiC also can be performed and presented in detail.

### **6.2.4 Fabrication of Potential Microdevices Based on 3C-SiC Membranes and Its Biocompatibility Study**

Potential Biomedical microdevices based on 3C-SiC membranes such as invasive micro blood pressure sensor can be fabricated and tested either in in vitro or in vivo environment. Prior to the fabrication of the device, microfluidic tests on the membrane can be performed using protein solution (bovine serum albumin in phosphate buffer saline solution) before real blood is used. This can reveal both mechanical and biocompatibility and hemocompatibility characteristic of the 3C-SiC membrane and the differences of the results due to the processes and the design involved in the fabrication. Performance of the BioMEMS can also be subject of interest since the effect biofouling due to protein adsorption can reduced the microdevice ability to sense pressure. Further biocompatibility assessments can be performed with animal testing and clinical testing on human.

# Appendix A

## A.1 Etching Simulation

Prior to the fabrication of 3C-SiC membranes, simulations were performed to determine the final outcome of the etching processes. The software used for this purpose was Anisotropic Crystalline Etching Simulation (ACES) Beta 2 (Build 200) version developed by Zhenjun (Alex) Zhu and Chang Liu from Micro Actuators, Sensors and Systems Group (MASS), University of Illinois at Urbana-Champaign [1]. The software is based on a continuous cellular automata method where the substrate is represented by an array of discrete cells which are interconnected in a crystalline lattice [1, 2]. The etching of the substrate abides to the etching rules where the

decision to remove or sustain a cell is based on the status of the neighboring cell number and their positions [1, 2].

Three (3) types of masks were used for this simulation. These masks were circular, square and rectangular masks as shown in Figure 2.1 a), 2.1 b) and 2.1c). The parameters set for the simulation were:

- The plan orientation for the etching: Face <100>, Edge <100>
- Substrate and type of etching: Silicon wet etching
- The etchant and the etching rate used: KOH (30%), 1.4  $\mu\text{m}/\text{min}$
- Etching time: 464 minutes

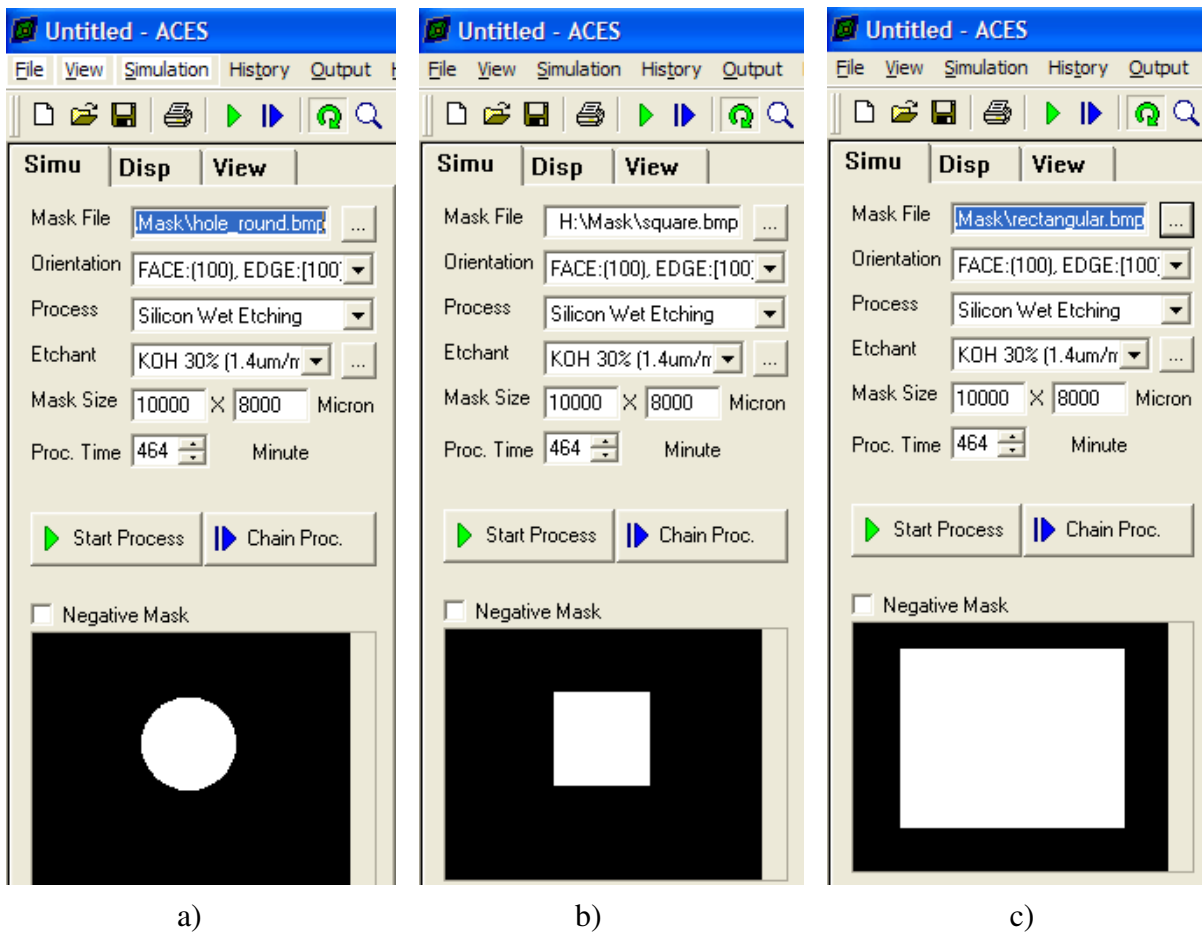


Figure A.1: The parameters set for the simulations of KOH etching of Si and the shape of masks used in the fabrication of 3C-SiC membranes, a) round mask and b) square mask c) rectangular mask

This simulated etching time was chosen due in regards to the thickness of the Si substrate which was approximately 650  $\mu\text{m}$ . By using this software, the size and the shape of the membrane can be predicted before the real etching process is performed.

## A.2 Simulation Results

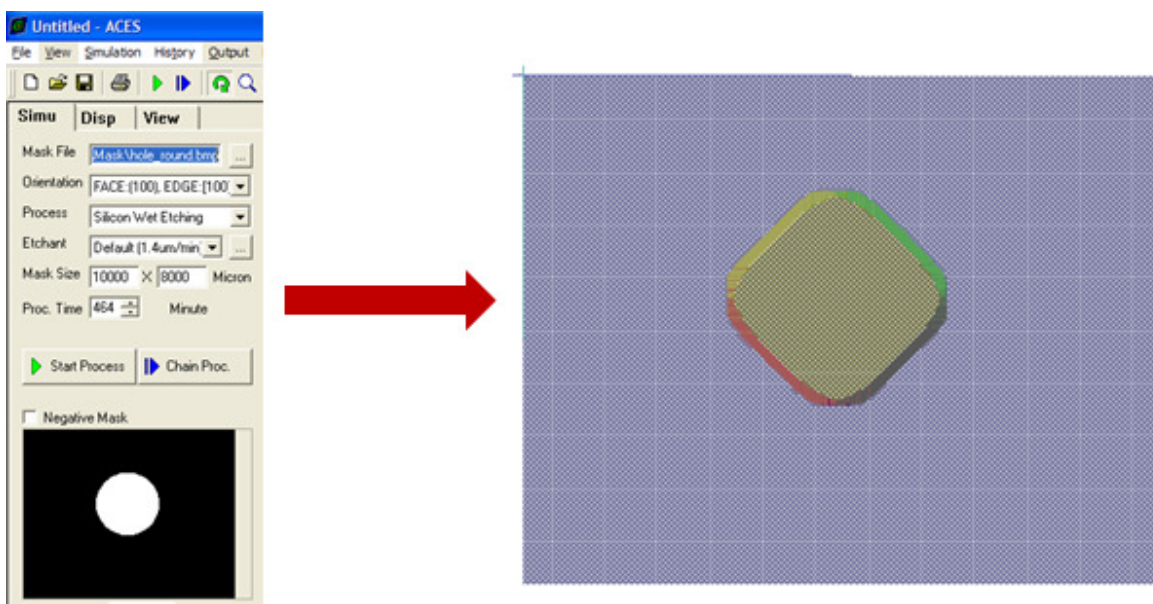


Figure A.2: The final outcome of the simulated etching of Si using circular mask.

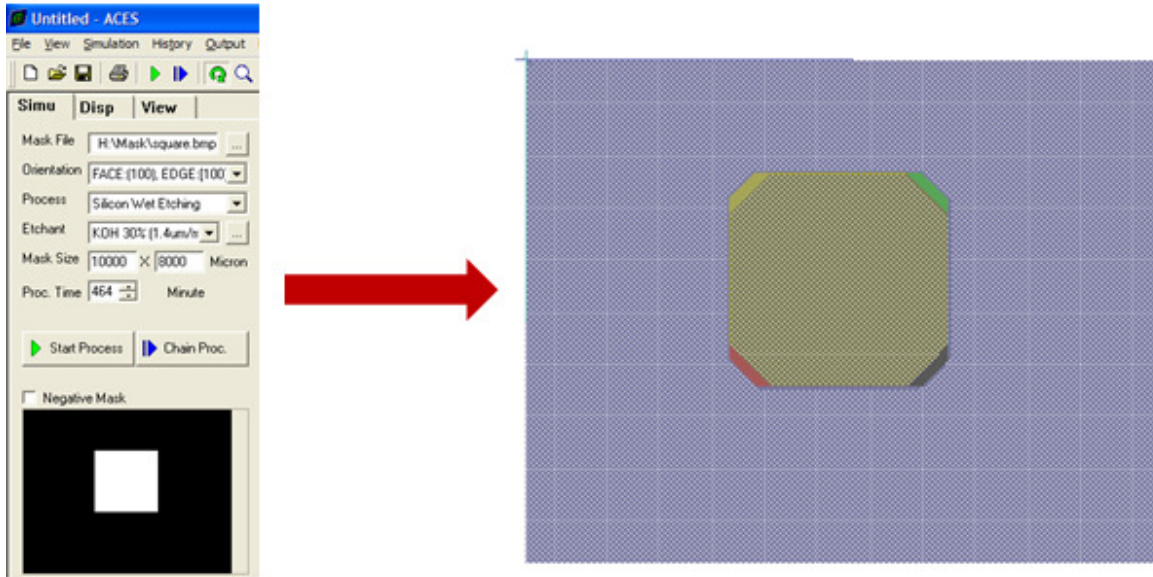


Figure A.3: The final outcome of the simulated etching of Si using square mask.

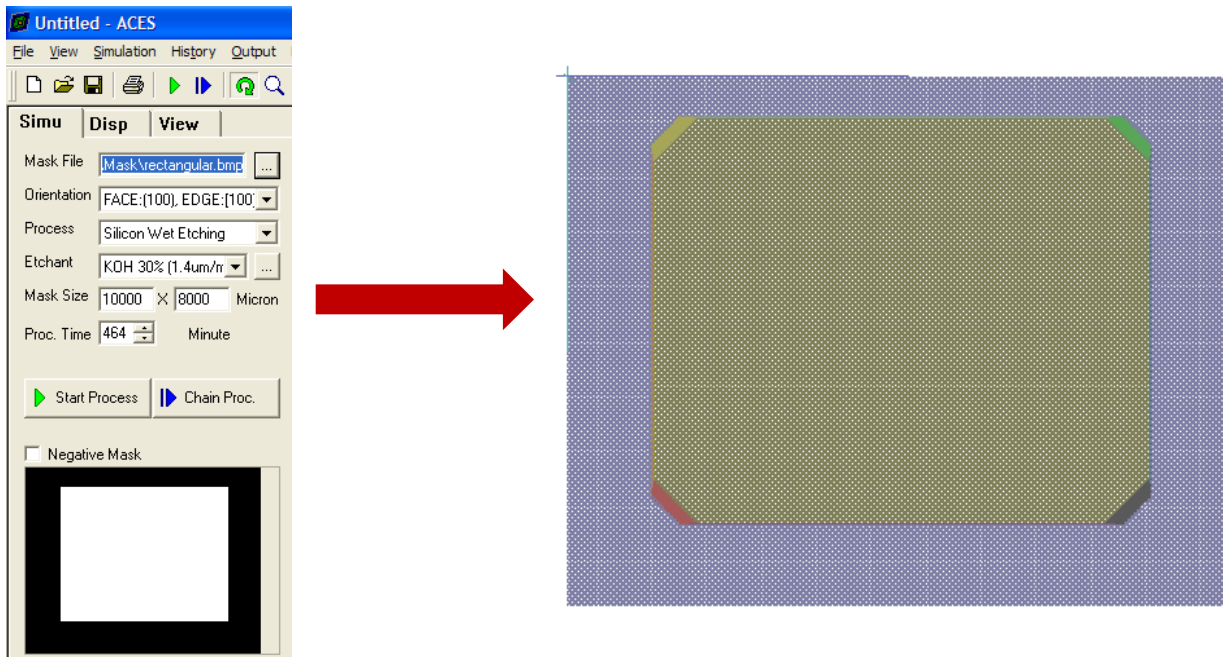


Figure A.4: The final outcome of the simulated etching of Si using rectangular mask.

The etching simulation shows the expected outcome of the etching using different mask shapes. KOH wet etching of Si <100> substrate using square and rectangular mask produced similar shape of the final products. However, the final produce from the substrate etching of the

circular shape mask was simulated to be square-like. Thus from the simulation of KOH wet etching using ACES software, all the 3C-SiC membrane produced for material, electrical and biological characterization would be square or rectangular in shape.

## A.3 References

- [1] Z. Zhenjun and L. Chang, "Micromachining process simulation using a continuous cellular automata method," *Microelectromechanical Systems, Journal of*, vol. 9, pp. 252-261, 2000.
- [2] Z. Zhu and C. Liu, "Simulation of anisotropic crystalline etching using a continuous cellular automata algorithm," *CMES - Computer Modeling in Engineering and Sciences*, vol. 1, pp. 11-19, 2000.

# Appendix B

## B.1 Micromilling

Micromilling was performed to remove some portion of 3C-SiC epitaxial layer on the backside of Si substrate using a Computer Numerical Control (CNC) machine, isel CPM 3020 micromiller. This was performed to create a window pattern in the SiC film on the backside of the Si substrate allows etching of the Si in the KOH solution as an alternative to RIE. In this process, a diamond bit was used due to the hardness of SiC which is about 9 Mohs hardness [1].





Figure B.1: isel CPM 3020 which was used to remove the 3C-SiC layer exposing the substrate for KOH wet etching of Si.

In this procedure, a drill with 3 mm diameter was used to create two holes (3 mm diameter) on the 3C-SiC samples. The 3C-SiC layer for the samples were  $0.95\ \mu\text{m}$  thick and the translation speed for isel CPM 3020 was set to  $0.25\ \text{mm/s}$  ( $250\ \mu\text{m/s}$ ) which is the slowest speed suggested by the manufacturer[2]. This speed is sufficient to remove the whole 3C-SiC layer from the substrate in a few seconds. Later, this procedure was followed by wet etching of Si using KOH solution at  $80^\circ\text{C}$  for the substrate removal to create 3C-SiC membranes.

## B.2 References

- [1] R. Cheung, "Introduction to Silicon Carbide Microelectromechanical Systems (MEMS)," in *Silicon Carbide Microelectromechanical Systems for Harsh Environments*, R. Cheung, Ed., 1st ed London: Imperial College Press, 2006, pp. 1-17.
- [2] B. Lenoir-Welter, "Machine Parameter," in *Galaad3 User's Manual*, B. Lenoir-Welter, Ed., 3.1 ed, 1999, pp. 9-9.

# Appendix C

## C.1 PrestoBlue™ Reagent Calculation

The common expression to calculate cell viability is based on this formula:

$$\frac{(OD_{552} \text{ Sample} - OD_{552} \text{ Background})}{(OD_{552} \text{ Control Sample} - OD_{552} \text{ Background})} \times 100 \quad (1)$$

In this formula, the measurement was performed by subtracting the background optical density, OD (which is defined as a blank) from the samples' OD. A blank usually consist of medium (with HEPES and Fetal Bovine Serum (FBS)) without any cells or assays/reagent. This formula is usually applied for MTT assay.

However, for PrestoBlue™ reagent, two measurements were taken which are at 595 nm and 630 nm. The 630 nm readings are referred to as those at the normalization wavelength. For each individual well, the OD<sub>630</sub> value is subtracted from the OD<sub>595</sub> value. The averages for the blanks were made after these subtractions. The value of the blanks averaged is subtracted from the answers of the subtraction of the OD<sub>630</sub> values from the OD<sub>595</sub> values of each well. These values are referred as background corrected values. For the positive control, the average value is considered as 100% which is the reference, and the other answer would be calculated against the positive control. Example of the measurement is tabulated below:

Measurement at OD <sub>595</sub>			Measurement at OD <sub>630</sub>			OD <sub>595</sub> -OD <sub>630</sub>		
Blank	Control	3C-SiC	Blank	Control	A	Blank	Control	A
0.078	0.792	0.774	0.041	0.378	0.367	0.037	0.414	0.407
0.071	0.759	0.746	0.038	0.374	0.361	0.033	0.385	0.385
0.077	0.758	0.768	0.041	0.367	0.363	0.036	0.391	0.405

Table C.1: The values for OD<sub>595</sub>, OD<sub>630</sub> and the OD<sub>595</sub>-OD<sub>630</sub>

The average for the blank: 0.035

Background Corrected Values: OD <sub>595</sub> -OD <sub>630</sub> -The Blank Average			
Control		A	
0.379		0.372	
0.350		0.350	
0.356		0.370	
Average	0.362	Average	0.364

Table C.2: The background corrected values

Thus, from Table C2, the cell viability percentage (using PrestoBlue™ reagent) of material A against positive control is 100.55%.

## C.2 References

- [1] L. T. Corporation. (2011, 7th May 2012). *Application Note: Processing Absorbance Data Obtained Using PrestoBlue™ Viability Reagent.*